RIGA TECHNICAL UNIVERSITY
Faculty of Civil Engineering
Institute of Materials and Structures

Pāvels Akišins
Doctoral Student of the Study Programme "Civil Engineering"

DESIGN OF ADVANCED PULTRUSION PROCESSES

Doctoral Thesis

Scientific supervisor
Professor *Dr. sc. ing.*
JEVGENIJS BARKANOVS

Riga 2017

ABSTRACT

This doctoral Thesis is devoted to the investigation, modelling, design and optimisation of advanced microwave assisted pultrusion processes. To provide better understanding of the pultrusion processes, to validate numerical simulation algorithms, conventional pultrusion processes are observed at the beginning of the research.

Two different approaches for a numerical simulation of pultrusion processes are proposed, compared and discussed. The first procedure is developed in the general-purpose finite element environment *ANSYS Mechanical* and based on the mixed time integration scheme and nodal control volumes method to decouple the coupled energy and species equations. The second procedure is performed by using computational fluid dynamics software *ANSYS CFX* and presents quite new approach not used widely for a pultrusion modelling. The developed procedures have been validated by the results of other authors and experimental results obtained in frames of *COALINE* project.

Accuracy of different curing kinetic models for resins with high microwave absorption properties has been evaluated and compared. Traditional description of the rate of the thermoset resin reaction by the Arrhenius relationship multiplied by a reaction function has been used. An engineering tool based on *Microsoft Excel* code has been developed by using the developed methodology. This tool has been successfully applied for a building of the curing kinetic models of resins with high microwave absorption properties used in the microwave assisted pultrusion processes.

To support the pultrusion tooling design and process control, new simulation methodology consisting of two sub-models has been developed. In the first step the electromagnetic sub-model is used to evaluate the electric field distribution by solving the Maxwell's equations with the *COMSOL Multiphysics*. In the second step an absorption energy field in the composite material determined with the electromagnetic sub-model is used as a heating source in the pultrusion process modelled with the thermo-chemical sub-model. This simulation procedure is developed in *ANSYS Mechanical* environment.

The developed procedure for numerical modelling of microwave assisted pultrusion process has been used for the design of multifunctional pultrusion die. The main idea of this die is to combine microwave assisted profile curing with an application of the coating in one pultrusion die. This process of pultruded coated profile manufacturing is free of VOCs and small particles emission. Also the proposed process has reduced labour and process cost. One more benefit is extraordinary interaction between coating and profile achieved by cure of the coating over a non-fully cured profile. After the coating application, the profile resin is fully cured together with coating.

At the end of the research, the designed microwave assisted pultrusion process with *in-line* coating technology has been optimised in terms of process and environment parameters with the objective to minimise energy consumption of the profile manufacturing. The defined optimisation problem has been solved by two methods: the random search method using *EDAOpt* optimisation software and the generalized reduced gradient algorithm utilized in *Microsoft Excel*. An engineering tool based on *Microsoft Excel* for a selection of optimal process parameters for different conditions has been developed using optimisation results.

ANOTĀCIJA

Promocijas darbs ir veltīts progresīvo ar mikroviļņiem veicinātu pultrūzijas procesu izpētei, modelēšanai, izstrādei un optimizācijai. Pultūzijas procesu labākai izprašanai un skaitlisko aprēķinu algoritmu validēšanai pētījuma sākumā ir apskatīti tradicionālie pultrūzijas procesi.

Divas dažādas pultrūzijas procesu skaitliskās simulēšanas metodes ir piedāvātas, salīdzinātas un apspriestas. Pirmā procedūra ir izstrādāta vispārējā pielietojuma galīgo elementu programmatūrā *ANSYS Mechanical* un izmanto jaukto laika integrācijas shēmu un mezglu kontroles tilpumu metodi saistīto enerģijas un pārneses vienādojumu atdalīšanai. Otrā procedūra ir izstrādāta izmantojot šķidrumu skaitļošanas dinamikas programmu *ANSYS CFX* un piedāvā jaunu līdz šim plaši neizmantotu metodi pultrūzijas modelēšanai. Izstrādātās simulācijas procedūras tika validētas, izmantojot citu autoru publicētus rezultātus un eksperimentālus rezultātus, iegūtus *COALINE* projekta ietvaros.

Pētījumā tika novērtēta un salīdzināta sveķu ar augstām mikroviļņu absorbcijas īpašībām dažādu saistīšanās kinētikas modeļu precizitāte. Tika izmantots tradicionāls termoreaktīvo sveķu reakcijas ātruma apraksts ar Arēniusa attiecību reizinātu ar reakcijas funkciju. Izmantojot izstrādātu metodoloģiju *Microsoft Excel* vidē tika izstrādāts rīks saistīšanās kinētikas modeļu izveidošanai. Dotais rīks tika veiksmīgi pielietots saistīšanās kinētikas modeļu izveidošanai sveķiem ar augstām mikroviļņu absorbcijas īpašībām, kuri tiks izmantoti ar mikroviļņiem veicinātos pultrūzijas procesos.

Ar mikroviļņiem veicināto pultrūzijas procesu labākai izprašanai, pultrūzijas iekārtu projektēšanas un procesa kontroles atbalstam tika izstrādāta jaunā simulēšanas metodoloģija, kas sastāv no diviem apakšmodeļiem. Pirmajā solī elektromagnētiskais apakšmodelis tiek izmantots elektriskā lauka sadales novērtējumam, risinot Maksvela vienādojumus ar *COMSOL Multiphysics*. Otrajā solī ar elektromagnētisko modeli noteikts absorbcijas enerģijas lauks kompozītā materiālā tika izmantots kā siltuma avots ar termoķīmisko modeli modelējamā pultrūzijas procesā. Dotā simulācijas procedūra ir izstrādāta *ANSYS Mechanical* vidē.

Izstrādāta ar mikroviļņiem veicinātu pultrūzijas procesu skaitliskās modelēšanas procedūra tika izmantota multifunkcionāla pultrūzijas veidņa projektēšanai. Progresīva procesa galvenā ideja ir apvienot ar mikroviļņiem veicinātu profila izveidi un pārklājuma uznešanu vienā veidnī. Dotais pārklātu pultrūdētu profilu ražošanas process ir raksturojams ar gaistošo organisko vielu savienojumu un mazu daļiņu emisijas neesamību. Piedāvātam procesam arī ir samazinātas tehnoloģiskas un personāla izmaksas. Papildus ieguvums ir ekstraordināra saiste starp profilu un pārklājumu, kas tiek iegūta ar pārklājuma saistīšanu uz nepilnīgi saistītās profila virsmas. Pēc pārklājuma uznešanas profila sveķi tiek pilnīgi saistīti kopā ar pārklājuma sveķiem.

Pētījuma nobeigumā izstrādāts ar mikroviļņiem veicināts pultrūzijas process ar *in-line* pārklājuma uznešanas tehnoloģiju tika optimizēts attiecībā uz procesa un vides parametriem ar mērķi samazināt profila ražošanai nepieciešamu enerģijas daudzumu. Definētā optimizācijas problēma tika risināta ar divām metodēm: gadījuma meklēšanas metodi izmantojot *EDAOpt* optimizācijas datorprogrammu un vispārināta samazināta gradienta algoritmu, izmantotu *Microsoft Excel* programmatūrā. Izmantojot optimizācijas rezultātus *Microsoft Excel* vidē tika izstrādās rīks optimālu procesa parametru izvēlei pie dažādiem nosacījumiem.

ACKNOWLEDGMENTS

I would like to thank my supervisor Prof. Evgeny Barkanov and head of the Institute of Material and Structures Prof. Andris Chate for they guidance and support throughout my career at the Riga Technical University and help on writing and presenting my work. It is a great benefit and honour to work with them.

I wish to thank colleagues Dr. Nora Lardiés Miazza and Santiago Gálvez from *AIMPLAS* (Spain) for the pultrusion trials and DSC scans of materials, Dr. Rudolf Emmerich and Matthias Graf from *FRAUNHOFER* (Germany) for the numerical calculation of electromagnetic field, and Nikos Pantelelis from *SYNTHESITES* (Greece) for the sensors and monitoring system used in pultrusion trials.

Finally, I want to thank my family for their support regardless of what I do.

This work was supported by the:

European Commission under *FRAMEWORK 7* program, contract no. NMP2-SL-2013-609149, project "Development of an Innovative Manufacturing Process for the In-Line Coating of Pultruded Composites (*COALINE*)".

TABLE OF CONTENT

INTRODUCTION

Pultrusion is a continuous and cost-effective process for a production of fibre-reinforced polymer composite structural components with a constant cross-sectional profile. It is an automated process requiring little labour and produces minimal waste material. Conventional pultrusion process that uses an electric heaters for heating of the pultrusion die is known since 1951 then in has been patented. At 2012, the volume of composites used in pultrusion processes sums up to 47 000 t, covering near 20 % of the total volume of currently used thermoset composites produced in Europe. During the last 5 years, the pultrusion market has experienced significant growth especially in transportation sector and construction applications and is expected to reach $ 1.7 billions in 2017. These points make pultrusion one of the fastest growing manufacturing processes within the composites market.

Although the sector demonstrates a healthy growth now but the continuous increase in the cost of electricity could considerably reduce this movement or even stop it. For this reason an urgent need appears for a considerable cost reduction of the pultrusion products which can be only reached by an improvement of the effectiveness of pultrusion processes.

Pultrusion process could be made more effective (less energy consumption and higher pultrusion speed) applying instead of conventional heaters a high frequency electromagnetic energy source. Also, the feature of the heating and, accordingly, the curing of the resin in case of microwave heating (cure starts on the centerline of the profile and then expands to the surface) allows the design of multifunctional pultrusion dies for coating application in the same die. In contrast, many manufacturing steps (profile pultrusion, surface preparing – sending and spraying, coating application) are necessary for obtaining of the coated pultruded profile in case of conventional pultrusion process.

1. LITERATURE REVIEW

1.1. Pultrusion processes

Pultrusion is a continuous and cost-effective process for a production of fibre-reinforced polymer (FRF) composite structural components with a constant cross-sectional profile. It is an automated process requiring little labour and produces minimal waste material. The pultrusion process allows high fibre volume fraction (60-70 %) [70]. The first work related to the pultrusion process has been published in 1951 [37]. A continuous production method for rod-like composite structures has been proposed in this patent. The first industrial pultrusion machine has been patented in 1959 [32]. The usage of the process has expanded worldwide due to the production of a wide range of pultruded profiles (Figure 1.1). At 2012, the volume of composites used in pultrusion processes sums up to 47 000 ton, covering near 20 % of the total volume of currently used thermoset composites produced in Europe [77]. During the last 5 years, the pultrusion market has experienced significant growth especially in transportation sector and construction applications and is expected to reach $ 1.7 billions in 2017. These points make pultrusion one of the fastest growing manufacturing processes within the composites market. According to a new market report [38], the future of the global pultrusion market looks bright with the growth at a CAGR of 4.6 % from 2016 to 2021. The major growth drivers for this market are the rise in demand for lightweight materials and increasing demand for durable products for corrosive environments, such as in rebar and gratings applications.

The pultrusion process is one of the most cost-effective and energy-efficient composite manufacturing process due to its high automation and production rate. The energy consumption of pultrusion process is around 3.1 MJ/kg (in comparison: for the autoclave moulding it is 21.9 MJ/kg and for the resin transfer moulding 14.9 MJ/kg) [9].

Thermosetting and thermoplastic resins are used in the pultrusion process. The most common thermosetting resins used in the pultrusion process are polyester, vinyl ester, polyurethane, epoxy, acrylic and phenolic [70]. Generally, the unsaturated resin is mixed with initiators and inhibitors to accelerate the chremical reaction of the resin during the process. Some of the thermoplastics that can be utilised in pultrusion process are polyamide, polyether ether ketone, polypropylene [9].

Figure 1.1. Pultruded profiles.

Glass and carbon fibre reinforcement can be employed in both types of matrix materials. The fibre reinforcement in forms of unidirectional (UD) roving, continuous filament mat (CFM), stitched fabric and woven fabric can be used for the production of FRF composites by pultrusion. The UD roving provides high tensile strength and Young modulus in longitudinal (pull) direction. The CFM, woven fabric and stitched fabrics are used to increase the strength and stiffness in the transverse direction [10].

During the conventional thermosetting pultrusion process the fibre reinforcements are saturated with the resin in a resin tank and then continuously pulled through a heated die by a puller. Inside the die the resin gradually cures and solidifies to form a composite part with the same cross-section profile of the die. At the final stage a travelling cut-off saw cuts the composite profile into desired lengths. A schematic view of this process is shown in Figure 1.2. The impregnation of the fibres take place at atmospheric pressure in this case. To increase the impregnation pressure the injection chamber can be used instead of the open resin bath (Figure 1.3).

Thermoplastic pultrusion tools have at least one additional die which is used for cooling the material. A schematic view of a thermoplastic pultrusion tool is shown in Figure 1.4. The molecular chains of thermoplastics are held together by weak van der Waals forces or by hydrogen bonds and do not undergo any chemical change during processing [9], therefore, the processing of thermoplastics requires consolidation under heat and pressure. The fibre reinforcements used in thermoplastic pultrusion are preimpregnated intermediate forms (commingled yarns, towpregs or prepregs) [47]. The thermoplastic resin and fibre bundle are heated in the preheating chamber and heating die to temperatures above the melting temperature of the thermoplastic matrix. After complete wet-out, the composite temperature decreases in the cooling die.

In many modern pultrusion processes the temperature measurements in different die points are executed by thermocouples to control the work of electrical heaters. By this way technologists could make pultrusion process more effective and control the degree of cure in pultruded profiles obtaining their desired quality.

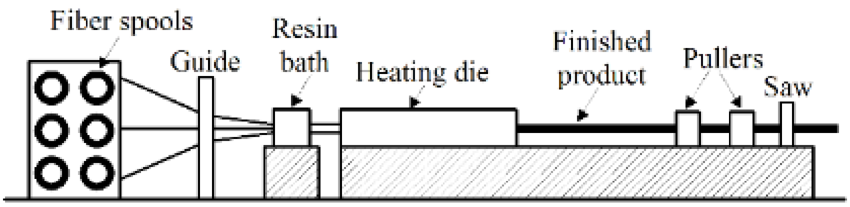

Figure 1.2. Conventional pultrusion tool for thermosetting pultrusion with an open resin bath.

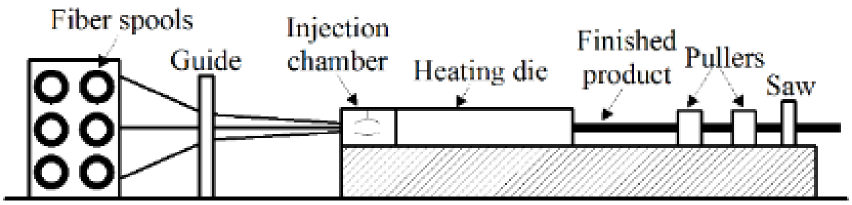

Figure 1.3. Conventional pultrusion tool for thermosetting pultrusion with a resin injection.

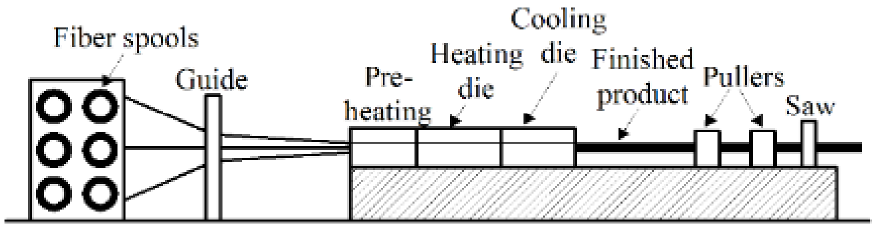

Figure 1.4. Conventional pultrusion tool for thermoplastic pultrusion.

Pultrusion technological process could be made more effective applying instead of conventional heaters a high frequency electromagnetic energy source characterized by the fast, instantaneous, non-contact and volumetric heating. It is necessary to note that at present time microwave heating [60] is successfully and widely used in different industrial curing processes [55, 74].

The high demand for durable composite products [38] requires the pultrusion of coated profiles with coatings providing specific properties to the composites, such as corrosion resistance in aggressive environments, UV radiation resistence, fire resistance or improved surface properties (brightness, aspect or colour). A primer type coating with bonding-on demand properties could be used for joining of the profile to other materials. At present time the profile coating is executed separately after profile pultrusion and cutting with an expensive and polluting sanding process used for a surface preparation.

1.2. Simulation of pultrusion processes

To provide better understanding of the pultrusion processes, to support the pultrusion tooling design and process control, a lot of numerical simulations have been done in the last thirty years [26, 34, 42]. Most of them are focusing on the analysis of the heat transfer and cure, on the pressure rise in the tapered zone of the die and on problems related to impregnation of reinforcing fibres to obtain a final product characterized by the desired mechanical properties. The effects of the processing parameters, like die temperature, pull speed, post cure temperature and time, filler and fibre type and content, on the mechanical properties of composites produced with a pultrusion have been also intensively investigated [24, 29, 30].

Thermochemical modelling has been developed for the transient and steady state analyses by using the finite difference [12, 27] and finite element methodologies [11, 33, 41, 58] with the control volume and nodal control volume methods. It is necessary to note that the steady state solution is more efficient for a simulation of the pultrusion with constant processing conditions. However, in the case, when the temperature of heaters is controlled by thermocouples or composite material properties are examined as dependent on time or temperature, the transient analysis should be applied. Recently, another numerical approach [23] using computational fluid dynamics model has been applied for the pressure and resin flow analysis at the tapered inlet of the die. The reinforcing fibres have been modelled as an anisotropic porous media with directional permeability in accordance with the Gebart model. As for the impregnation model, the software *ANSYS CFX* has been also used in [23] to solve the porous thermal model employing the finite volume numerical scheme. The porous model examines the pultrusion process as a reactive liquid (resin) flow through a moving porous media (reinforcement) inside a defined rigid boundary (die cavity). In the porous thermal model the degree of cure is treated as an additional scalar variable with transport properties existing only in the fluid phase and varying according to a source term generated by the reaction rate.

It is necessary to note that numerical simulations of the pultrusion processes are carried out by using non-commercial FE codes and general-purpose FE software. In most cases the developed numerical models are firmly connected with the final product and applied technology. So the finite difference and finite element methodologies have been used for a simulation of pultrusion process of the composite profile with C cross-section made of epoxy resin and fiberglass [26]. Three-dimensional thermochemical analysis has been applied for a simulation of pultrusion process of the composite flat plate using transient and steady-state approaches in paper [11]. In paper [23] the pultrusion process of unidirectional graphite/epoxy composite rod with circular cross-section has been analysed applying the finite element methodology (*ABAQUS*) with nodal control volume method and *ANSYS CFX* with finite volume numerical scheme by using continuous and porous models, respectively.

The review of the literature shows that less attention has been paid for the analyses of pultrusion processes with a temperature control [27, 31, 46, 58]. Paper [27] indicates an importance of controlling the processing parameters in producing quality pultruded products by thermostatical control of three heating zones of the die to maintain the prescribed temperatures. Simulating the transient pultruder operation by using the finite difference analysis, heaters have been turned on or off at the end of each time step to compensate for changes of more than 1 °C in the pre-set temperatures in the places where thermostats are located. Heaters power control along the die for a start-up heating process has been executed by three thermocouples in [31]. When the pre-set temperatures have been reached, the start-up heating process ends and simulation of the pultrusion process for the flat plate profile starts right away by the developed computer code. More complicated control of the pultrusion process of I-beam profile has been performed in [58] for the heating system consisting of four electrical heat platens located on the top and bottom surfaces of the die and two electrical strip heaters placed on its both sides. For a time step, the applied heating powers have been turned on or off automatically by the finite element numerical procedure according to the temperatures at the control nodes. Unfortunately, due to a lack of some data in [58], the control algorithm is not clearly described. Recently, the control algorithm for the heaters and duty cycle based on a simple on/off control with a location of the control temperature at the interface between die and profile has been investigated in [46]. By using cyclic variation of the die temperature as a result of the simulated control algorithm, the so-called duty cycle of the typical pultrusion process has been established. Simplified numerical analysis has been performed in *MATLAB* solving the energy equation for a composite by the implicit finite difference method and integrating the reaction term by the fourth order Runge-Kutta method.

Due to the complexity of the multiphysical problem to be solved for a microwave assisted pultrusion process, initially these processes have been analysed experimentally [45, 54, 69]. A brief review of the potential for microwave heating in the pultrusion manufacturing processes of fiber reinforced composites is presented in paper [61]. Recently, due to the rapid development of the finite element software for a solution of multiphysical problems, a computational modelling of the microwave assisted pultrusion processes has started. In paper [25] the finite element model and corresponding analysis have been developed for the microwave assisted pultrusion process of a fiberglass-epoxy cylindrical profile with the diameter of 5 mm pultruded in cylindrical die with the length of 183 mm. (Figure 1.5). Several die external radius and two different sets of material die properties (Table 1.1) have been investigated to obtain an effective manufacturing process. The pull speed was constant and equal to 60 cm/min. The temperature and the degree of cure distributions along the profile centerline are presented in Figure 1.6 and 1.7 respectively. It is important to note that it is not correct to conclude about the effectiveness of the pultrusion process using the degree of cure obtained for the profile centerline in the case of microwave assisted pultrusion. In this case the heating and resin chemical reaction starts from the centerline and the degree of cure inside the profile is greater than on the surface.

Experimental investigation of microwave assisted pultrusion process and corresponding coupled electromagnetic and thermal finite element simulation using *COMSOL Multiphysics* have been carried out in [45]. Scheme of the experimental setup for microwave assisted pultrusion of 9 mm diameter rod made of *24K Torayca* fiber of type *T700S* and resin *EPONOLTM* type *2509* in combination with acid catalyst *EPONOUM 25011B* and the internal release agent *INT-1850HT* is shown in Figure 1.8. Pultrusion die is ceramic tube with inner diameter 9 mm and outer diameter 20 mm. Ceramic has low dielectric losses at the microwave frequency and is used as microwave conductor. Metal base is used for positioning of the ceramic die, waveguide and electromagnetic chokes that avoid microwave leakage (Figure 1.9). Experiment was successful (the resin is fully cured that is confirmed by DSC tests executed after the pultrusion) for pull speed of 15 cm/min and applied microwave energy of 430 W. Simulation model created in *COMSOL Multiphysics* is shown in Figure 1.10. It is necessary to note that no chemical simulation has been performed. It means that only energy and temperature (Figure 1.11) distributions in pultruded profile and die are obtained. Resin reaction (degree of cure) is not evaluated numerically.

Additionally pultrusion processes have been investigated experimentally for various unidirectional composite profiles [53, 57, 65]. In these studies, experimental temperatures have been measured by using thermocouples inserted into the die or moved composite, but the degree of cure has been obtained from the differential scanning calorimetry analysis of samples prepared from the pultruded profiles. It is necessary to note that allocation of thermocouples on the surface of moving composite or inside it is complicated and time consuming procedure. The experimental results have been used in most cases for a validation of the developed numerical algorithms [28, 31, 58]. Recently, the electrical resistivity of resins has been measured with the direct current based dielectric system and used for a calculation of the on-going degree of cure and glass transition temperature in the resin transfer moulding and vacuum infusion processes. Later the same direct current sensing technology has been successfully applied for monitoring the quality of out of the die ultraviolet-cured pultrusion line [73]. In contrast to the resin transfer moulding and vacuum infusion processes, measurement of the resistivity of a composite profile in the pultrusion possess is more complicated since the profile is moving over the sensor and, for this reason, the contact between specimen and electrodes is not ideal.

The reliably or probabilistic analysis provides a probability distribution of the desired properties of the product caused by variations of material properties, resin and fibre-reinforcement content, presence of defects and void formations inside the composite and so on. Effects of the manufacturing process parameters – heating temperatures, pull speed – also are studied in the reliably analysis.

Table 1.1.

Numerical simulation

Simulation	Die external radius	Die material
Simulation 1	Empty cavity	
Simulation 2	10 mm	Unfilled PTFE
Simulation 3	10 mm	Filled PTFE
Simulation 4	15 mm	Unfilled PTFE
Simulation 5	15 mm	Filled PTFE
Simulation 6	20 mm	Unfilled PTFE
Simulation 7	20 mm	Filled PTFE
Simulation 8	41.5 mm	Unfilled PTFE
Simulation 9	41.5 mm	Filled PTFE

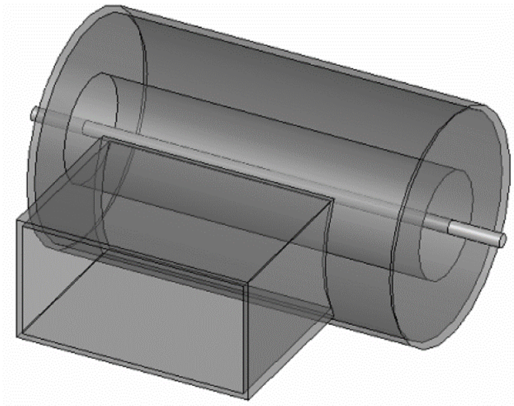

Figure 1.5. Simulation domain [25].

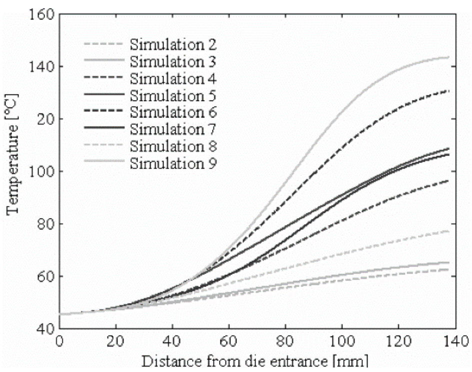

Figure 1.6. Temperature distribution along centerline [25].

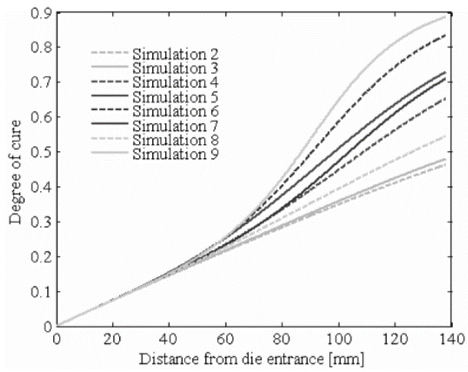

Figure 1.7. Degree of cure distribution along centerline [25].

In [13], a probabilistic analysis has been carried out for a circular rod pultrusion process presented in [56, 72, 76]. The Monte Carlo Simulation (MCS) and Response Surface Method (RSM) have been employed separately in this investigation. The selected random input parameters were: the pull speed, fibre volume content, inlet temperature, all the characteristic material properties and the resin curing kinetic parameters. Coefficients of variation for input parameters have been taken in range 0.01… 0.05. The centerline degree of cure at die exit has been taken as output response. The linear correlation coefficients between the input parameters and output response and corresponding sensitivities are shown in Figure 1.12.

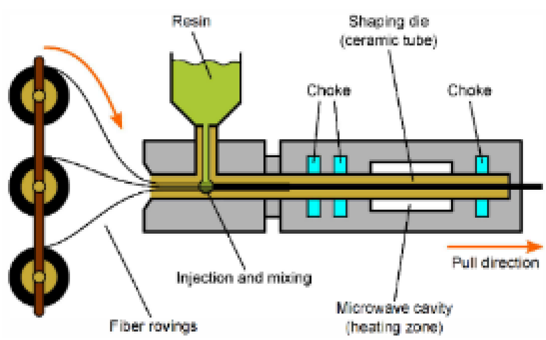

Figure 1.8. Experimental pultrusion setup [45].

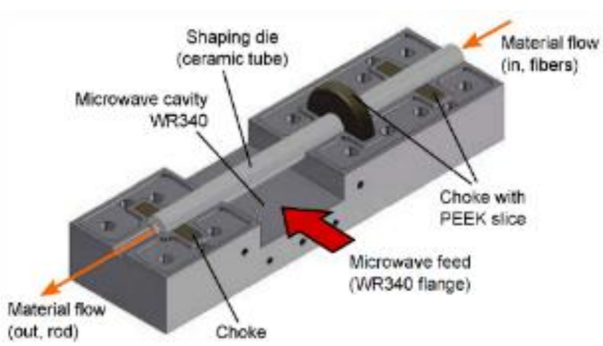

Figure 1.9. CAD model of the fabricated microwave pultrutor [45].

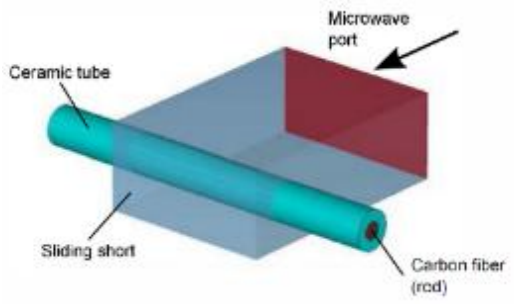

Figure 1.10. Simulation model of the microwave cavity [45].

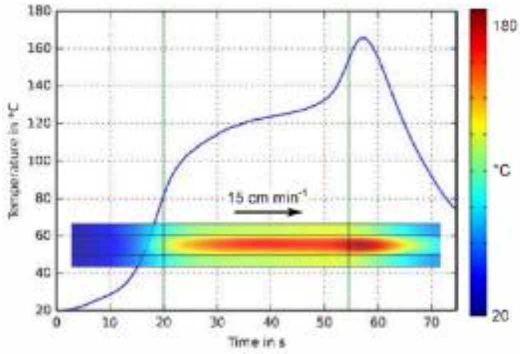

Figure 1.11. Simulated temperature as function of time for a point fixed on the axis of the moving fiber composite rod. The field plot shows the temperature distribution inside the rod for t = 75 s. [45].

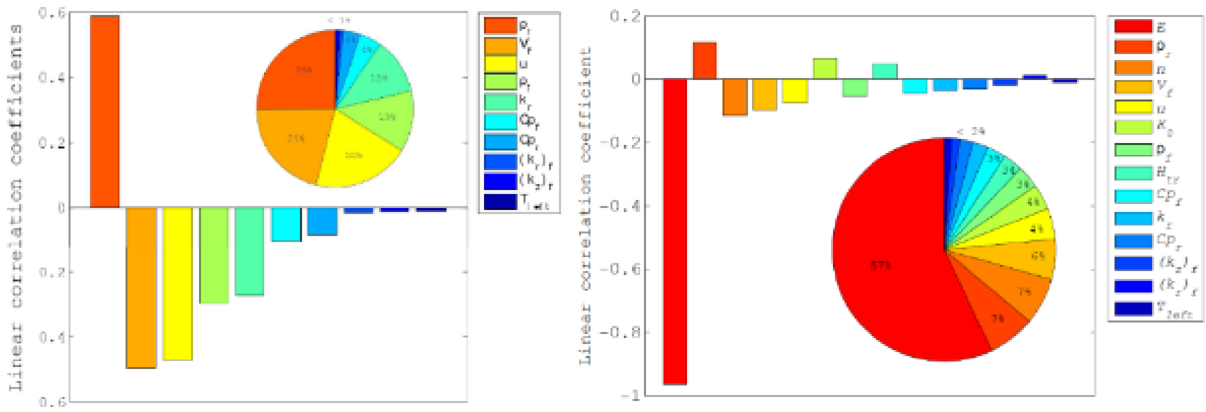

a *b*

Figure 1.12. Linear correlation coefficients (bar plots) and sensitivities (pie charts) obtained by MCM (*a*) and RSM (*b*) [13].

The similar investigation has been performed in [14] for the pultrusion of a flat plate described in [28, 56]. The First-order Reliability Method (FORM) and MCS have been utilized to study the sensitivity of the resin degree of cure at die exit and maximal temperature in the profile to 15 random input parameters (process parameters and material properties).

It has been determined by reliable analyses that process parameters – heating temperature and pull speed – have significant effect on the resin degree of cure and temperature. These output parameters are also very sensitive to the resin activation energy and density, therefore these material properties should be determined with high accuracy.

1.3. Optimisation of pultrusion processes

In order to achieve a better product quality, a high degree of process safety, reduced manufacturing costs and higher production rates, a systematic optimisation procedures are used. Use of numerical process models and solving of optimisation problem avoid expensive and time-consuming experimental approaches for determination of appropriate process parameters.

In [52], a mathematical relationship between the cure quality and the heater temperatures has been developed to find the optimum heater temperatures which gave the highest degree of cure. The Gradient-based Algorithm has been used to minimize the objective function relating the heaters temperature and the uniformity of C-shape profile cure. The optimisation algorithm was numerically stable and worked well for die with 6 heaters (Figure 1.13). The iterative optimisation procedure has been terminated after 11 iteration, because the maximal temperature inside composite reached 240 °C, which was the allowable temperature for the resin. The degree of cure was 0.875 at this iteration, so it has been shown that it is impossible to obtain fully cured profile at used pull speed of 5 mm/s.

An improved optimisation procedure has been developed in [43] for the same problem. Additionally, effects of pull speed and die preheating temperature have been studied. It has been find that the optimal pull speed is 2.3 mm/s that is more than two times lower than initial value of 5 mm/s. The obtained mean degree of cure at the die exit was 0.892 (desired value was 0.9) with a standard deviation of 0.0045 after 20 optimisation iterations.

Finally, the optimisation of heating power control for the same C-shape profile pultrusion die by using the concept of "heater switch-on and -off" upon receiving feedback from a thermocouple mounted on the heater pads has been performed in [44]. It has been identified that the optimisation of the die heating with the heater power control is more accurate and realistic. When this case has been compared with the results of optimisation without heater power control, initial die-heater temperature was significantly lower. It has been found that the degree and uniformity of cure with heater power control approached the desires values more steadily. Also it has been indicated that that the heater power plays an important role in obtaining of a quality product. In case considered in [44] has been showed that heater pads with power of 900 W are not enough to achieve 90 % cure, but by increasing the power to 2000 W, the desired properties could be achieved. Results obtained after each optimisation iteration are shown in Figure 1.14. Obtained optimal algorithm of heaters work is shown in Figure 1.15.

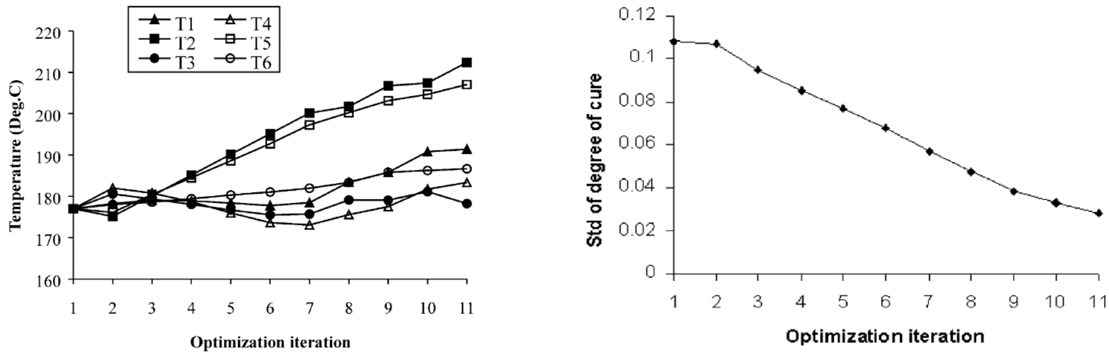

a *b*

Figure 1.13. Results obtained after each optimisation iteration: heater temperature (*a*) and standard deviation of degree of cure (*b*) [52].

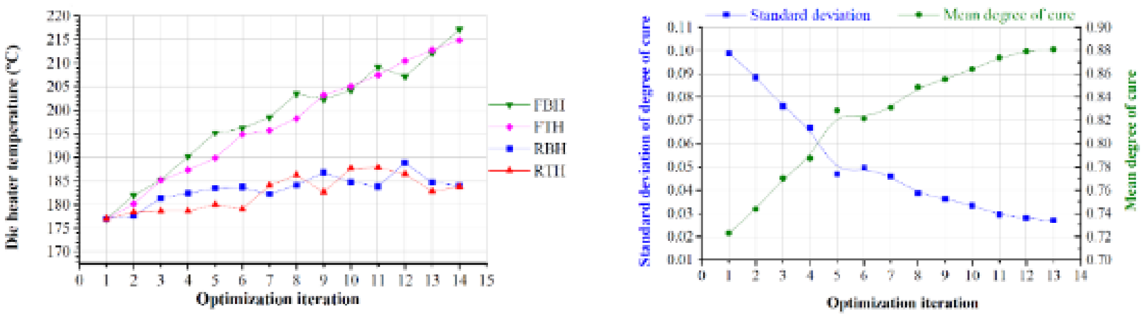

a *b*

Figure 1.14. Results obtained after each optimisation iteration: heater temperature (*a*) and degree of cure and its standard deviation (*b*) [44].

The surrogate methodology which is composed of a statistical learning technique (Kriging) and a constrained optimisation methodology based on this surrogate method have been used in [75] for optimisation of a square profile (25.4 mm × 25.4 mm) pultrusion (Figure 1.16). The single objective function was to maximise the average degree of cure at the die exit. 13 design variables, including not only process parameters (pull speed and heater temperatures), but also geometrical dimensions of die and positions of 3 heaters, have been varied during the optimisation procedure. 15 constraint functions based on the die geometry and process parameters (heater temperatures, maximum part temperature, pull speed) have been introduced to the optimisation procedure. The initial sample set is prepared with 65 design sets and 130 more are added along the optimization procedure. The progress of the optimization is shown in Figure 1.17. The global optimum is found at 177*th* iteration out of 195 iterations. In Figure 1.18, the distance between each iterative solution and the global optimum is also drawn in order to show the progress of the algorithm in the design space rather than only the objective space. The mean degree of cure equal to 0.9971 is achieved for the resin at die exit. The worst value of the degree of cure for the resin at die exit is equal to 1.9969, that means that homogenous field of the degree of cure is obtained at the die exit.

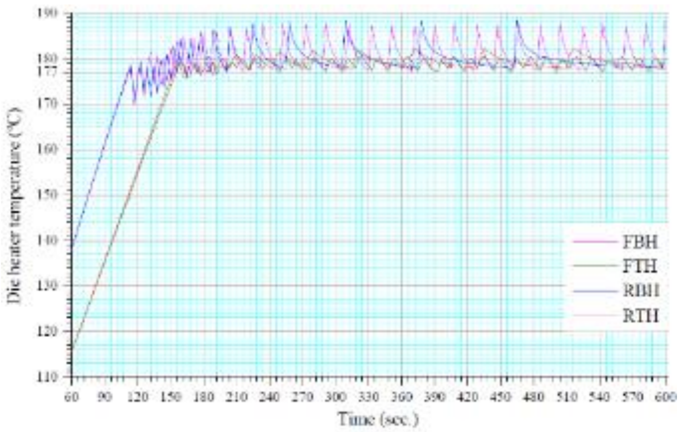

Figure 1.15. Fluctuations in die heater temperature due to “switch-on and –off” power control [44].

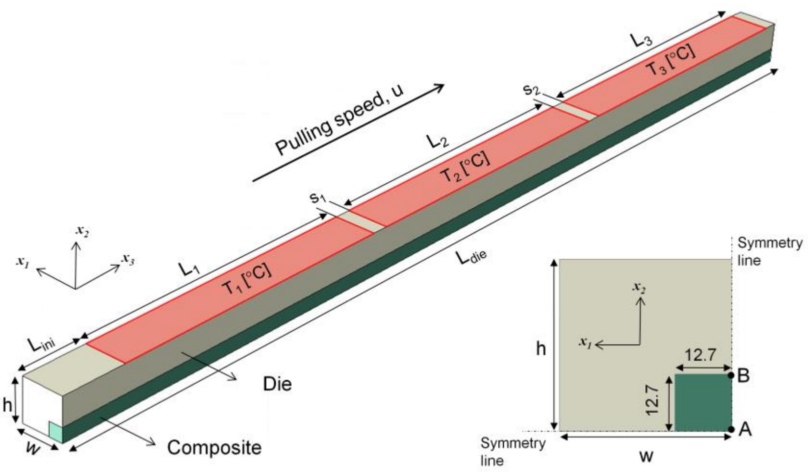

Figure 1.16. Schematic view of the quarter pultrusion domain [75].

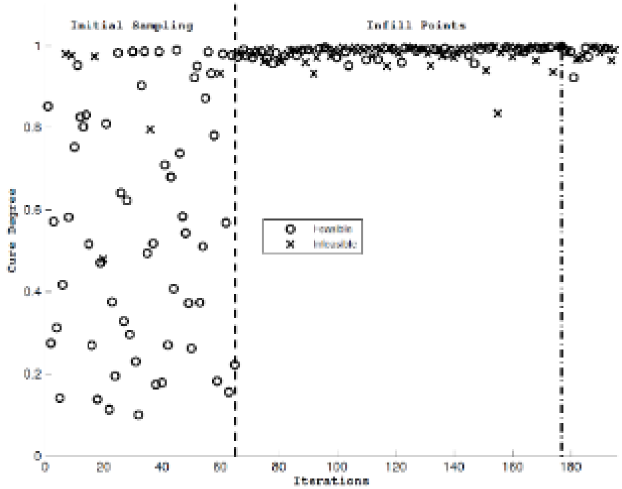

Figure 1.17. Evolution of the norm for the optimisation problem [75].

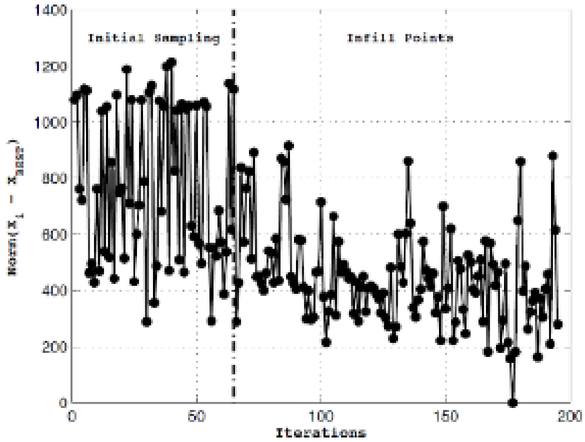

Figure 1.18. Evolution of the norm for the optimisation problem [75].

1.4. Thesis objectives

Conventional process for manufacturing of coated pultruded profiles is time-consuming and labour-intensive (Figure 1.19). Also this process is “dirty” because of VOCs and small particles emission during sanding, painting or spraying.

The development, design and optimisation of advanced pultrusion process is performed in this Thesis. This new manufacturing process allows to obtain coated pultruded profile in one-stage (Figure 1.20). The proposed process has reduced labour and process cost because of the reduced number of manufacturing steps in comparison with conventional process. This process is more ecological, because all “dirty” manufacturing steps are removed.

The resin injection and microwave aided cure, as well as coating application and cure take place in one multifunctional pultrusion die (Figure 1.21). The coating is injected over the composite profile by means of a special chamber in order to obtain the desired thickness of the coating. Cure of the coating over a non-fully cured profile gives extraordinary interaction between coating and profile that is one more benefit of this process.

The main aim of the present Thesis is to develop new methodology for simulation, design and optimisation of the advanced microwave assisted pultrusion processes. This methodology is based on the joint use of different finite element codes, planning of experiments and response surface technique and allows to obtain parameters of the technological process that give the minimal energy consumption for manufacturing of coated pulruded profile.

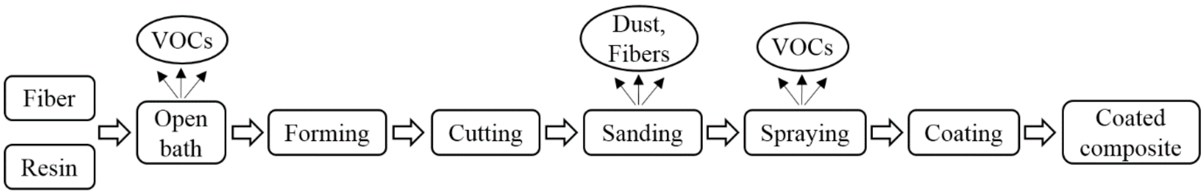

Figure 1.19. Conventional manufacturing of coated pultruded profile.

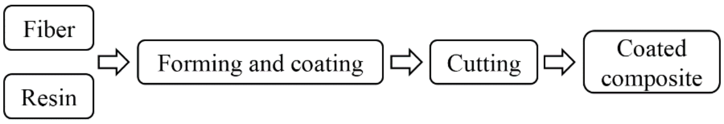

Figure 1.20. Advanced manufacturing of coated pultruded profile.

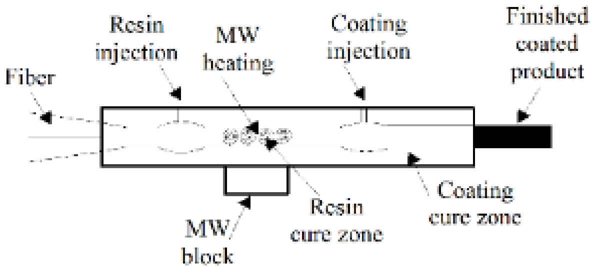

Figure 1.21. Scheme of advanced pultrusion die.

To achieve the Thesis objective the following problems should be solved:

1. Study of scientific literature related to the simulation and experimental investigation of the pultrusion process.
2. Development of reliable holistic numerical procedure for simulation of pultrusion processes.
3. Development of curing kinetic models for resins with high microwave absorption properties.
4. Experimental validation of developed numerical simulation procedures.
5. Development of numerical simulation procedures for microwave assisted pultrusion processes.
6. Design of microwave assisted pultrusion process for a multifunctional pultrusion die.
7. Formulation and solution of the optimisation problem for the advanced microwave assisted pultrusion process.

1.5. Structure of Thesis

The present Thesis consists of eight chapters, which are organized as follows:

Chapter 1 presents general overview on the pultrusion processes, their simulation and optimisation.

Chapter 2 presents general formulation and numerical implementation of the thermochemical analysis of pultrusion processes. Two numerical procedures based on different finite element codes (*ANSYS Mechanical* and *ANSYS CFX*) are developed for a solution of thermochemical problem. The validation of these procedures by experimental and numerical results published in scientific literature is also presented.

Chapter 3 presents development and validation of the methodology for a building of curing kinetic models for thermoset resins with high microwave absorption properties. The developed methodology has been implemented in *Microsoft Excel* tool.

Chapter 4 presents experimental validation of the developed procedures for numerical simulation of pultrusion processes. An influence of different process parameters and die material properties on temperature and degree of cure in composite material is shown. Correction of initial data using experimental and simulation results is performed with the aim to obtain reliable results.

Chapter 5 is devoted to the numerical simulation and study of advances microwave assisted pultrusion process. An influence of capacity of the absorption energy field, application of thermal insulation on the die, preheating of steel die, heating of resin bath and reduction of the steel die length on the parameters of pultrusion process are studied with the purpose to increase its effectiveness.

Chapter 6 is devoted to the design of multifunctional pultrusion die used in the advanced pultrusion process with microwave assisted heating and *in-line* coating technology.

Chapter 7 describes an optimisation methodology, based on the planning of experiments and response surface technique for optimisation of advanced microwave assisted pultrusion process with *in-line* coating technology.

Finally, the research achievements of the present Thesis are summarized in the **Chapter 8**. Recommendations for the future work are also discussed.

2. MODELLING OF CONVENTIONAL PULTRUSION PROCESSES

The statement of thermochemical problem of pultrusion process is described in this Chapter. Two numerical procedures based on different finite element codes are developed for solving of thermochemical problem [17]. The validation of these procedures used experimental and numerical results published in scientific literature is also presented.

2.1. Statement of the thermochemical problem

To study numerically pultrusion processes, the following thermochemical problem consisting of three governing equations should be solved:

$$\begin{cases} \rho c_p \dfrac{\partial T}{\partial t} - \dfrac{\partial}{\partial x}\left(k_x \dfrac{\partial T}{\partial x}\right) - \dfrac{\partial}{\partial y}\left(k_y \dfrac{\partial T}{\partial y}\right) - \dfrac{\partial}{\partial z}\left(k_z \dfrac{\partial T}{\partial z}\right) - q_b = 0 \\ \bar{\rho}\, \bar{c}_p \left(\dfrac{\partial T}{\partial t} + u \dfrac{\partial T}{\partial x}\right) - \dfrac{\partial}{\partial x}\left(\bar{k}_x \dfrac{\partial T}{\partial x}\right) - \dfrac{\partial}{\partial y}\left(\bar{k}_y \dfrac{\partial T}{\partial y}\right) - \dfrac{\partial}{\partial z}\left(\bar{k}_z \dfrac{\partial T}{\partial z}\right) - q = 0 \\ \left(\dfrac{\partial \alpha}{\partial t} + u \dfrac{\partial \alpha}{\partial x}\right) = R_r \end{cases} \tag{2.1}$$

where T is the temperature, °C;

ρ is the density of the tooling material, kg/m^3;

c_p is the specific heat of the tooling material, J/(kg · °C);

k_x, k_y, k_z are the thermal conductivities of the tooling material in x, y, z directions, J/(m · °C · s);

q_b is the rate of energy exchange at the boundary, J/(m^3 · s);

u is the pull speed, m/s;

$\bar{\rho}$ is the lumped density for the composite material, kg/m^3;

$\bar{c}_p$ is the lumped and specific heat for the composite material, J/(kg · °C);

$\bar{k}_x$, $\bar{k}_y$, $\bar{k}_z$ are the lumped thermal conductivities of the composite material in x, y, z directions, J/(m · °C · s);

q is the generative term related to the internal heat generation due to the exothermic resin reaction, J/(m^3 · s);

$\alpha = H(t)/H_{tr}$ is the degree of cure;

$H(t)$ is the amount of heat evolved during the curing up to time t, J/kg;

H_{tr} is the total heat of reaction, J/kg.

It is necessary to note that the first equation in the system presents the energy equation for the tool, second – the energy equation for the composite moving in the pull direction and third – the species equation (transport equation) for the resin.

Heat transfer in the composite occurs as a result of conduction and the generation of heat resulting from the exothermic chemical reaction initiated by the die temperature. The generative term related to the internal heat generation due to the exothermic resin reaction could be written as:

$$q = V_r \rho_r H_{tr} R_r \tag{2.2}$$

where V_r is the resin volume fraction;
ρ_r is the resin density, kg/m^3;
R_r is the rate of resin reaction, 1/s, determined as:

$$R_r(\alpha, T) = \frac{\partial \alpha}{\partial t} = \frac{1}{H_{tr}} \frac{dH(t)}{dt} = K(T) \cdot f(\alpha) \tag{2.3}$$

where $f(\alpha)$ depends on the resin properties and varies with the applied resin reaction model;
$K(T)$ is defined by the Arrhenius relationship:

$$K(T) = K_0 \exp\left(-\frac{E}{RT}\right) \tag{2.4}$$

where $R = 8.314$ is the universal gas constant, (J/(mol · °C);
E is the activation energy, J/mol;
K_0 is the frequency factor, 1/s.

It is necessary to note that coefficients of the Arrhenius relationship: activation energy E and frequency factor K_0 are the physical values and determined by the Kissinger method or *ASTM E 698* standard methodology from the DSC tests. Coefficients of the selected function $f(\alpha)$ could be obtained in a simple way by a fitting of the experimental heat flow curves applying the least squares method.

The reinforcement is saturated with the resin before entering the heated die in pultrusion process. Therefore, it is reasonable to assume that the resin does not flow. Therefore the lumped properties of composite material are evaluated by the rule of mixture:

$$\begin{gathered}
\bar{\rho} = (1 - V_r)\rho_f + V_r \rho_r \\
\bar{c}_p = \frac{(1 - V_r)\rho_f c_{pf} + V_r \rho_r c_{pr}}{\bar{\rho}} \\
\bar{k} = \frac{k_f k_r \bar{\rho}}{(1 - V_r)\rho_f k_r + V_r \rho_r k_f}
\end{gathered} \tag{2.5}$$

where indexes f and r relates to the fibres and resin, respectively.

The above system of three governing equations (Equation (2.1)) could be solved by using the prescribed initial and boundary conditions. It is assumed that at time $t = 0$, for a curing composite the temperature is $T = T^0$ and the degree of cure is $\alpha = \alpha^0$, where index 0 denotes the initial values. The temperature of the composite at the die entrance and everywhere in the composite at the first step of numerical algorithm is prescribed as the pre-heat resin temperature. The value of the degree of curing at the die entrance and everywhere in the composite at the first step of numerical algorithm is taken as zero or very small value depending on the resin curing kinetic model. In some pultrusion processes this value could be much higher in relation to the ambient room temperature which is used also as the boundary conditions for a die to describe the convection effect demonstrating the thermal energy transfer between a pultrusion die and an air surrounding it as a result of a temperature difference. It is important to note that the power flux at the entrance and exit of the composite in the die is specified as zero. The insulated boundary conditions could be applied also to reduce unnecessary heat losses and conserve energy in pultrusion processes.

2.2. Algorithms for a numerical simulation

The developed algorithms simulate the pultrusion phenomenon by solving a set of coupled energy and species equations (Equation (2.1)). The equations are coupled because the exothermic heat release term appears as a heat source term in the energy equation.

2.2.1. Procedure based on *ANSYS Mechanical*

The first procedure has been developed in *ANSYS Mechanical* environment and based on the mixed time integration scheme and nodal control volumes method to solve simultaneously the coupled temperature state and degree of cure by using an iteration technique [1]. A uniform finite element discretization of the pultruded composite profile is applied in the pull direction. The nodal control volumes are constructed based on the finite element mesh as presented in Figure 2.1. The centres of the control volumes coincide with the nodal points of the finite element. In the control volume the distribution of a field variable is assumed constant and its value is defined by the field variable calculated at the representative finite element node.

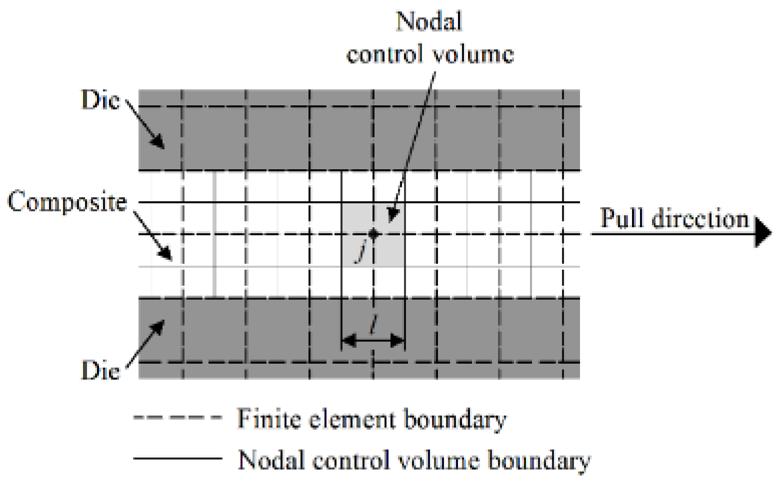

Figure 2.1. Finite element and nodal control volume meshes.

At the beginning it is assumed that the degree of cure has the same value α^0 in each nodal control volume of the composite. In most cases it equals zero. Then the transient thermal finite element analysis is performed to obtain an initial state of temperatures for each element. From the temperature field, the rate of cure for the nodal control volume j at any type step i is calculated outside the finite element software by the user developed program:

$$\frac{\partial \alpha_j^i}{\partial t} = \left[\frac{\Delta \alpha_j^i}{\Delta t} \right] = K_0 \exp\left(-\frac{E}{RT_j^i} \right) f(\alpha_j^{i-1}) \tag{2.6}$$

For $t > 0$, the degree of cure can be obtained continuously by using the following relation:

$$\alpha_j^i = \alpha_j^{i-1} + \left[\frac{\Delta \alpha_j^i}{\Delta t} \right] \Delta t \tag{2.7}$$

where Δt is the time step, s, determined as:

$$\Delta t = \frac{1}{p} \cdot \frac{l}{u} \tag{2.8}$$

where l is the length of nodal control volume in the pull direction, m;
u is the pull speed, m/s;
p is the number of sub-steps. If the procedure of sub-stepping is not applied, $p = 1$.

The exothermic effects of cure reaction are evaluated as the equivalent nodal heat power for a nodal control volume or node j by the following relation:

$$q = V_r \rho_r H_{tr} R_r = V_r \rho_r H_{tr} \left[\frac{\Delta \alpha_j^i}{\Delta t} \right] \tag{2.9}$$

These values will be applied to calculate the temperature field for a new step of iteration. Thereby, a movement of the resin-saturated composite is simulated by shifting the temperature and degree of cure fields after each calculation step. It is necessary to note that at the entrance of the die, the degree of cure remains unchanged and equals to α^0 at any step of iterations. In general, the algorithm can be summarized as a flowchart presented in Figure 2.2.

The main advantage of the procedures based on the mixed time integration scheme and nodal control volumes method is the possibility to take into account all the required parameters of the technological process. Moreover, their accuracy and reliability have been confirmed by numerous experiments. As a disadvantage, the necessity of the user developed programs for a solution of the coupled thermochemical problem could be examined.

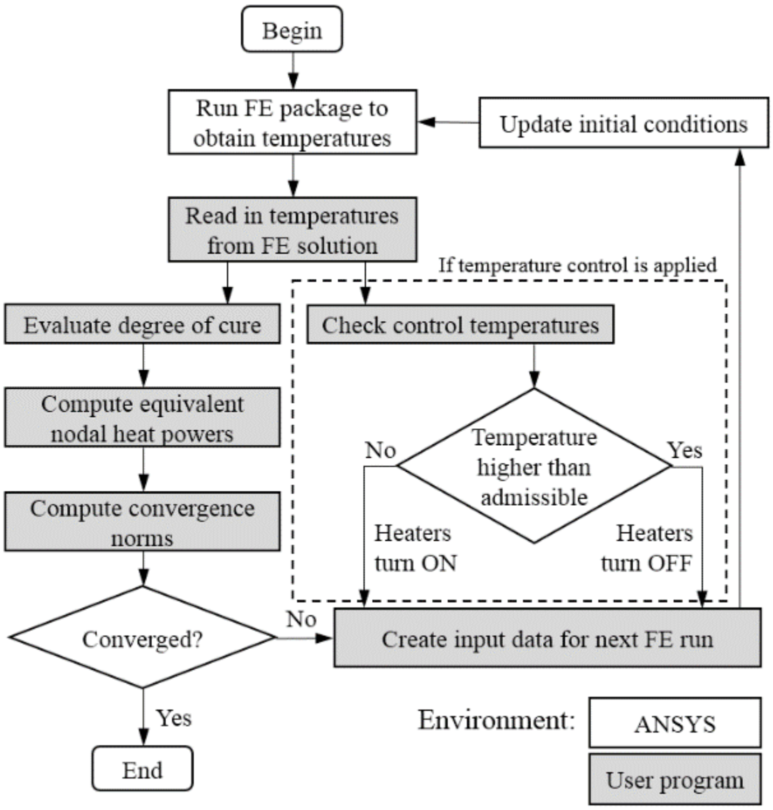

Figure 2.2. Flowchart of the numerical procedure based on *ANSYS Mechanical*.

2.2.2. Procedure based on *ANSYS CFX*

The second procedure has been developed by using *ANSYS CFX* software. It should be noted that the calculation using *ANSYS CFX* are based on more complex system of equations than Equation (2.1), containing the Navier-Stokes equations for the velocity component of the medium, and terms accounting for the turbulence, viscosity and diffusion. However, in the absence of turbulence and velocity gradients all additional terms are equal to zero, and additional equations become identities. In the pultrusion problems composite is modelled as a heterogeneous mixture of two components with the same physical characteristics which represent the reacted and unreacted material [16]. The degree of cure α is modelled as a mass fraction of the reacted substance. During the reaction, a phase transition occurs between two components. The speed of the phase transition can be specified in the dimension of kg/(m^3 · s) and is calculated as follows:

$$massTransfer = \frac{\partial \alpha}{\partial t} \overline{\rho} \tag{2.10}$$

Unfortunately, at this point a latent heat release during the phase transition is not implemented in *ANSYS CFX*, so it is necessary to imitate this effect in the form of additionally distributed heat source in the volume of the composite according to the law corresponding to the speed of the phase transition W/m^3:

$$heatSource = \frac{\partial \alpha}{\partial t} \rho_r H_{tr} V_r \tag{2.11}$$

The model of the phase transition in *ANSYS CFX* has an additional technical limitation - it cannot be used when a contact is modelled between liquid and solid volumes. Therefore, for the problems where a calculation of the temperature field for the surrounding shapes is also required, the composite is modelled in another way - by an introducing of additional scalar parameter equal to α with an intensity of the distributed source of this scalar corresponded to the $heatSource$. In this case the composite can also be modelled not as a uniform flow in the liquid volume but as the solid volume with a predetermined constant speed and including an advection at the input section.

The main advantage of the calculation in *ANSYS CFX* is that regardless of the method of implementation, the calculation changes of the degree of cure are done with a built-in methods coupled with the calculation of thermodynamics and thus the higher speed, accuracy and stability of the design scheme is achieved which is especially important when the degree of cure very fast at some stage of the process. In addition, there is no need for a connection of the calculation time step with a size of the finite element in a pull direction. The main disadvantage of the procedure based on *ANSYS CFX* is the impossibility to use anisotropic thermal conductivities. At the same time, *ANSYS CFX* provides no ability to control and correct calculations, as an entire process of the numerical calculations is done automatically with the build-in methods which can be a disadvantage. Also, due to a separate modelling of the degree of cure and heat release, it is necessary to introduce some limitations to the Equation (2.11) avoiding an excessive heat realize of the unreacted resin. This can be done by limitation of the rate of cure:

$$\frac{\partial \alpha}{\partial t} = \min\left[K(T) \cdot f(\alpha), \frac{1\text{-}\alpha^{i-1}}{\Delta t}\right] \tag{2.12}$$

2.3. Algorithms' numerical validation

The developed procedures have been successfully validated by the temperature and degree of cure fields described in the literature studying the pultrusion of cylindrical rod [56, 72, 76], flat plate [28, 56] and I-beam profiles [58].

2.3.1. Pultrusion of cylindrical rod

The dimensions of the pultruded composite profile and die are presented in Figure 2.3. The materials used for a production of the cylindrical rod are graphite fibres *Hercules AS4-12K* rovings with the fibre volume content of 62.2 % and thermoset epoxy resin *SHELL EPON 9420/9470/537*. Their thermal properties are given in Table 2.1. The rate of resin reaction is described by using the *n*-th order curing kinetic model:

$$R_r(\alpha, T) = \frac{\partial \alpha}{\partial t} = K_0 \exp\left(-\frac{E}{RT}\right)(1-\alpha)^n \tag{2.13}$$

with the parameters presented in Table 2.2.

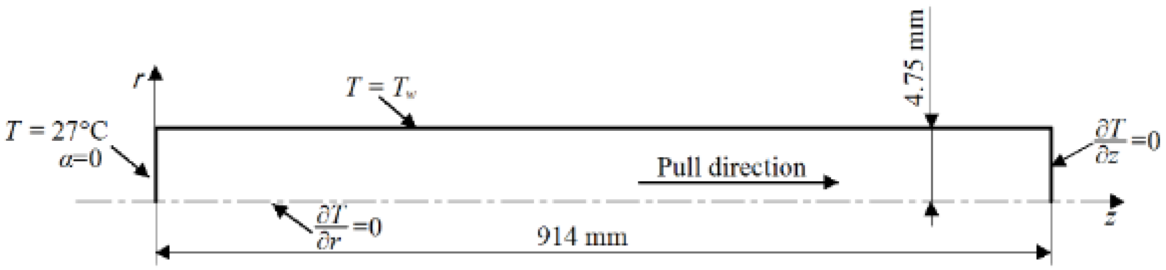

Figure 2.3. Simplified model of the cylindrical rod pultrusion.

Table 2.1.

Thermal properties of materials

	ρ, kg/m^3	c_p, J/(kg · °C)	k_z, W/(m · °C)	k_r, W/(m · °C)
Epoxy resin	1260	1255	0.2	0.2
Graphite fibers	1790	712	66.0	11.6
Lumped properties (V_r =0.378)	1589.7	874.7	0.66284	0.64167

Table 2.2.

Kinetic parameters of the resin

H_{tr}, J/kg	K_0, s^{-1}	E, J/mol	n
323 700	191 400	60 500	1.69

Table 2.3.

Temperatures distribution on the die-composite interface

z, cm	0	6.0	12.4	18.8	25.2	31.2	37.6	43.6
T_w, °C	45	51	62	92	139	175	188	190
z, cm	50.0	56.0	62.4	68.8	75.2	81.2	87.6	91.6
T_w, °C	189	188	187	189	187	179	172	170

The pull speed is 30 cm/min. The die wall temperatures have been plotted in [76]. Then they have been treated and presented in a tabular form in [56] for a number of points measured from the graph in paper [76]. In the present analyses for an application of thermal boundary conditions for a larger number of points than presented in [56], the temperature of die wall between two adjacent points in Table 2.3 has been linearly approximated. Initial conditions are applied at time $t = 0$ when all nodal points have the ambient room temperature of 27 °C and zero degree of cure. The temperature gradient at the exit end of the composite is specified as zero $\partial T/\partial z = 0$ to separate the modelling domain from the rest of the composite. The symmetry boundary conditions $\partial T/\partial r = 0$ are applied to decrease the dimension of the finite element problem.

The formulated pultrusion problem has been simulated as steady-state problem in [72, 76] and solved by using the finite difference approach with a fixed control volumes [76], and approach based on the *ABAQUS* finite element code used for a solution of heat-transfer sub-model and numerical approximation of curing kinetic [72]. The finite element procedure based on control volumes has been applied for a solution of the same problem in transient formulation in paper [56].

The finite element model for a simulation of the rod pultrusion has been created in *ANSYS Mechanical* by using 2-D thermal solid finite element *Plane 55*. The element has four nodes with a single degree of freedom, temperature, at each node and the orthotropic material properties. The finite element mesh is regular and has 229 elements in pull direction and 3 elements in radial direction. The time step defined by Equation (2.8) is 0.8 s. During this time the composite travels in the pull direction on the distance equal to the dimension of one element (4 mm). It is necessary to note that iterations (sub-steps) are not performed in the finite element analysis.

Another finite element model for a simulation of the rod pultrusion has been created in *ANSYS CFX* by using unstructured tetrahedral mesh. The tetra-element has four nodes and several degrees of freedom based on the used model. In the present case there are three velocity components, pressure, temperature and volume ratio of components. The pressure and velocity components are computed independently from the temperature and volume ratio, and correspond to a trivial solution for the uniform flow. The finite element mesh is irregular and has 110 893 elements and 23 956 nodes. The characteristic size of elements is 1.5 mm. Due to *ANSYS CFX* software limitation, an isotropic thermal conductivity of the composite material had to be considered with the average value (Table 2.1) having been taken as $\bar{k} = 0.652255\ \text{W/(m} \cdot {}^\circ\text{C)}$.

The predicted temperature and degree of cure distribution at centreline agree well with the published results (Figures 2.4-2.5). The slight difference could be explained by a different time integration schemes applied in the finite element modelling, ambient room temperature which differs from the cited in papers [56, 72, 76] and different finite element software used for a simulation. Nevertheless, the numerical procedure based on *ANSYS CFX* predicts the same degree of cure and temperature at the exit end of the die like it is described in papers [56, 76]. At the same time the results obtained with *ANSYS Mechanical* is quit closer to the degree of cure and temperatures obtained by the algorithm developed with *ABAQUS* and presented in paper [72].

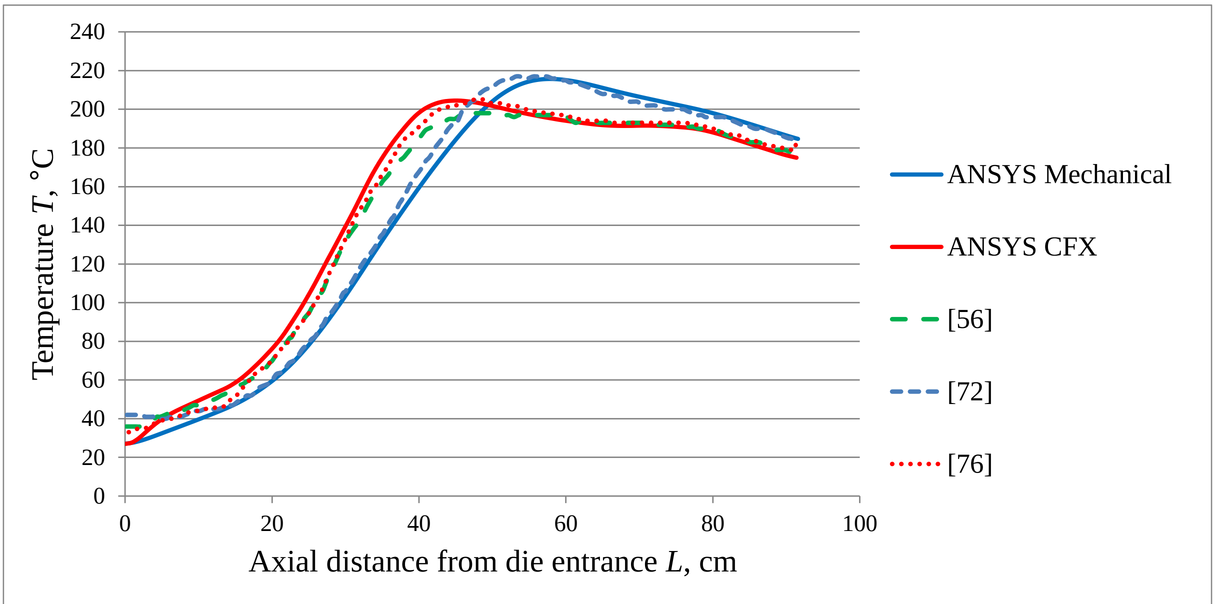

Figure 2.4. Temperature distribution at the centreline.

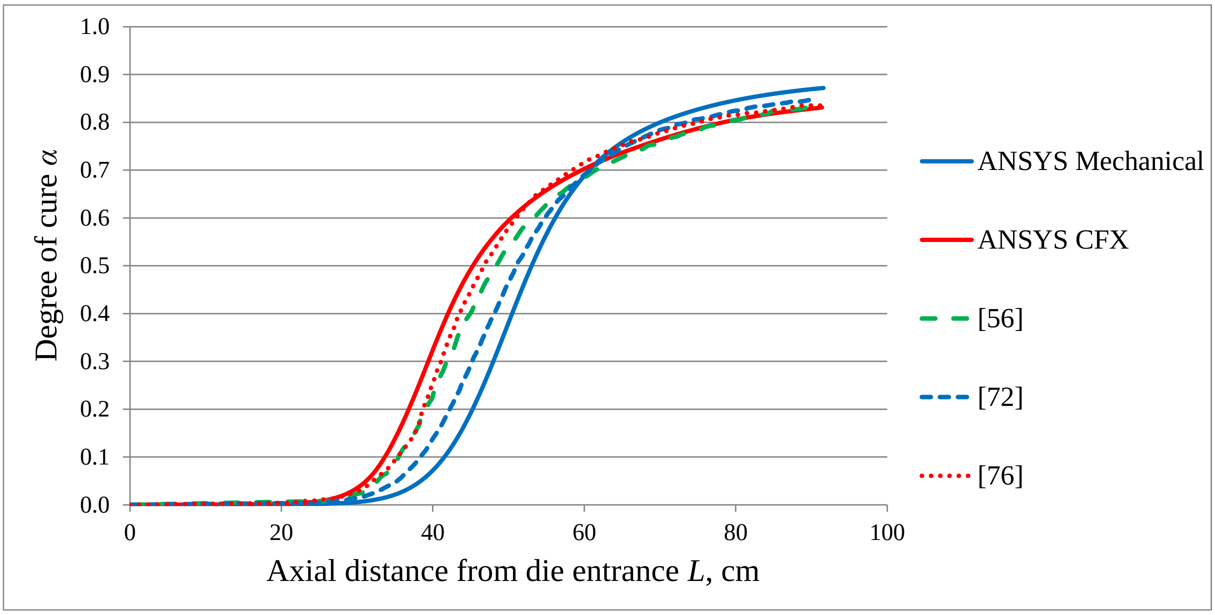

Figure 2.5. Degree of cure distribution at the centreline.

2.3.2. Pultrusion of flat plate

The dimensions of the pultruded composite profile and die, as well as the locations and dimensions of the heating zones and cooling holes are presented in Figure 2.6. The materials used for a production of the flat plate are glass fibres *PPG Industries 2001* with the fibre volume content of 63.9 % and thermoset epoxy resin *SHELL EPON 9420*. Their thermal properties are given in Table 2.4. The rate of resin reaction is described by using the *n*-th order curing kinetic model (Equation (2.13)) with the parameters presented in Table 2.5.

The pull speed is 20 cm/min. The heaters are simulated as zones with a constant temperature as presented in Figure 2.6. The exterior surfaces of the die, except those under the heaters, are assumed to be exposed to the air and hence are simulated as convective boundaries with a convective heat transfer coefficient of 10 W/m^2 · °C. The ambient room temperature is 20 °C. To prevent premature resin gelation at the die entrance, the water cooling is applied. Each water channel is located at the distance of 60 mm from the beginning of the die and in the distance of 6.35 mm from the top and bottom surfaces of the die (Figure 2.6). Their cross-section dimensions are 100 mm × 12.7 mm. The cooling water temperature is taken from the papers [28, 56] and equals to 50 °C. Initial conditions are applied at time $t=0$ when all nodal points of composite have the preheat resin temperature of 30 °C and zero degree of cure. The temperature gradient at the exit end of the composite is specified as zero $\partial T/\partial z = 0$ to separate the modelling domain from the rest of the composite.

Table 2.4.

Thermal properties of materials

	ρ, kg/m^3	c_p, J/(kg · °C)	k_z, W/(m · °C)	$k_x = k_y$, W/(m · °C)
Epoxy resin	1260	1255	0.21	0.21
Glass fibers	2560	670	11.4	1.04
Lumped properties (V_r=0.361)	2090.7	797.27	0.90526	0.55917
Steel (die)	7860	486	40	40

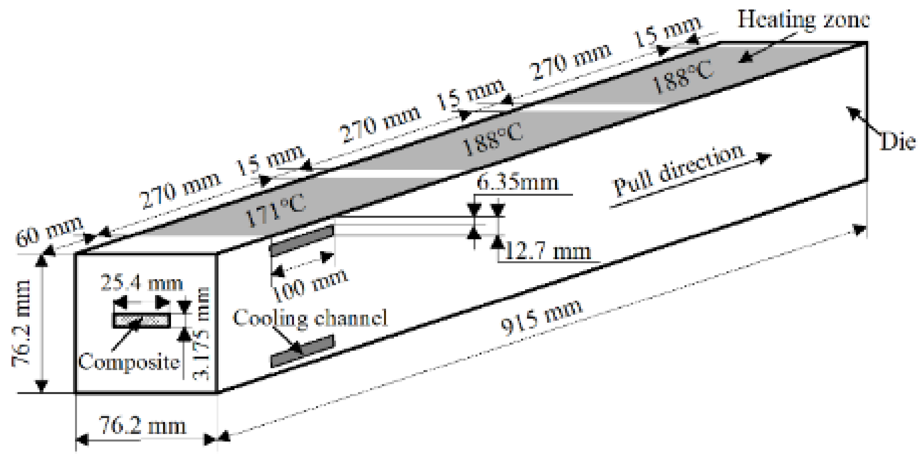

Figure 2.6. Simplified model of the flat plate pultrusion.

Table 2.5.

Kinetic parameters of the resin

H_{tr}, J/kg	K_0, s^{-1}	E, J/mol	n
324 000	192 000	60 000	1.69

The formulated pultrusion problem has been simulated as transient in [56] and solved by using the developed finite element procedure based on control volumes and finite difference grids. The same transient heat conduction and chemical reaction problem has been solved in paper [28] by using the finite difference technique based on control volumes.

The finite element model for a simulation of the flat plate pultrusion has been created in *ANSYS Mechanical* by using 3-D thermal solid finite element *Solid 70*. The element has eight nodes with a single degree of freedom, temperature, at each node and the orthotropic material properties. Taking into account symmetry of the examined problem, only a quarter of the die is modelled. The finite element mesh is presented in Figure 2.7*a*. It is regular in pull direction and has there 61 elements. The total number of finite elements is 2684 and it consists of 183 elements used for the composite modelling and 2501 elements used for the die. The time step defined by Equation (2.8) is 4.5 s. During this time the composite travels in the pull direction on the distance equals to the dimension of one element (15 mm). It is necessary to note that iterations (sub-steps) are not performed in the finite element analysis.

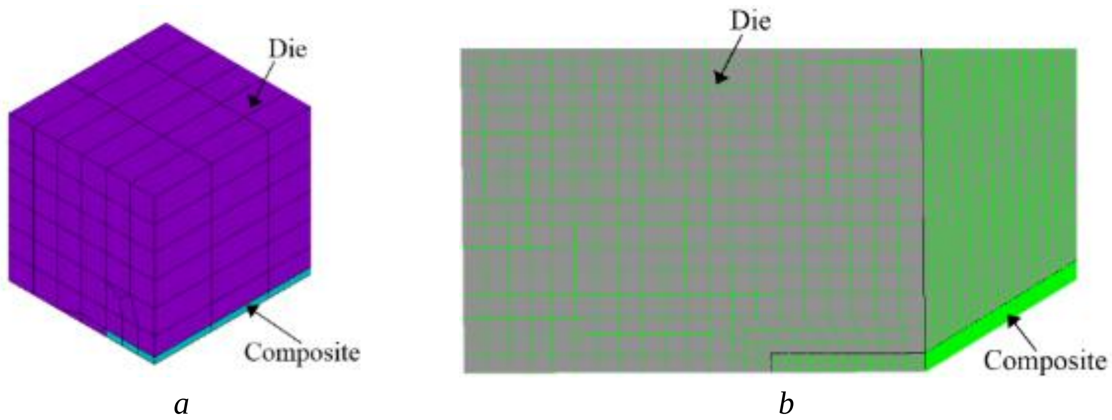

Figure 2.7. Finite element mesh used for a simulation of the flat plate pultrusion: in *ANSYS Mechanical* (*a*) and in *ANSYS CFX* (*b*).

Another finite element model for a simulation of the flat plate pultrusion has been created in *ANSYS CFX* by using two structured hexahedral meshes (Figure 2.7*b*): one defined for the composite and another - for the die. The hexa-element has eight nodes and several degrees of freedom based on the used model. The composite-mesh finite elements have three velocity components, pressure, temperature and volume ratio of components. The pressure and velocity components for the composite mesh are computed independently from the temperature and volume ratio, and correspond to a trivial solution for the uniform flow. The die-mesh finite elements have a single degree of freedom which is the temperature. Taking into account symmetry of the examined problem, only a quarter of the die and composite is modelled. Both finite element meshes are regular in pull direction. The composite mesh has 190 320 elements and 247 185 nodes. The characteristic size of elements is 0.5 mm. The die mesh has 202 540 elements and 225 108 nodes. The characteristic size of elements is 2 mm. An average value of the lumped thermal conductivities given in Table 2.4: $\bar{k} = 0.732215$ W/(m · °C) has been used for a description of the isotropic thermal conductivity of composite material.

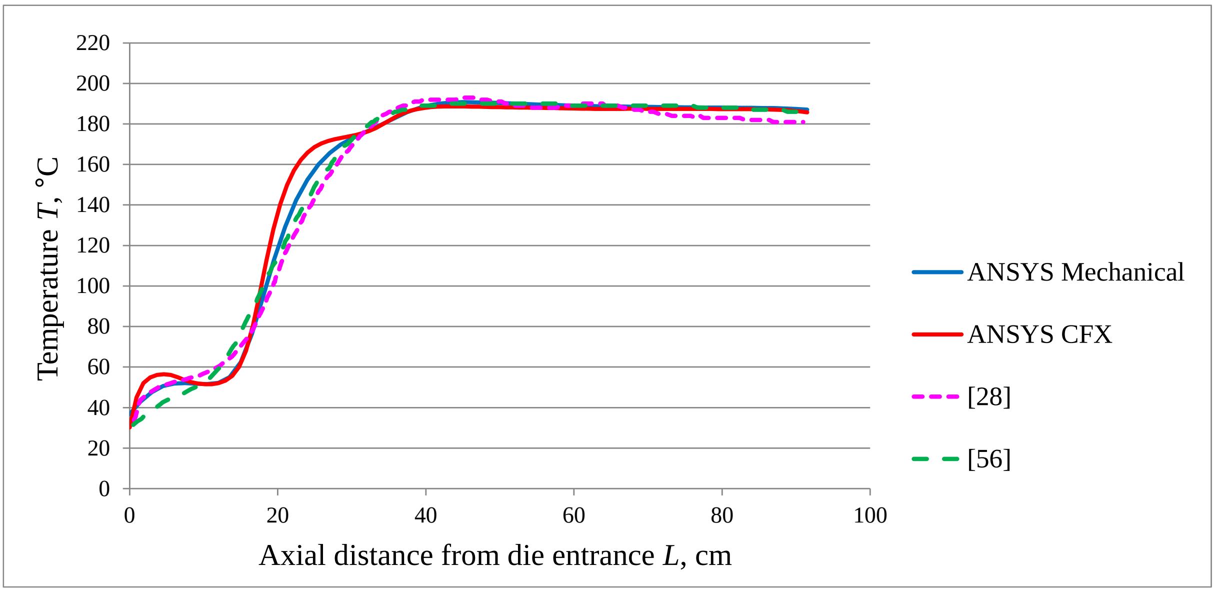

Figure 2.8. Temperature distribution at the centreline.

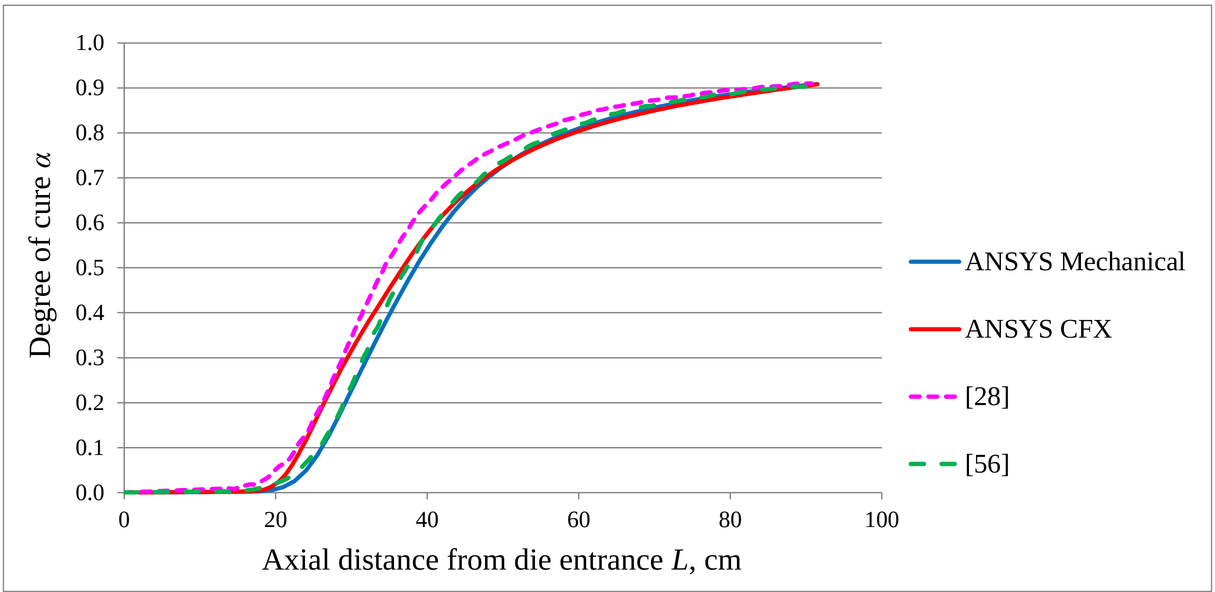

Figure 2.9. Degree of cure distribution at the centreline.

The predicted temperature and degree of cure distribution at centreline agree well with the published results (Figures 2.8 and 2.9). The slight difference could be explained by a different time integration schemes applied in the finite element modelling and different finite element software used for a simulation. The larger difference is observed in the temperature predictions near the die entrance. This is due to the fact that the dimensions and locations of the heaters and cooling channels differs a little bit from the cited in papers [28, 56]. Finally, it is important to note that the degree of cure predicted by all the procedures in the die exit is very close.

2.3.3. Pultrusion of I-beam

The present example has been chosen to demonstrate an application of the developed numerical procedures for a simulation of the pultrusion process with the temperature control. The corresponding scheme of the pultrusion set-up is given in Figure 2.10. The dimensions of the pultruded composite profile and die, as well as the locations and dimensions of the heat platens, strip heaters and cooling pipes are presented Figures 2.11 and 2.12. An additional length of 285 mm of the I-beam is arranged at the die exit to extend the thermochemical analysis to the post-die region (Figure 2.12*a*). The materials used for a production of the I-beam are glass fibres with the fibre volume content of 45 % and vinyl ester resin *VE3*. Their thermal properties are given in Table 2.6. The rate of resin reaction is described by using the Prout-Tompkins curing kinetic model:

$$R_r(\alpha,T)=\frac{\partial\alpha}{\partial t}=K_0\exp\left(-\frac{E}{RT}\right)\alpha^m\left(\alpha_{\max}-\alpha\right)^n,\ m+n=2 \tag{2.14}$$

with the parameters presented in
Table 2.7.

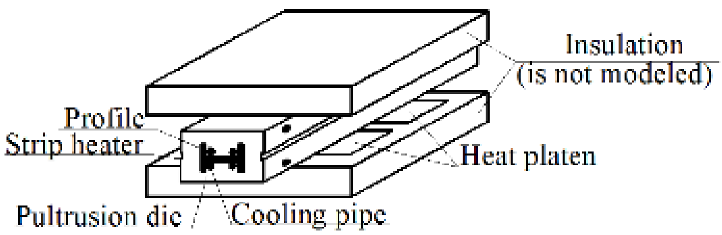

Figure 2.10. Scheme of the pultrusion set-up.

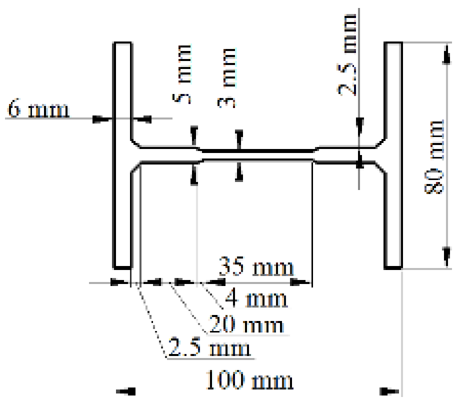

Figure 2.11. Cross-section of the I-beam.

Table 2.6.

Thermal properties of materials

	ρ, kg/m^3	c_p, J/(kg · °C)	k_z, W/(m · °C)	$k_x = k_y$, W/(m · °C)
Vinyl ester	1100	1640	0.169	0.169
Glass fibers	2560	670	11.4	1.04
Lumped properties (V_r =0.55)	1757	1004	0.4773	0.3748
Steel (die)	7860	486	51	51
Aluminium (heat platens)	2700	896	180	180

Table 2.7.

Kinetic parameters of the resin

H_{tr}, J/kg	K_0, s^{-1}	E, J/mol	n	m	$\alpha_{\max}$
398 440	186 958 305	71 688	1.2853	0.7147	0.97

The pull speed is 30 cm/min. Heating is provided by four electrical heat platens placed on the top and bottom surfaces with the heater's power of 1600 W and two electrical strip heaters placed on the both die's sides with the heater's power of 1500 W (Figure 2.10). The heat platens are insulated excepting the contacting surfaces with the die. The exterior surfaces of the die, except those under the heaters, and the I-beam are assumed to be exposed to the air and hence are simulated as convective boundaries with a convective heat transfer coefficient of 10 W/(m^2 · °C). The ambient room temperature is 20 °C. The die is cooled at the distance of 100 mm from the die entrance by water with the temperature of 20 °C to prevent an excessive curing at the die entrance. Initial conditions are applied at time $t = 0$ when all nodal points of composite have the preheat resin temperature of 20 °C and zero degree of cure.

Unfortunately the temperature control points - location of thermocouples and algorithms of the heaters work are not properly formulated and described in paper [58]. For this reason the control temperature of 123 °C for the second and strip heaters is taken on the line C. In the control algorithm the first heat platen works permanently but the second heat platen and strip heaters are switched on if the maximal temperature on the line C is not higher than 123 °C in any point and otherwise they are switched off.

The finite element model for a simulation of the I-beam pultrusion has been created in *ANSYS Mechanical* by using 3-D thermal solid finite element *Solid 70*. The element has eight nodes with a single degree of freedom - temperature at each node and the orthotropic material properties. Taking into account symmetry of the examined problem, only a quarter of the die is modelled. The insulation materials surrounding the heat platens are not included into the finite element model but the surfaces of the platens, excepting those that contact with the die, are assumed as fully insulated. The strip heaters located on both sides of the die are simulated as surface powers directly applied on the surface of the die. The finite element mesh is presented in Figure 2.13*a*. It is regular in pull direction and has 87 elements on the beam. The total number of finite elements is 34 329 and it consists of 6873 elements used for the composite modelling, 25 296 elements used for the die and 2160 elements used for the heat platens. The time step defined by Equation (2.8) is 3 s. During this time the composite travels in the pull direction on the distance equals to the dimension of one element (15 mm). It is necessary to note that iterations (sub-steps) are not performed in the finite element analysis.

Another finite element model for a simulation of the I-beam pultrusion has been created in *ANSYS CFX* by using one structured hexahedral mesh for a composite and three unstructured tetrahedral meshes, one for a die and two for heaters (Figure 2.13*b*). The tetra-element has four nodes and single degree of freedom – temperature. The hexa-element has eight nodes and several degrees of freedom based on the used model. In the present case there are three velocity components, pressure, temperature and extra scalar parameter equals to α. The pressure and velocity components are computed independently from the temperature and scalar parameter, and correspond to a trivial solution for the uniform flow. Taking into account symmetry of the examined problem, only a quarter of the die and composite is modelled (Figure 2.13*b*). The finite element meshes for the die and heaters are irregular. The die mesh has 215 578 finite elements and 40 866 nodes. 40 707 finite elements and 8141 nodes have been used for a modelling of the first heater, and 40 826 finite elements and 8177 nodes for the second. The characteristic size of elements is 7.3 mm for the die and 10 mm for the heaters. The composite mesh is regular in pull direction and has 30 290 finite elements and 46 332 nodes. The characteristic size of elements is 4 mm for a thick plate of composite and 1 mm for a thin plate. An average value of the lumped thermal conductivities given in Table 2.6: $\bar{k} = 0.42605$ W/(m · °C) has been used for a description of the isotropic thermal conductivity of composite material. The transient analysis is applied for a simulation of the pultrusion process.

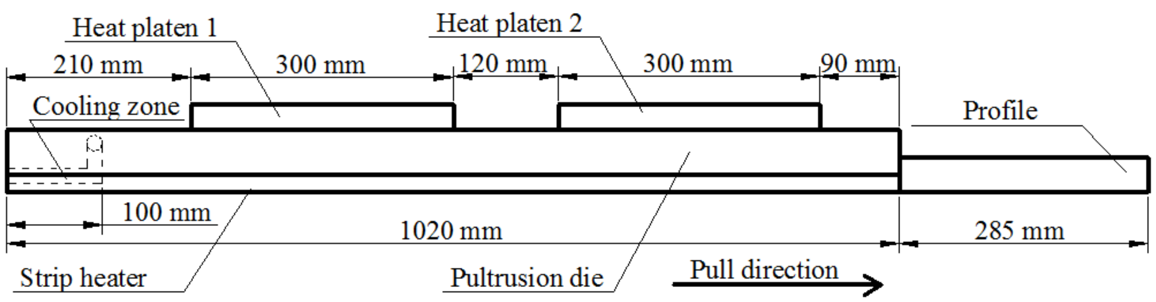

a

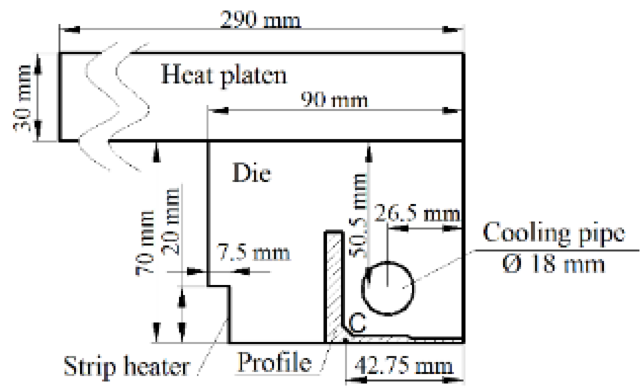

b

Figure 2.12. Section of the pultrusion die: in the longitudinal direction (*a*) and in the transverse direction (*b*).

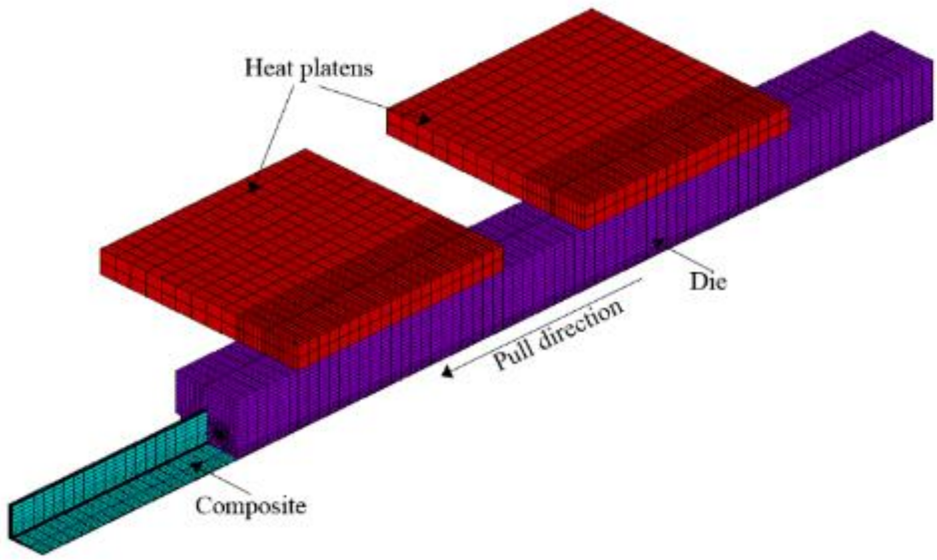

a

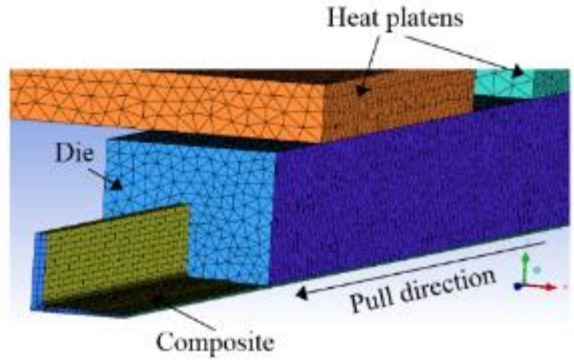

b

Figure 2.13. Finite element mesh used for a simulation of the I-beam pultrusion: in *ANSYS Mechanical* (*a*) and in *ANSYS CFX* (*b*).

The temperature and degree of cure distribution in the pull direction have been investigated at the line C (Figures 2.14 and 2.15). The figures show that both investigated parameters are predicted well by using the developed numerical procedures based on *ANSYS Mechanical* and *ANSYS CFX*. Small difference could be explained by a lack of data in paper [58] necessary for a development of the control algorithms. Moreover, the difference in the finite element models exists. In paper [58] the interface between the part and die is modelled as a thermal contact surface. This interface is absent in the developed finite element model due to an absence of the value describing the thermal conductance of the contact surface. Besides that in paper [58] the convergence study of the finite element solution is not presented and coarser finite element mesh is used than built in the present simulations.

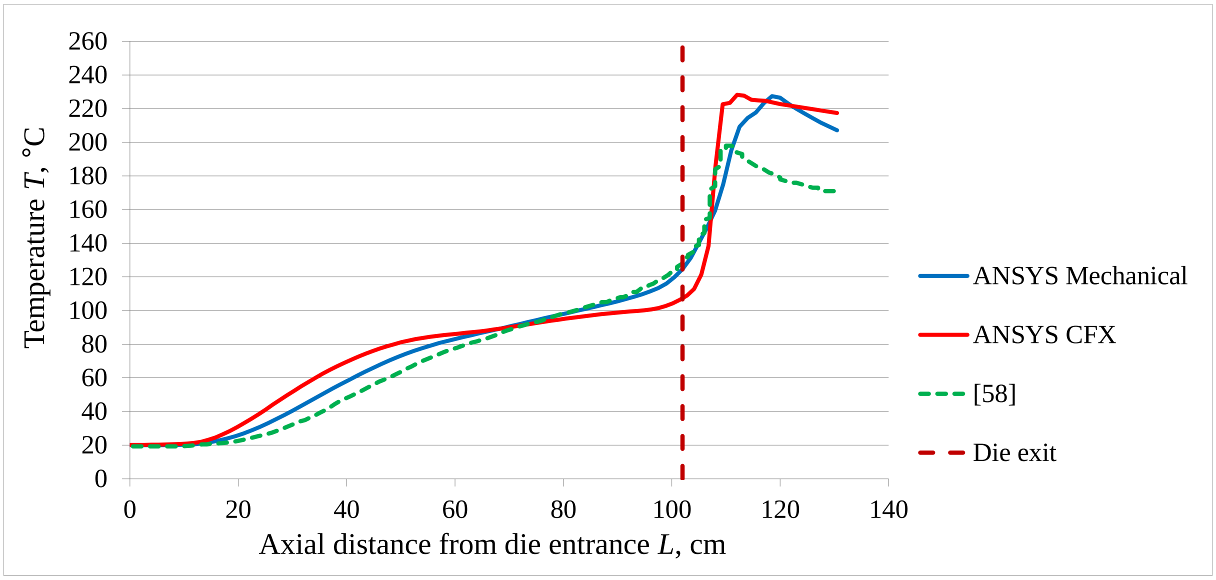

Figure 2.14. Temperature distribution at the line C.

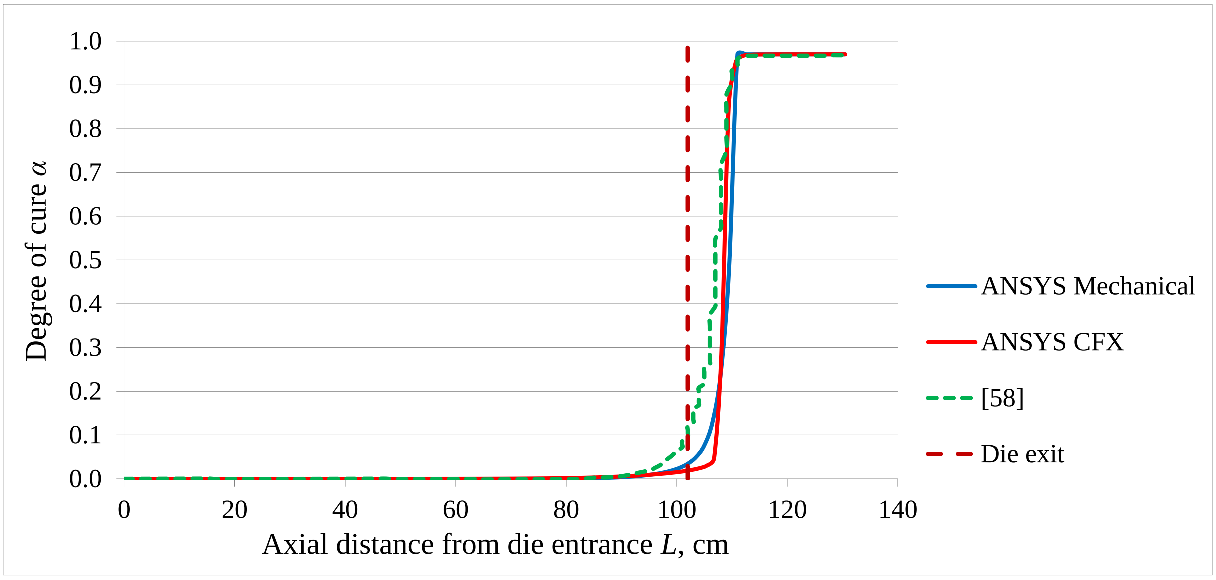

Figure 2.15. Degree of cure distribution at the line C.

3. CURING KINETIC MODELLING

For a simulation of the pultrusion process, the curing kinetic model for the matrix material should be developed. The resin curing process is an exothermic reaction. Heat generation depends on the resin absolute temperature and the degree of cure, which can be measured by a DSC (Differential Scanning Calorimetry) apparatus. There are two types of DSC test: dynamic and isothermal. In the isothermal DSC, the resin is kept in a constant temperature until the curing process completes. In the dynamic DSC, resin is heated with a constant rate (1… 15 °C/min) [51]. In the pultrusion process, except near the wall of the die region, resin temperature rises almost in the constant rate [3, 68]. So, in the present work the dynamic DSC test method has been applied to obtain the heat generation of the resin, which has been used for a building of the curing kinetic model. The *Microsoft Excel* engineering tool for a characterisation of the parameters of curing kinetic models has been developed.

In kinetic analysis, it is generally assumed that the rate of resin reaction can be described by Equation (2.3) [2] consisting of two separable functions, the Arrhenius relationship $K(T)$ (Equation (2.4)) and the reaction function $f(\alpha)$, depending on the resin properties and varying with the applied resin reaction model. For the thermoset resins, traditional forms of the reaction function are

$$f(\alpha) = (1-\alpha) \text{ - first order kinetic model,} \tag{3.1}$$

$$f(\alpha) = (1-\alpha)^n \text{ - } n\text{-th order kinetic model,} \tag{3.2}$$

$$f(\alpha) = (1-\alpha)^n (1+K_2\alpha) \text{ - } n\text{-th order kinetic model with autocatalysis,} \tag{3.3}$$

$$f(\alpha) = \alpha^m (1-\alpha)^n,\ m+n=2 \text{ - Prout-Tompkins autocatalytic model,} \tag{3.4}$$

where m, n and K_i are empirical reaction constants.

In some cases two or even more sets of equations are used to describe the reaction. As a modified approximation for the rate of curing of thermoset resins, Kamal-Sourour autocatalytic model is more widely used:

$$\frac{\partial \alpha}{\partial t} = \left(K_1 \exp\left(-\frac{E_1}{RT}\right) + K_2 \exp\left(-\frac{E_2}{RT}\right) \cdot \alpha^m \right) \cdot (1-\alpha)^n \tag{3.5}$$

It is necessary to note that other models could be used also for an approximation of the thermoset resin curing kinetic.

3.1. Coefficients of Arrhenius relationship

Coefficients of the Arrhenius relationship, activation energy E and frequency factor K_0, are the physical values and they could be determined by the Kissinger method [48] or *ASTM E 698* standard methodology [6] from the DSC dynamic tests. For a proper accuracy at least 3 DSC tests at different heating rates (usually 1… 10 °C/min) are required.

In the case of Kissinger method, the following equation is used:

$$\ln\left(\frac{\beta}{T_p^2}\right) = \ln\left(\frac{K_0 R}{E}\right) - \frac{E}{RT_p} \tag{3.6}$$

where β is the heating rate, °C/s;

T_p is the peak temperature, °C.

By plotting $\ln(\beta / T_p^2)$ versus $1/T_p$, the values of activation energy E and frequency factor K_0 can be estimated by calculating the slope of the linear fit a_s and the *y*-intercept b_{int}, as shown in Figure 3.1. In this case the value of activation energy is determined as:

$$E = -a_s R \tag{3.7}$$

and the value of frequency factor is determined as:

$$K_0 = \frac{Ee^{b_{\text{int}}}}{R} \tag{3.8}$$

In the case of application of *ASTM E 698* standard methodology, the plot of $\lg(\beta)$ versus $1/T_p$ (Figure 3.2) is examined. Now the value of activation energy is determined as:

$$E = -2.19 a_s R \tag{3.9}$$

and the value of frequency factor is determined as:

$$K_0 = \beta \frac{Ee^{\frac{E}{RT_p}}}{RT_p^2} \tag{3.10}$$

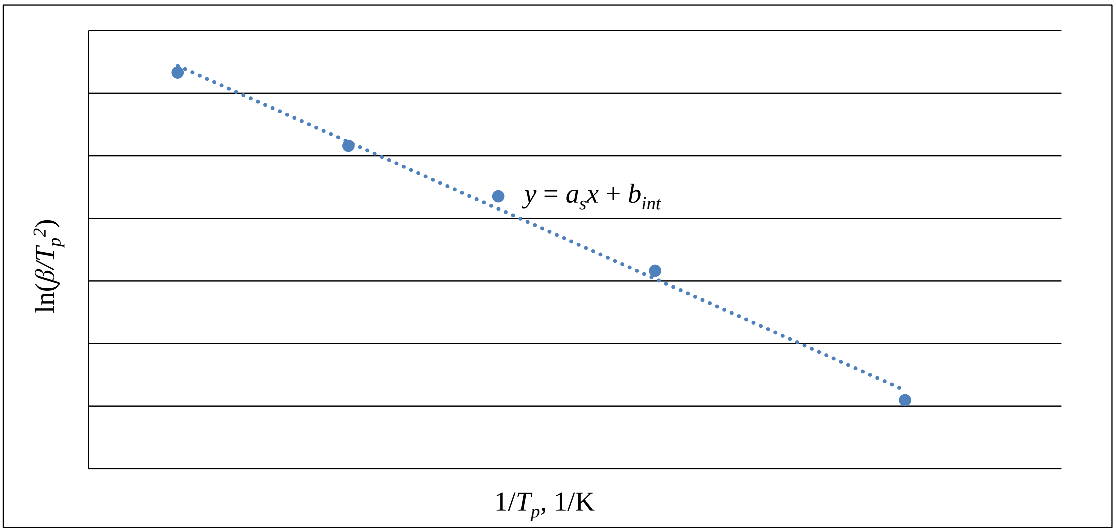

Figure 3.1. Kissinger plot.

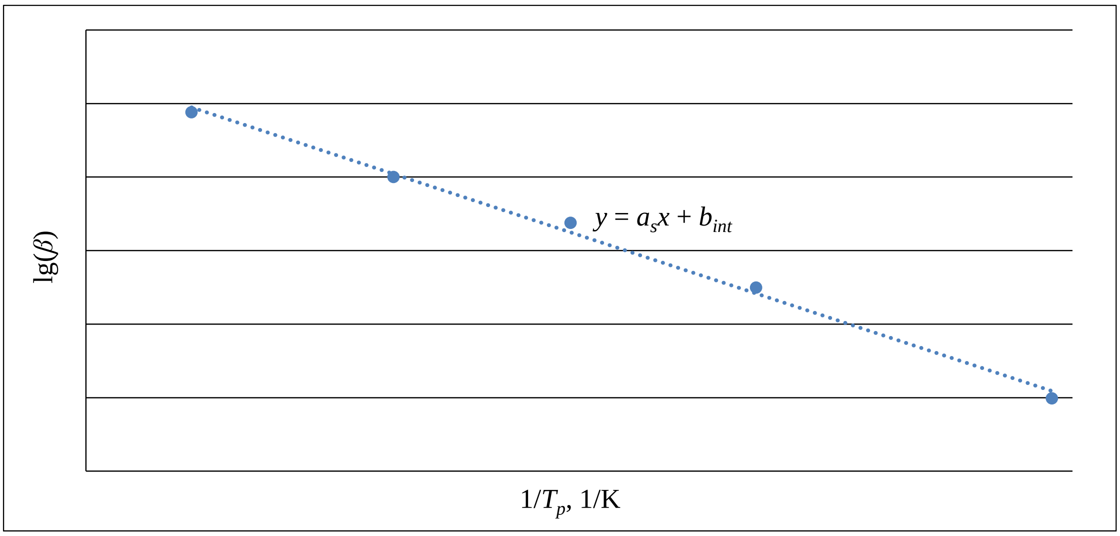

Figure 3.2. ASTM E 698 plot.

3.2. Coefficients of reaction function

Coefficients of the function $f(\alpha)$ are obtained by a fitting of the experimental heat flow curves applying the least squares method:

$$\Delta = \sum_{i=1}^{n}\sum_{j=1}^{m}(\alpha_{ij}^{\exp} - \alpha_{ij})^2 \to \min \tag{3.11}$$

where n is the number of DSC tests at different heating rates;

m is the number of sampling points.

3.3. Validation of *Microsoft Excel* tool

The developed *Microsoft Excel* tool for a building of the curing kinetic models (Figure 3.3) has been successfully validated by using DSC data obtained with *Netzsch DSC-204 Phenix* analyser for an epoxy resin in paper [5]. In this paper measurements of the resin curing have been performed at five heating rates: 2.5, 5.0, 7.5, 10.0 and 15.0 °C/min (Figure 3.4). To validate the developed *Microsoft Excel* tool, only three of them, namely curing at heating rates of 2.5, 7.5 and 15.0 °C/min have been utilised.

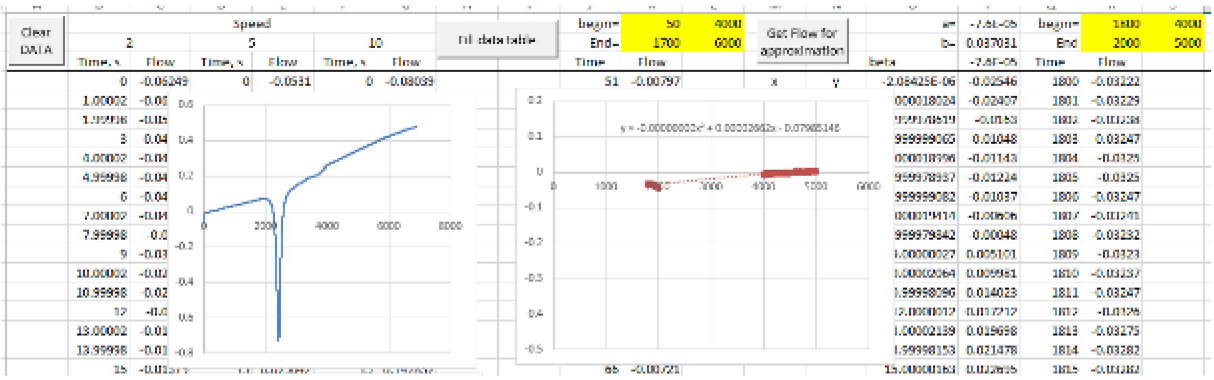

Figure 3.3. Fragment of *Microsoft Excel* tool developed for building of curing kinetic models.

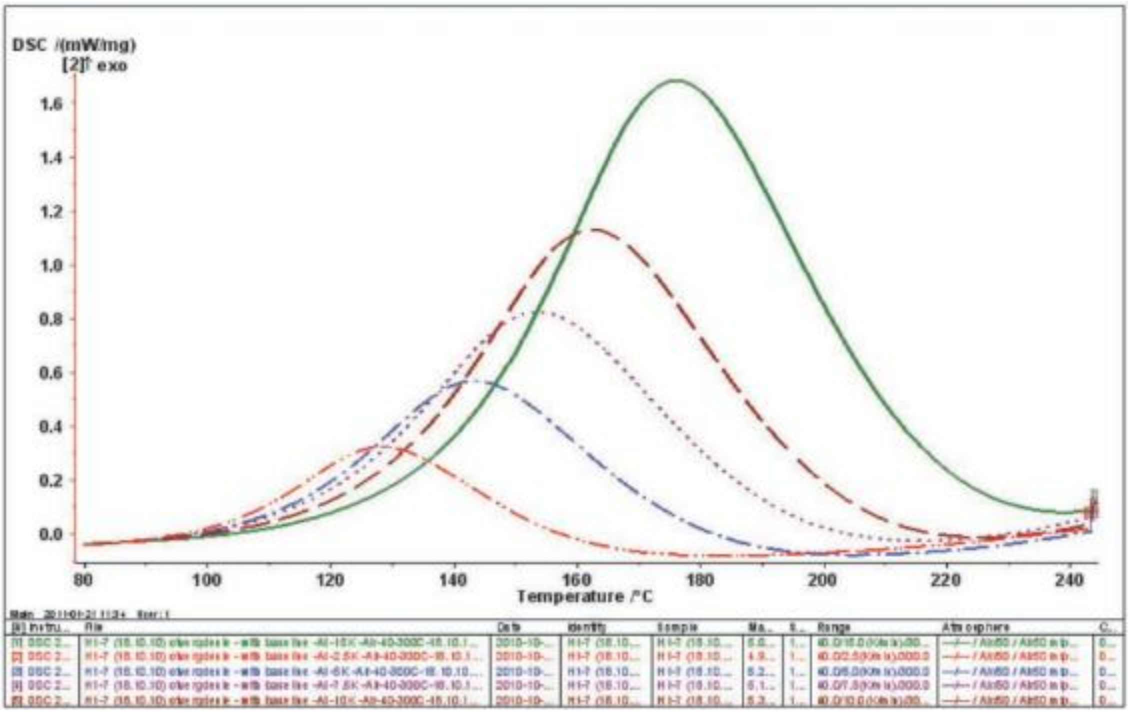

Figure 3.4. DSC curves of epoxy resin curing [5].

Validation of *Excel* tool presents a comparison of experimental dependencies of the degree of cure on time and the same dependencies obtained by the developed curing kinetic models for different heating rates. For this reason the experimental degree of cure $\alpha = H(t)/H_{tr}$ at arbitrary time t should be calculated by using the scheme presented in Figure 3.5. In this case the total heat of reaction H_{tr} is preliminary determined by using a numerical integration of the normalized heat flow on time. To define an integrated area (Figure 3.5), the baseline (red line) is built. The values of the total heat of reaction H_{tr} for three chosen heating rates are given in Table 3.1. The obtained curves showing experimental dependences of the degree of cure on time are presented in Figure 3.6.

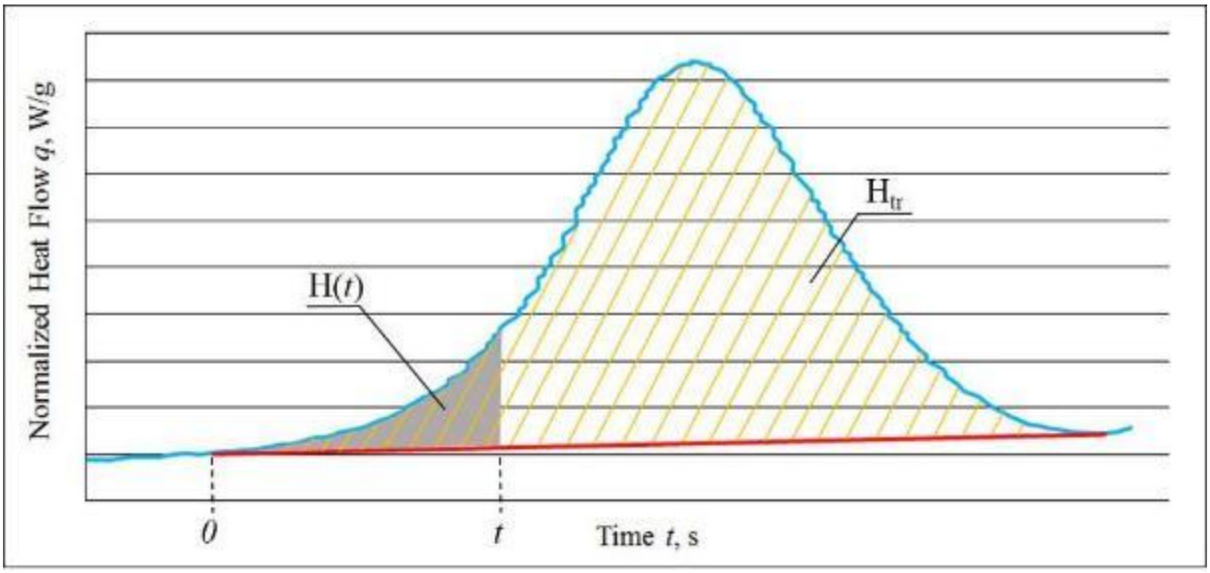

Figure 3.5. Heat flow at heating rate of 15 °C/min.

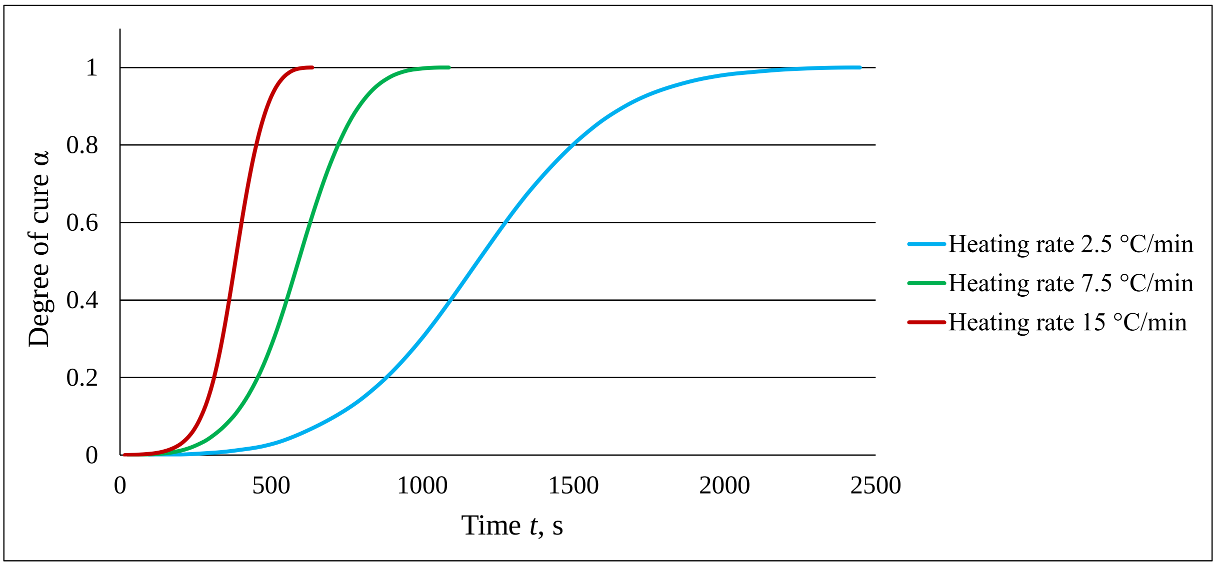

Figure 3.6. Experimental dependences of the degree of cure on time for different heating rates.

Table 3.1.

Total heat of reactions

Heating rate, °C/min	H_{tr}, J/g
2.5	339.37
7.5	330.55
15.0	331.25
Averaged:	333.7

Table 3.2.

Coefficients of Arrhenius relationship

Parameter	Kissinger method	ASTM E 698 procedure
E, kJ/mol	49.4	50.5
K_0, s^{-1}	4444	6457

Table 3.3.

Coefficients of selected reaction functions

Model	Parameters						Δ, %
	n	m	K_1, s^{-1}	E_1, J/mol	K_2, s^{-1}	E_2, J/mol	
n-th order	1.12	-	-	-	-	-	3.84
Prout-Tompkins	0.66	0.23	-	-	-	-	0.35
Kamal-Sourour	1.14	0.47	0.002	137 343	3568	46 349	0.06

To build the corresponding curves obtained by the curing kinetic models, it is necessary to define the coefficients of Arrhenius relationship and coefficients of selected reaction functions. The parameters of Arrhenius relationship obtained by the Kissinger method and *ASTM E 698* procedure are given in Table 3.2. *n*-th order, Prout-Tompkins and Kamal-Sourour models have been chosen to fit the experimental heat flow curves. The coefficients of selected reaction functions obtained by the least squares method are given in Table 3.3

The results of experimental curves' fitting are presented in Figures 3.7-3.9 for different heating rates. It is necessary to note that the coefficients of Arrhenius relationship obtained by the Kissinger method have been used in the developed curing kinetic models.

Table 3.3 and Figures 3.7-3.9 demonstrate clearly that the best precision has been obtained with the Kamal-Sourour model but the *n*-th order model gave the worst result.

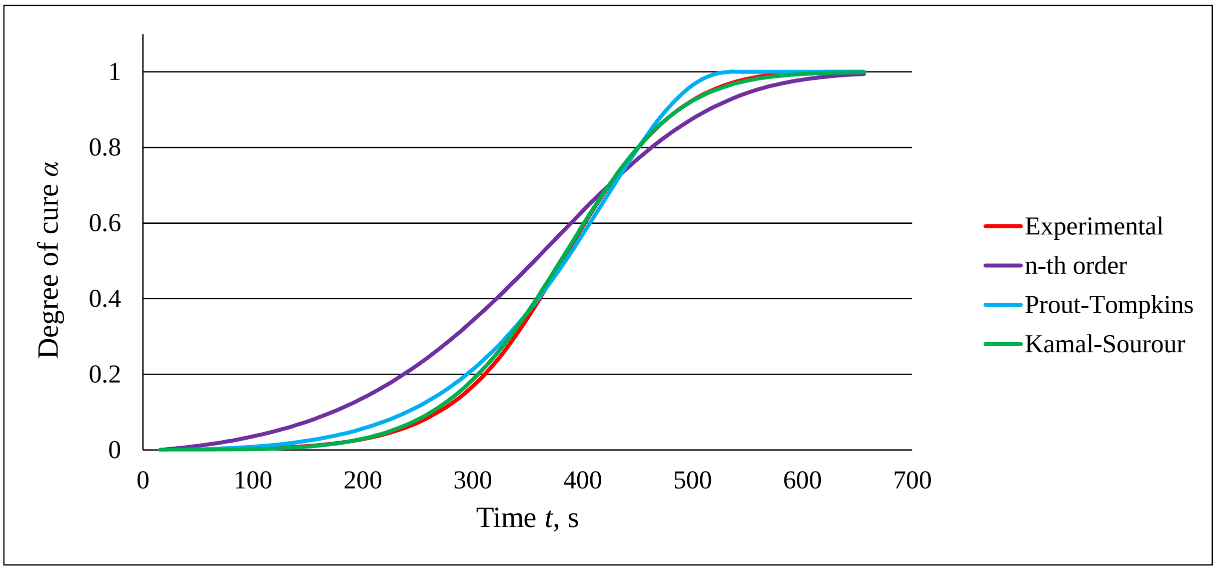

Figure 3.7. Dependences of the degree of cure on time for the heating rate of 15 °C/min.

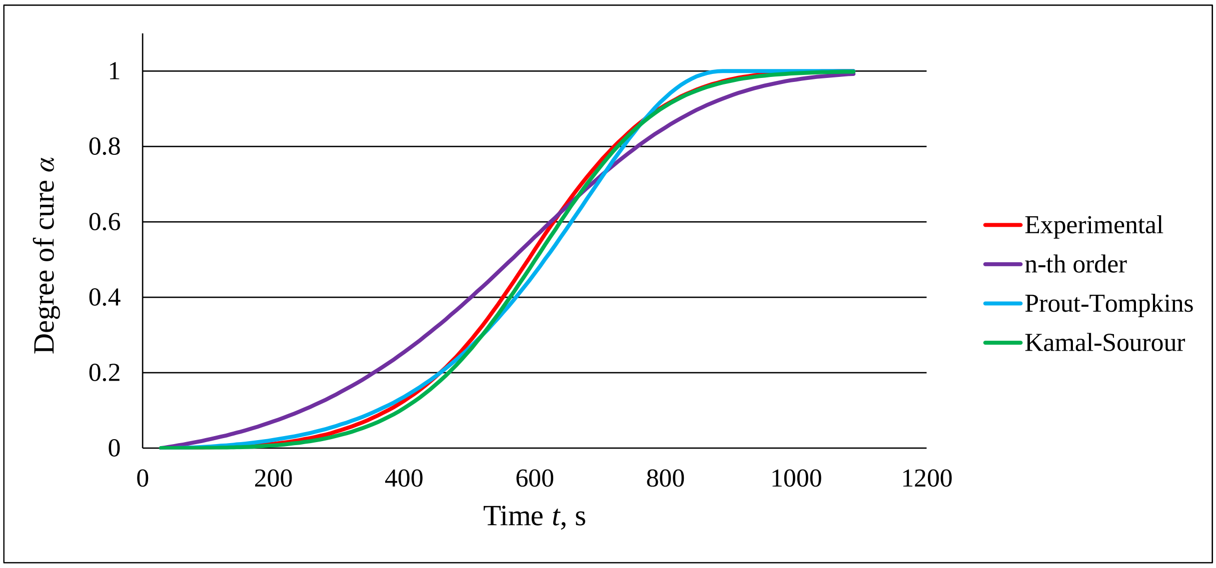

Figure 3.8. Dependences of the degree of cure on time for the heating rate of 7.5 °C/min.

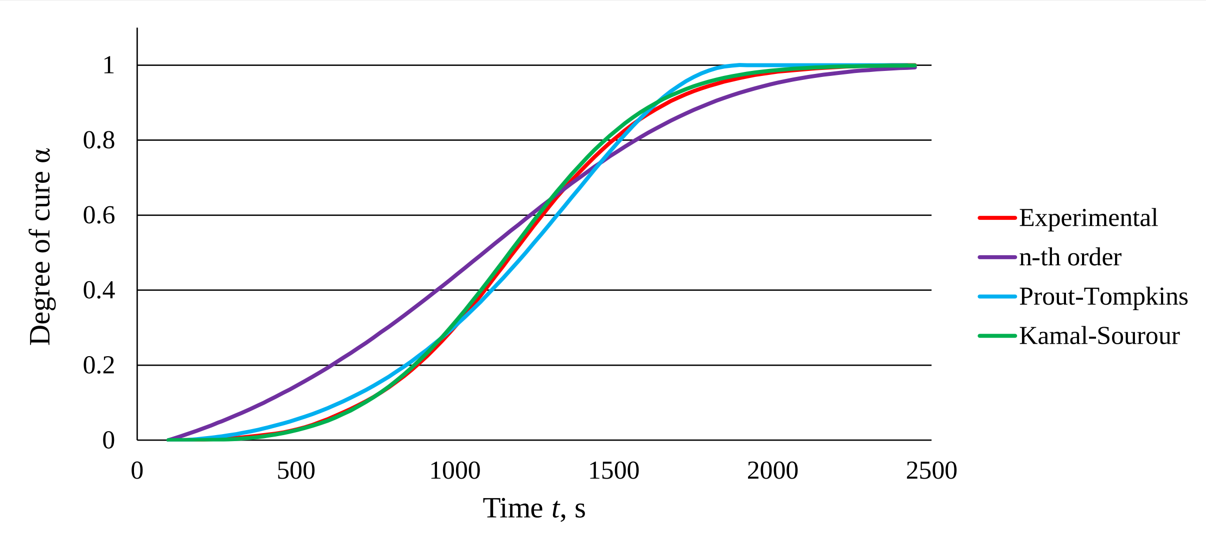

Figure 3.9. Dependences of the degree of cure on time for the heating rate of 2.5 °C/min.

3.4. Curing kinetic models for the resins with high microwave absorption properties

Finally the developed methodology has been successfully applied for a building of the curing kinetic models of resin and coating with high microwave absorption properties to be used in the advanced pultrusion processes. The following materials have been chosen for an application:

- Resin:
  POLRES 305BV (polyester)
- Coating:
  RESOLTECH RESOLCOAT 2010 FGCS (epoxy)

To define the curing kinetic parameters, results of DSC scans performed in *AIMPLAS* (Spain) by *Perkin Elmer Diamond HeperDCS* machine heating samples from 20 °C to 250 °C at heating rates of 2, 5, 10 °C/min are used. It is necessary to note that the parameters of Arrhenius relationship, activation energy and frequency factor, are determined by using the Kissinger method and, as the reaction function, the Kamal-Sourour model (Equation (3.5)) is used. The normalised heat flows in temperature and time domains (Figures 3.10, 3.11, 3.14, 3.16), Kissinger plots (Figures 3.12 and 3.16), determined kinetic parameters (Tables 3.4 and 3.5), and experimental and modelled dependences of the degree of cure on temperature at different heating rates (Figures 3.13 and 3.17) are given below for chosen resin and coating.

It is necessary to note that experimental and modelled dependences of the degree of cure on temperature at different heating rates (Figures 3.13 and 3.17) demonstrates a good correlation for most experiments excluding DSC scan performed at heating rate of 2 °C/min for the resin *POLRES 305BV* (polyester). In this case DSC scan made at heating rate of 2 °C/min for the resin *POLRES 305BV* (polyester) demonstrates the behaviour different from all other scans and, on this reason, could be presumed that carried out measurements are incorrect. The developed curing kinetic models only reflect in this case inaccuracies of the physical experiments.

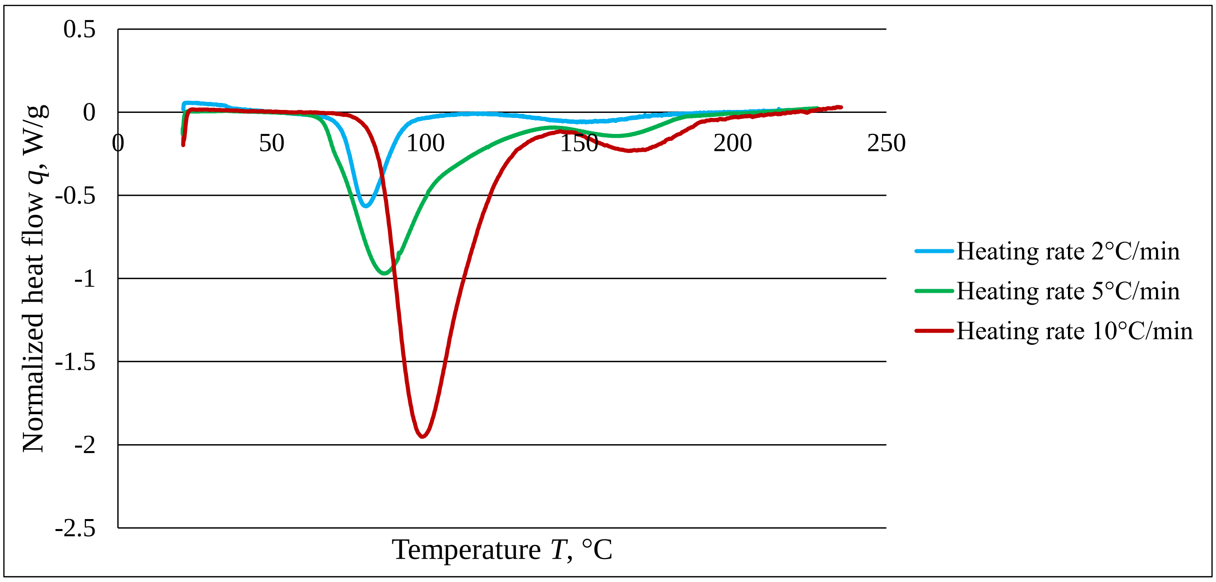

Figure 3.10. Dependence of the normalised heat flow on temperature of *POLRES 305BV*.

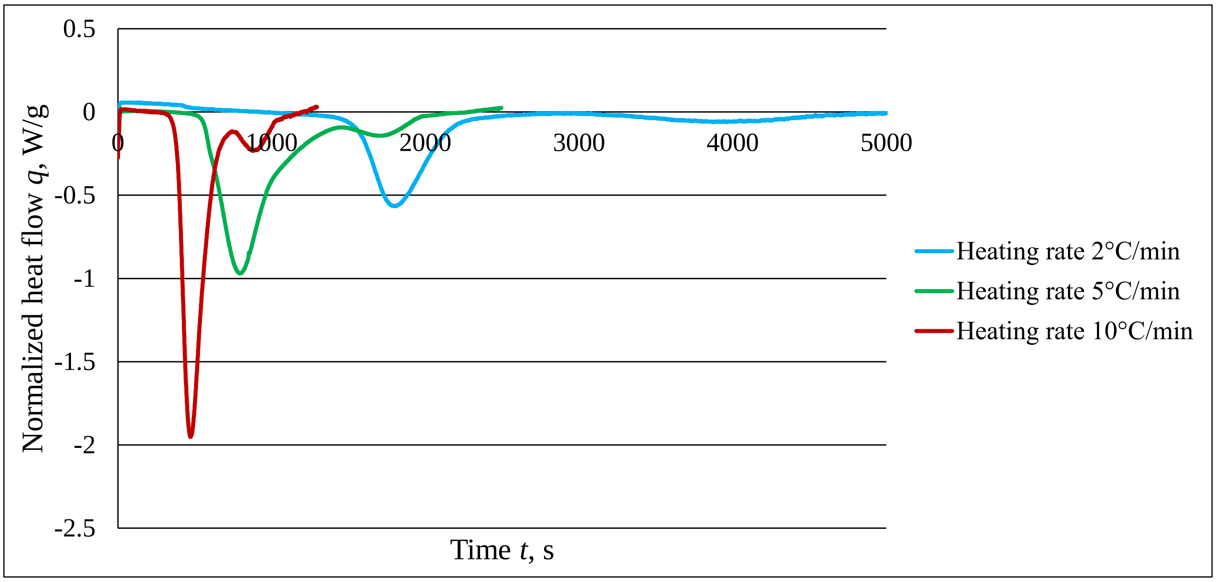

Figure 3.11. Dependence of the normalised heat flow on time of *POLRES 305BV*.

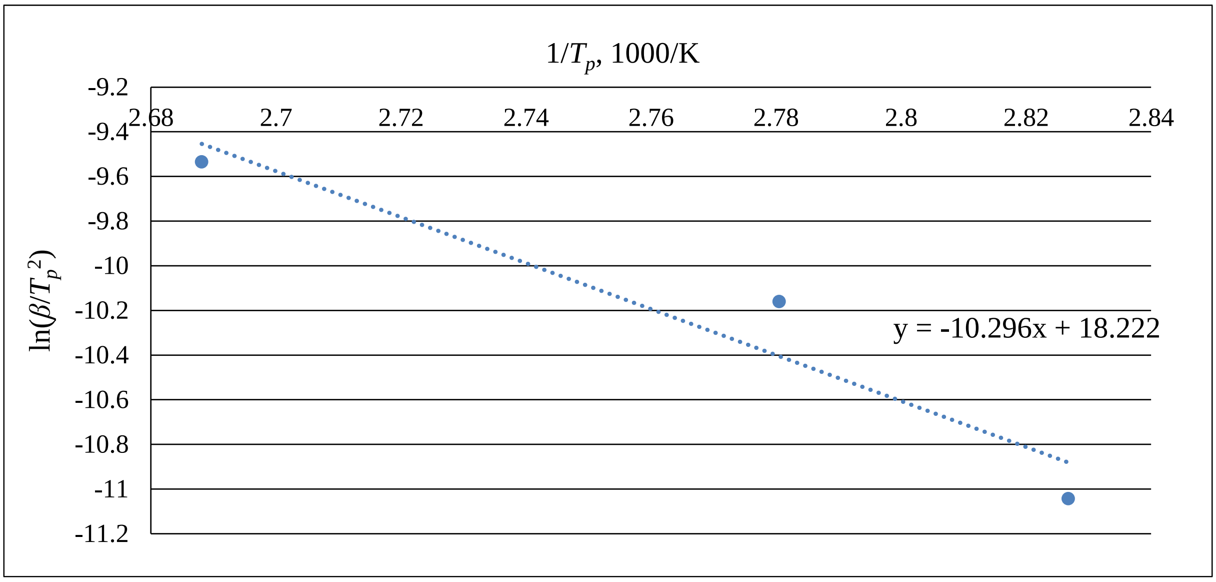

Figure 3.12. Kissinger plot of *POLRES 305BV*.

Table 3.4.

The determined parameters of curing kinetic model of *POLRES 305BV*

H_{tr}, J/kg	K_1, s^{-1}	K_2, s^{-1}	E_1, J/mol	E_2, J/mol)	n	m
323 074	14 289 310 986	285.870	85 573	33 141	2.342	0.519

Table 3.5.

The determined parameters of curing kinetic model of *RESOLTECH RESOLCOAT 2010 FGCS*

H_{tr}, J/kg	K_1, s^{-1}	K_2, s^{-1}	E_1, J/mol	E_2, J/mol)	n	m
152 907	2416 288	186 069 445 590 610	609 443	192 271	1.700	0.190

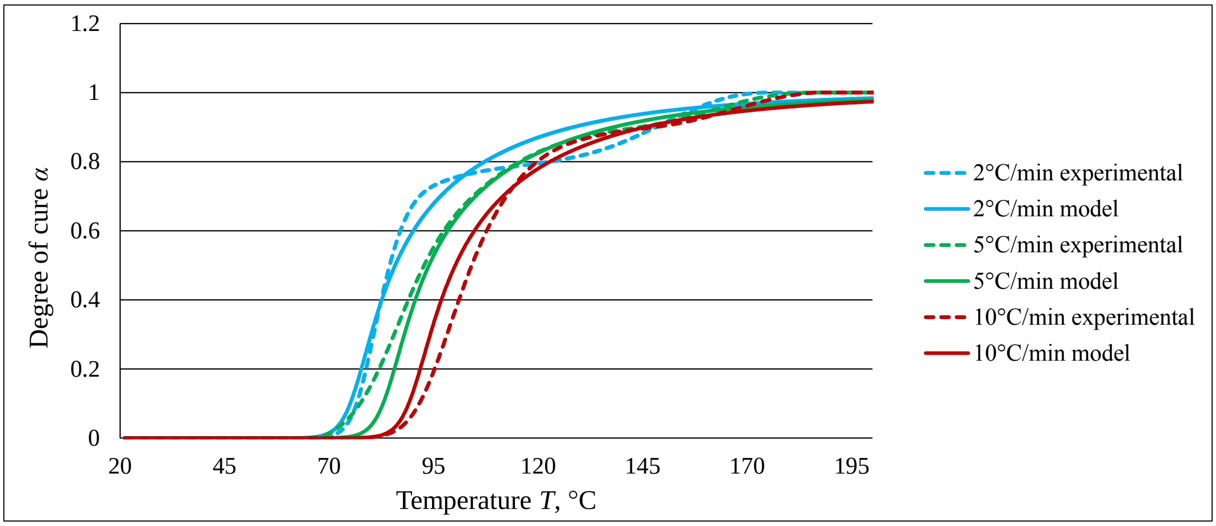

Figure 3.13. Dependences of the degree of cure on temperature at different heating rates of *POLRES 305BV*.

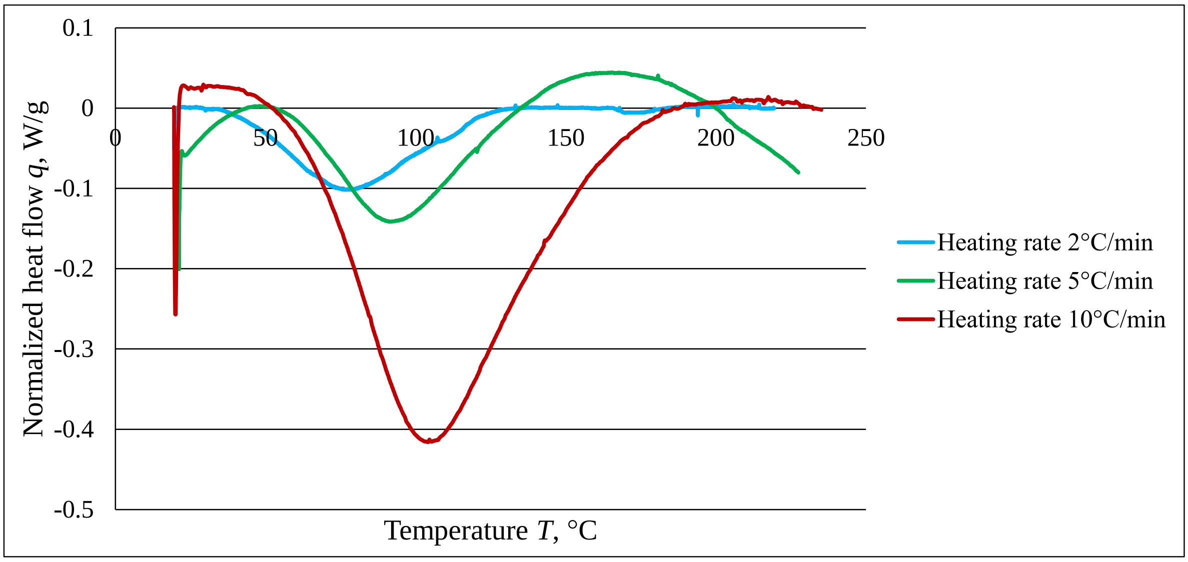

Figure 3.14. Dependence of the normalised heat flow on temperature of *RESOLTECH RESOLCOAT 2010 FGCS*.

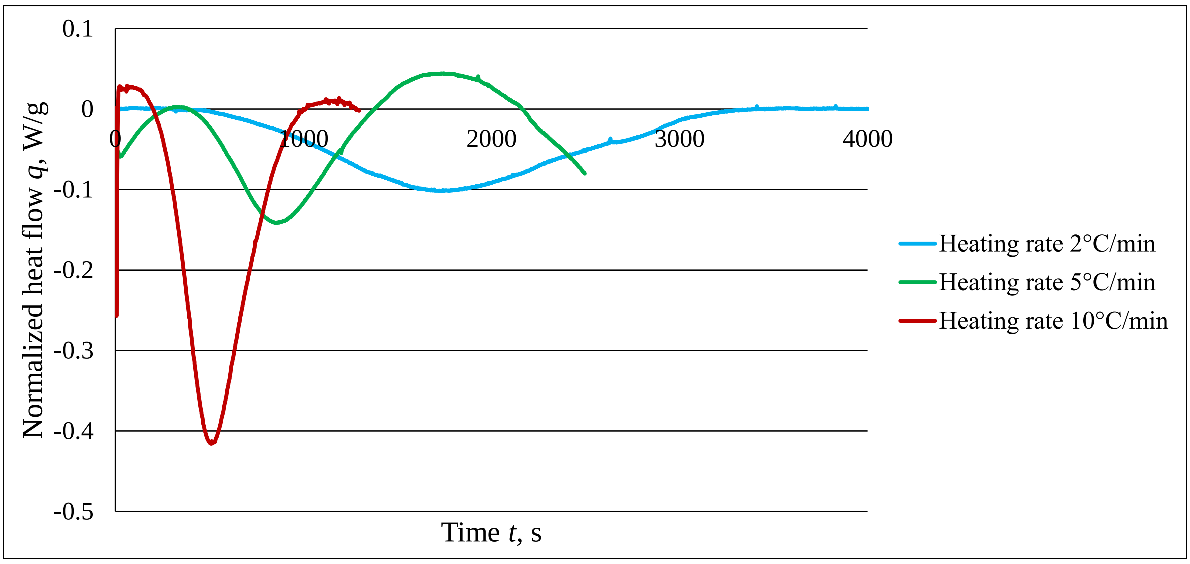

Figure 3.15. Dependence of the normalised heat flow on time of *RESOLTECH RESOLCOAT 2010 FGCS*.

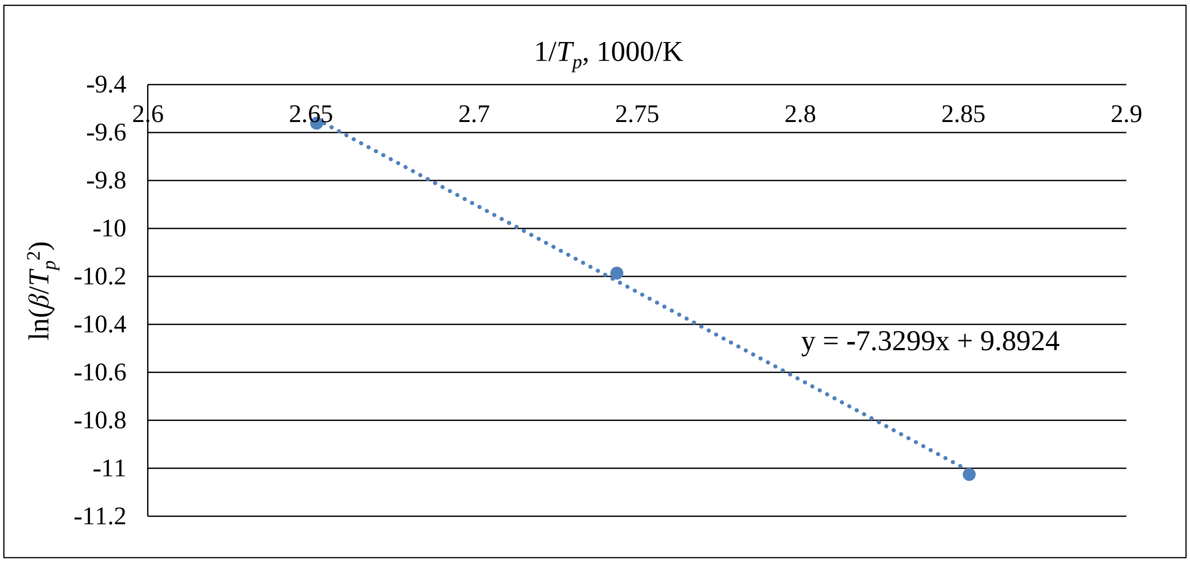

Figure 3.16. Kissinger plot of *RESOLTECH RESOLCOAT 2010 FGCS*.

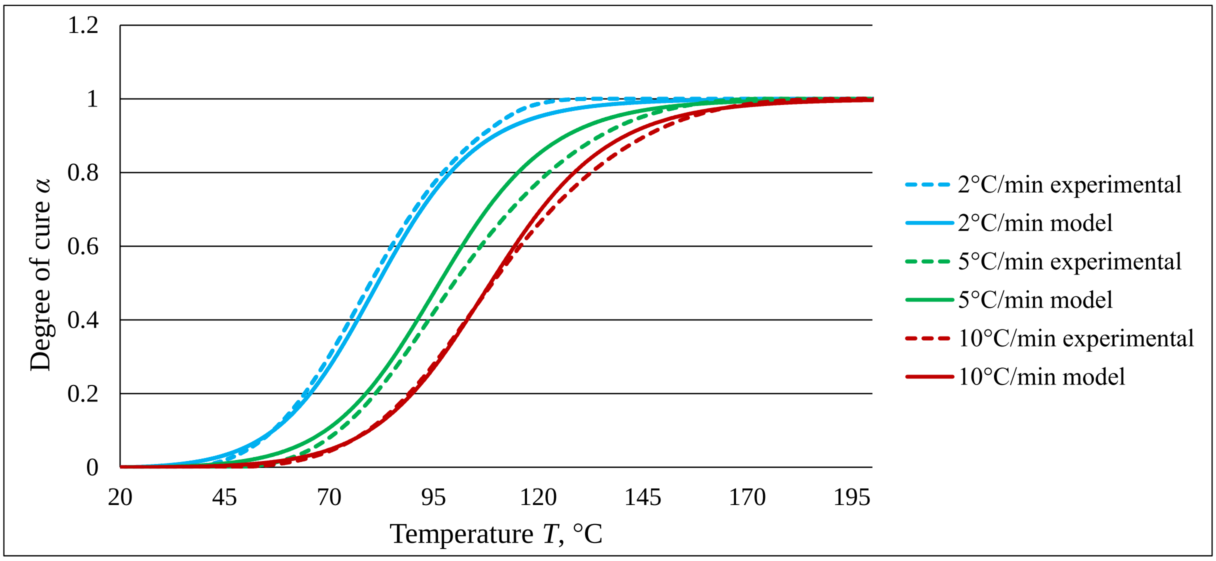

Figure 3.17. Dependences of the degree of cure on temperature at different heating rates of *RESOLTECH RESOLCOAT 2010 FGCS*.

4. EXPERIMENTAL VALIDATION OF SIMULATION ALGORITHMS

This Chapter presents experimental validation of developed procedures for numerical simulation of pultrusion process. Results of the conventional pultrusion made for the cylindrical rod with the diameter of 16 mm in *AIMPLAS* (Spain) are used. The influence of the adjustment and correction of process parameters and material properties on results obtained for transient process in time domain is shown. Correction of initial data using experimental and simulation results is performed with the aim to obtain reliable results

4.1. Experimental set-up and measurement methodology

Experimental set-up and simplified model of the pultrusion tool is presented in Figure 4.1. Heating of the die is realized by 12 electrical heaters split to 3 groups controlled by the proportional-integral derivative (PID) controller and thermocouples located between each heaters group. Electrical power of each heater is 315 W. The controller turns off the heaters groups when the temperature on the corresponding thermocouples reaches 100, 120 or 140 °C (Table 4.1) [18]. Parameters of the pultrusion process, temperature and electrical resistance on the surface of the running pultruded profile, have been measured by three specifically designed sensors (Figure 4.2) located on the die top and newly developed by *Synthesites Innovative Technologies* (Greece). The sensors are connected to the *Optimold* system [39] that can measure the resistivity up to 10^{14} Ohm at the shop-floor using a unique technology based on application of direct current or constant voltage excitation to the electrodes of the sensor.

It has been shown [59, 73] that the ionic conductivity equal to the inverse electrical resistivity of thermoset resin correlates well with the degree of cure of resin. For this reason, for a constant temperature the degree of cure could be calculated using the following equation:

$$\alpha = \frac{\log(RES(T)) - \log_0(RES(T))}{\log(RES_{\max}(T)) - \log_0(RES(T))} \tag{4.1}$$

where *RES* is the measured resistivity of the resin, Ohm;
RES_0 is the resistivity of the unreacted resin, Ohm;
RES_{max} is the maximum value of the resistivity reached by the end of an isothermal cure, Ohm.

However, resistivity is significantly affected by a temperature so when the temperature is not constant, a decoupling of the effect of temperature is required. Most of the thermoset resins present a linear behaviour of the logarithm of the resistivity as a function of the inverse temperature when the resin is at glassy or rubbery states and could be well represented by an Arrhenius relationship:

$$RES_{\max}(T) = A \cdot \exp\left(\frac{K}{T}\right) \tag{4.2}$$

where parameters A and K can be easily calculated using the experimental resistivity/temperature data measured for a fully cured resin. Following this parameter fitting, the temperature-decoupled resistivity is introduced as:

$$RES = \frac{RES(T)}{A \cdot \exp\left(\frac{K}{T}\right)} \tag{4.3}$$

Dimensions (in mm) of the pultrusion die and locations of the heaters, thermocouples and sensors are shown in Figure 4.1. Pultrusion die has been made of steel *40Cr*. The materials used for a production of the cylindrical rod are glass fibres *Unifilo 4800 tex* and polyester resin *POLRES 305BV*. The fibre volume content in the pultruded material is 55 %. The thermal properties of the applied materials are given in Table 4.2. The rate of resin reaction is described by using the Kamal-Sourour curing kinetic model (Equation (3.5)) developed in Chapter 3.4. The experimental pultrusion process is realized at pull speed of 18 cm/min. Room temperature is 17 °C, resin temperature is equal to the room temperature since no resin preheating is used.

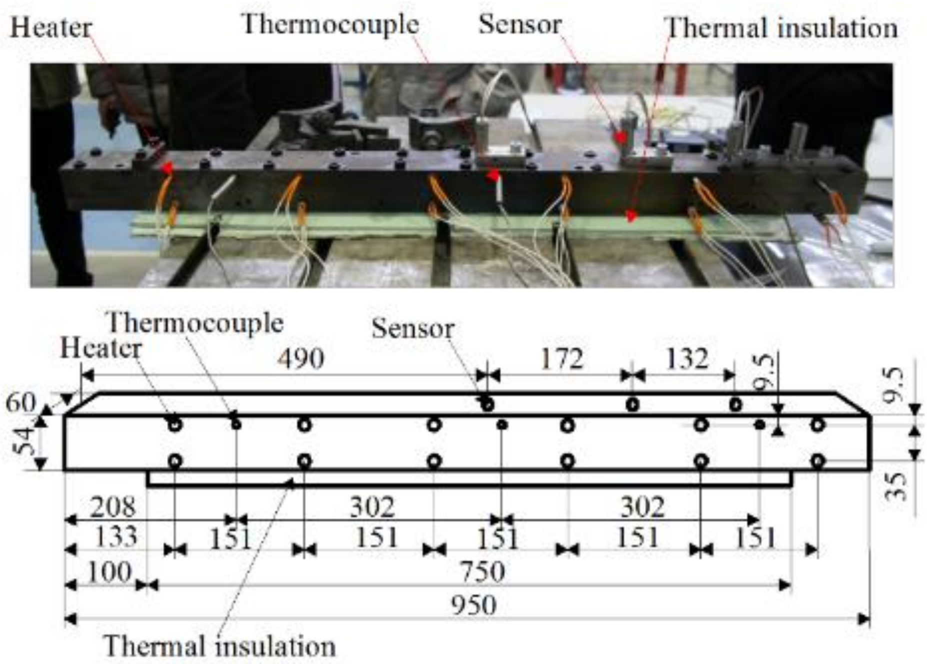

Figure 4.1. Set-up of conventional pultrusion.

Figure 4.2. Curved sensor.

Table 4.1.

Control temperatures

Thermocouple	Initial, °C	Corrected 1, °C	Corrected 2, °C	
			First switch- off	Main control
1	100	85	65	85
2	120	105	85	105
3	140	125	105	125

Table 4.2.

Thermal properties of materials

	ρ, kg/m^3	c_p, J/(kg · °C)	k_x, W/(m · °C)	$k_y = k_z$ W/(m · °C)	Max allowable *T*, °C
Polyester *POLRES 305BV*	1100	1360	0.209	0.209	190
Glass fibers *Unifilo 4800 tex*	2500	1235	11	1	1200
Lumped properties	1870	1268	0.750	0.500	-
Steel *40Cr* (initial)	7850	460	46	46	-
Steel *40Cr* (corrected)	7850	460	33	33	-

4.2. Finite element simulation in *ANSYS Mechanical*

The first finite element model for a simulation of the cylindrical rod pultrusion has been created in *ANSYS Mechanical* by using 3-D thermal solid finite elements *Solid 70*. The finite element has eight nodes with a single degree of freedom, temperature, at each node and the orthotropic material properties. Thermal insulation under the die is not taking into account in the finite element model. In this case symmetry of the simulated domain is used and only a quarter of the die is modelled. To analyse heat transfer and curing processes in the post-die region, the modelling of the profile is continued at the distance of 250 mm from the die exit. A fragment of the finite element model is presented in Figure 4.3. The finite element mesh is regular in pull direction and has 240 elements along the profile. The total number of finite elements is 73 040 and it consists of 7680 elements used for the composite modelling and 65 360 elements used for the die including heaters and thermocouples. The time step of the solution is 1.67 s. During this time the composite travels in the pull direction on the distance equals to the dimension of one finite element (5 mm). It is necessary to note that iterations (sub-steps) are not performed in the finite element analysis. Initial conditions are applied at time $t = 0$ when all nodal points of the composite have the room temperature and degree of cure equals to $\alpha = 10^{-10}$.

Results of simulation, temperature and degree of cure obtained on sensors 1-3, together with experimental measurements are presented in Figures 4.4-4.6. Final distribution of the temperature and degree of cure along the composite profile is given in Figure 4.7. Figures 4.4-4.6 demonstrate that close agreement between experimental and simulation results has not been obtained. If to suppose that experimental results are correct, a disagreement should be identified. However it is necessary to note that sensor 1 located closely to the die entrance is dirty what is confirmed by a more smooth temperature curve at the end of measurement time. This could be explained by the fact that it is not screwed till the final position and on this reason an appeared cavity has been filled by the uncured material. This is why sensor 1 not properly reacts on the heaters switch off or switch on. This phenomenon should be taken into account additionally analysing the experimental and simulation results.

4.2.1. Correction of control temperatures

To identify a disagreement between experimental and simulation results, the control temperatures of 100, 120 or 140 °C have been checked firstly since the controller regulating these temperatures has been used by technologists as “the black box”. From Figure 4.1 it is seen that sensor 1 is located very closely to the thermocouple 2. Figure 4.8 shows that the distance between axis of the thermocouple and the sensor is only 20 mm. It is reasonable to assume that temperatures on sensor 1 and thermocouple 2 are very close or the same. The results of the finite element simulation confirm this assumption (Figure 4.9).

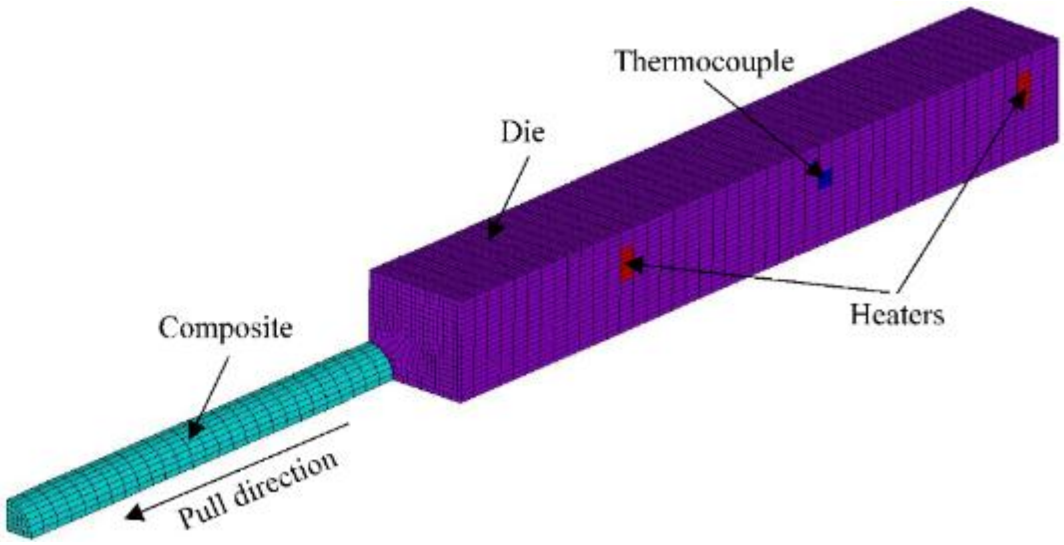

Figure 4.3. Fragment of the finite element model.

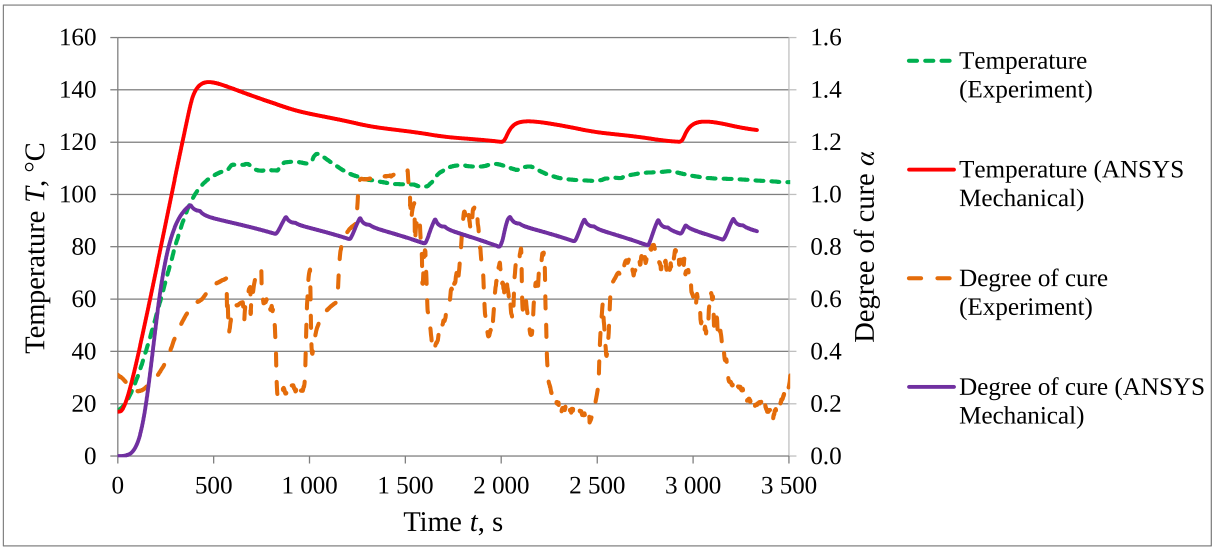

Figure 4.4. Temperature and degree of cure on sensor 1.

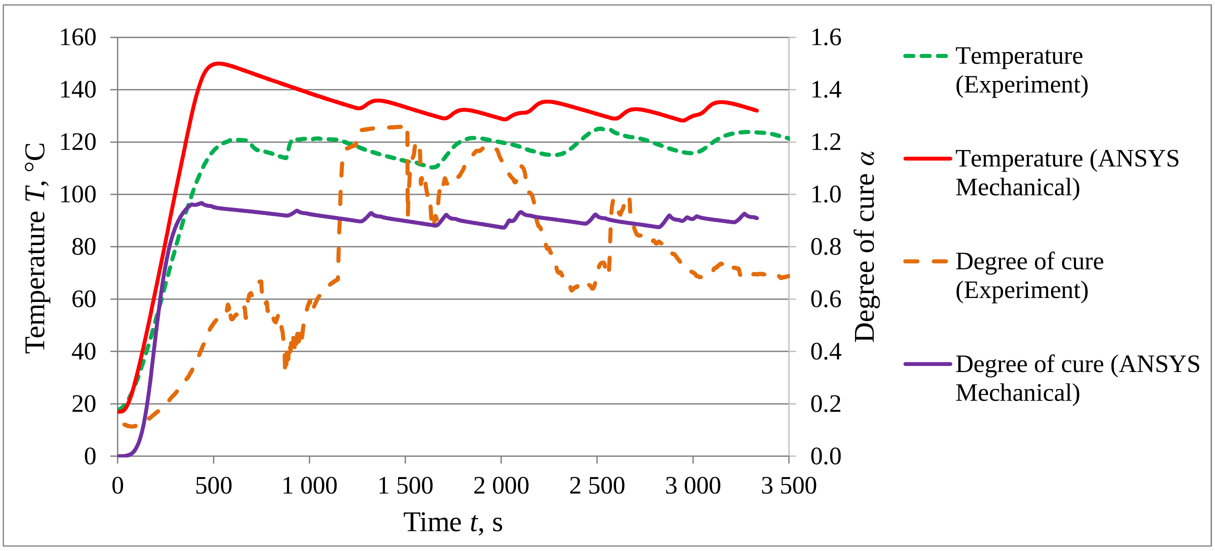

Figure 4.5. Temperature and degree of cure on sensor 2.

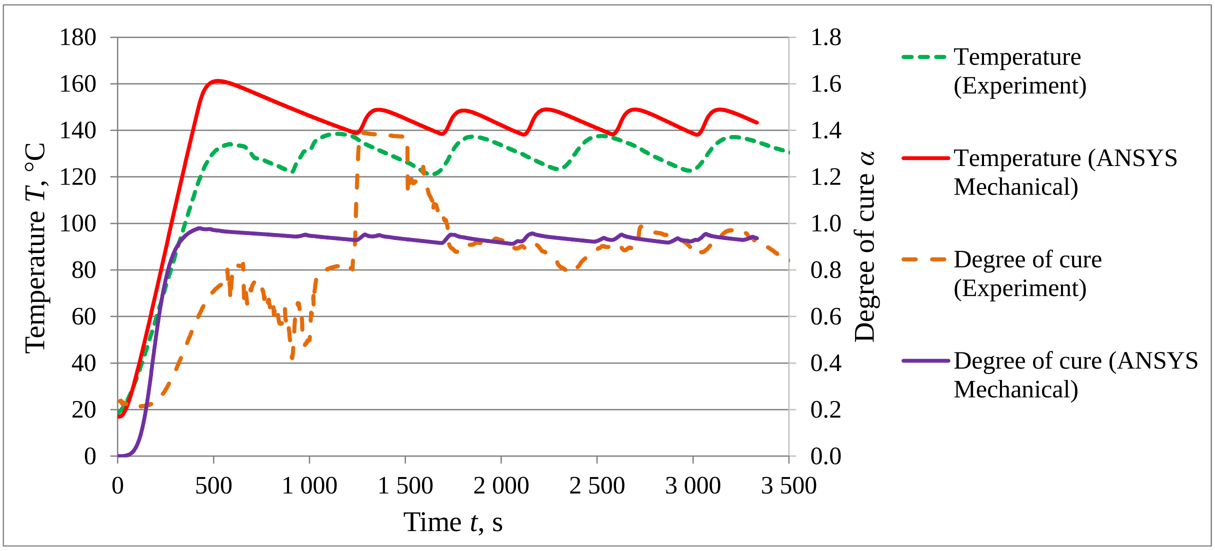

Figure 4.6. Temperature and degree of cure on sensor 3.

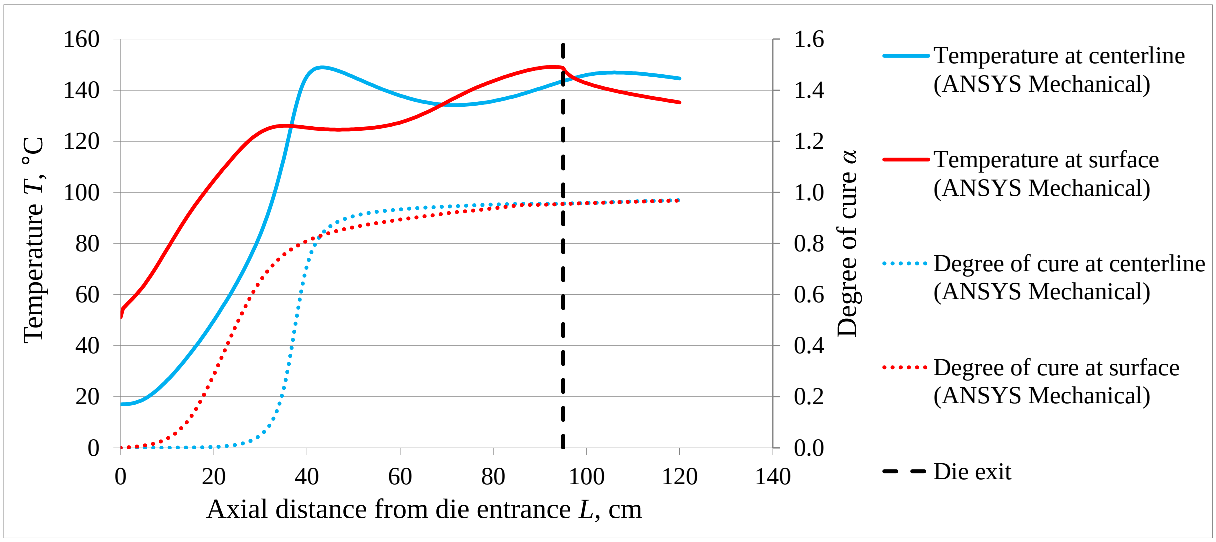

Figure 4.7. Final distribution of temperature and degree of cure along the composite profile.

It is seen from Figure 4.9 that the temperature on sensor 1 is lower than the controlled temperature on thermocouple 2. Also Figures 4.4-4.6 show that the simulated temperatures on all sensors any time are greater than the temperatures obtained experimentally. As the conclusion it is possible to say that the temperatures really controlled by thermocouples during an experiment are lower than the given in Table 4.1. For this reason additional calculations have been performed with the corrected control temperatures. For thermocouples 2 and 3 they have been taken from the experimental results for sensors 1 and 3 respectively as presented in Figures 4.10 and 4.11. The control temperature for thermocouple 1 has been taken proportionally to the temperatures on thermocouples 2 and 3. The corrected values of the control temperatures are given in Table 4.1 (Corrected 1).

Experimental measurements together with the results of simulation, temperature and degree of cure obtained on sensors 1-3 with the corrected control temperatures (Table 4.1, Corrected 1), are presented in Figures 4.12-4.14. The modified final distribution of the temperature and degree of cure along the composite profile is given in Figure 4.15. Figures 4.12-4.14 demonstrate that simulation temperatures curves have moved down and more close agreement between experimental and simulation results has been obtained with the corrected control temperatures. A big disagreement is visible now for temperatures after the first switch-off of the heaters (at time about 400 s from the process beginning): temperature in the simulation continues to rise because of thermal inertia of the steel pultrusion die.

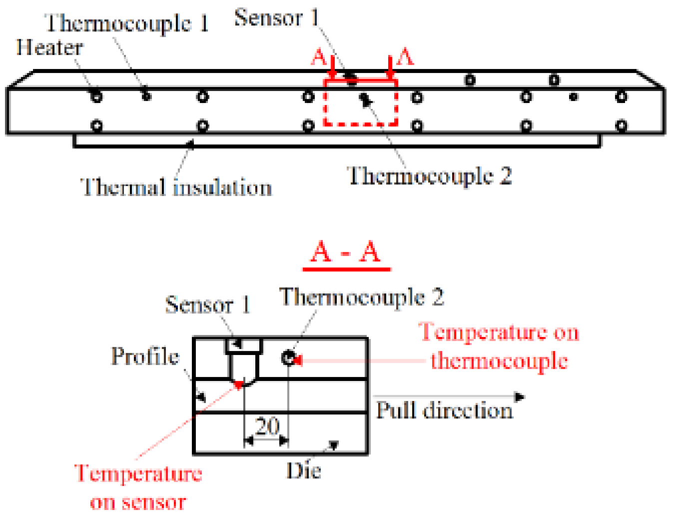

Figure 4.8. Location of sensor 1 and thermocouple 2 in the die.

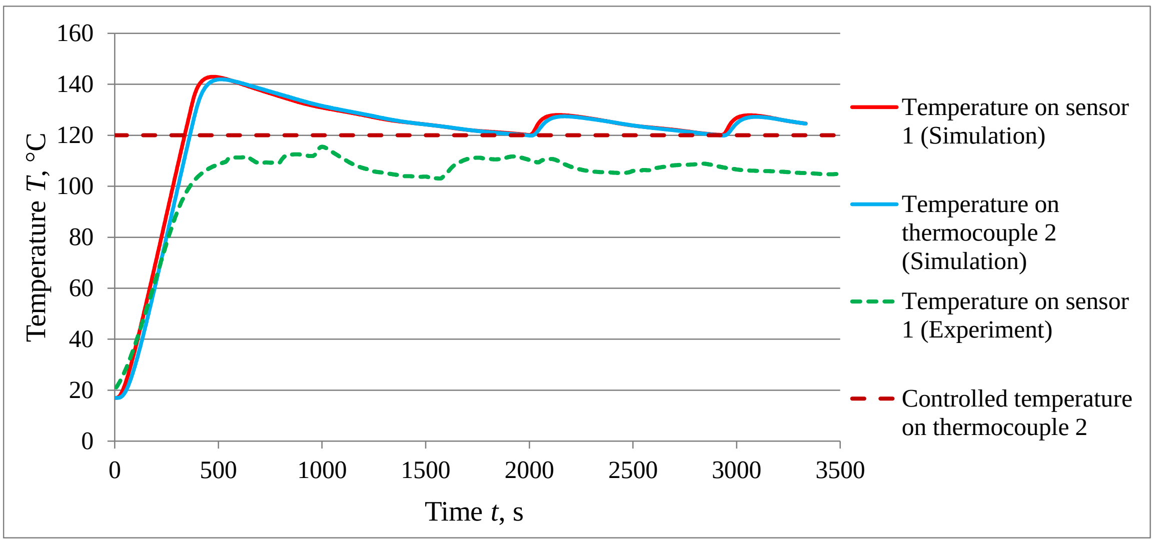

Figure 4.9. Simulated and experimental temperatures on sensor 1 and thermocouple 2.

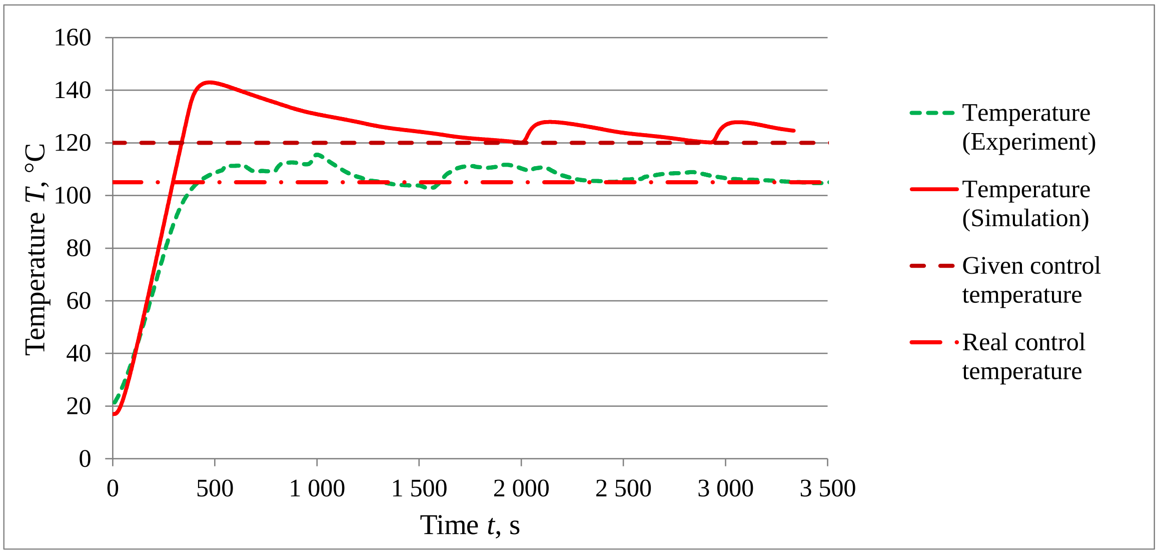

Figure 4.10. Correction of the control temperature on thermocouple 2 by using measurements on sensor 1.

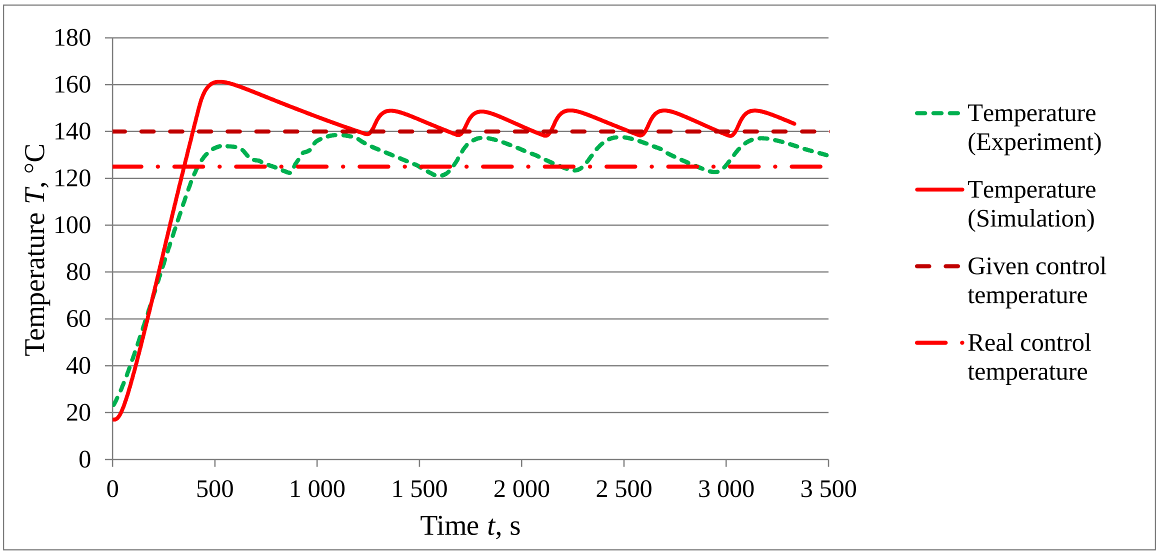

Figure 4.11. Correction of the control temperature on thermocouple 3 by using measurements on sensor 3.

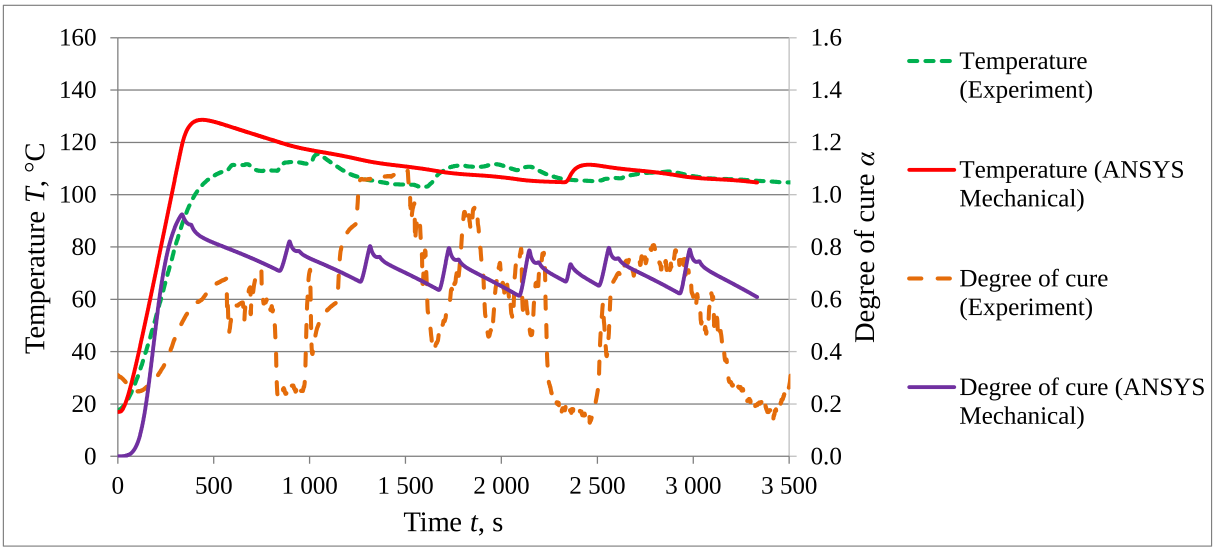

Figure 4.12. Temperature and degree of cure on sensor 1 after correction of the control temperatures.

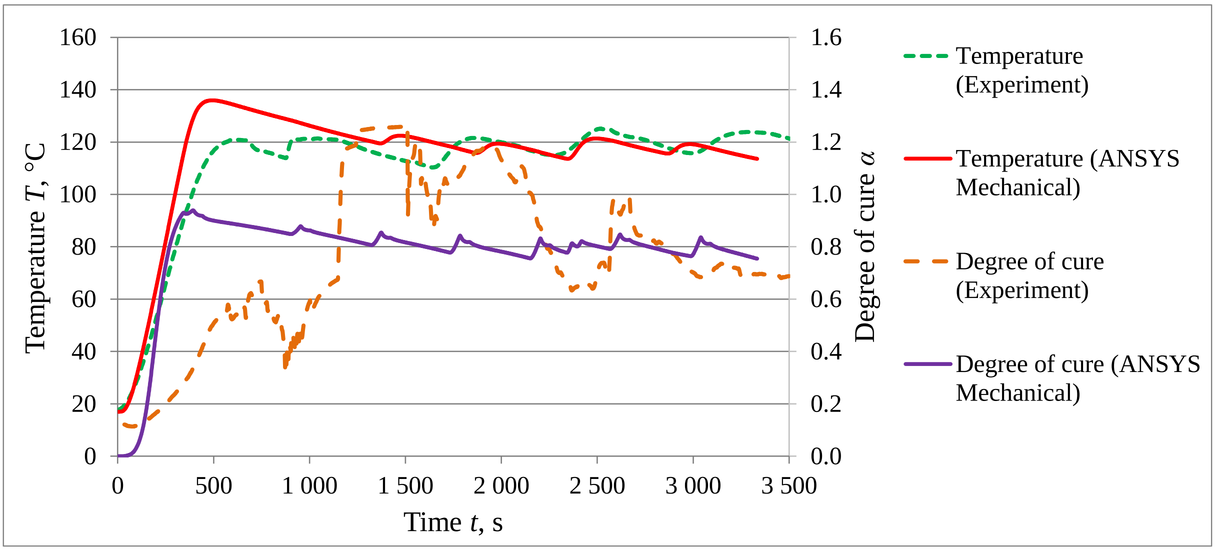

Figure 4.13. Temperature and degree of cure on sensor 2 after correction of the control temperatures.

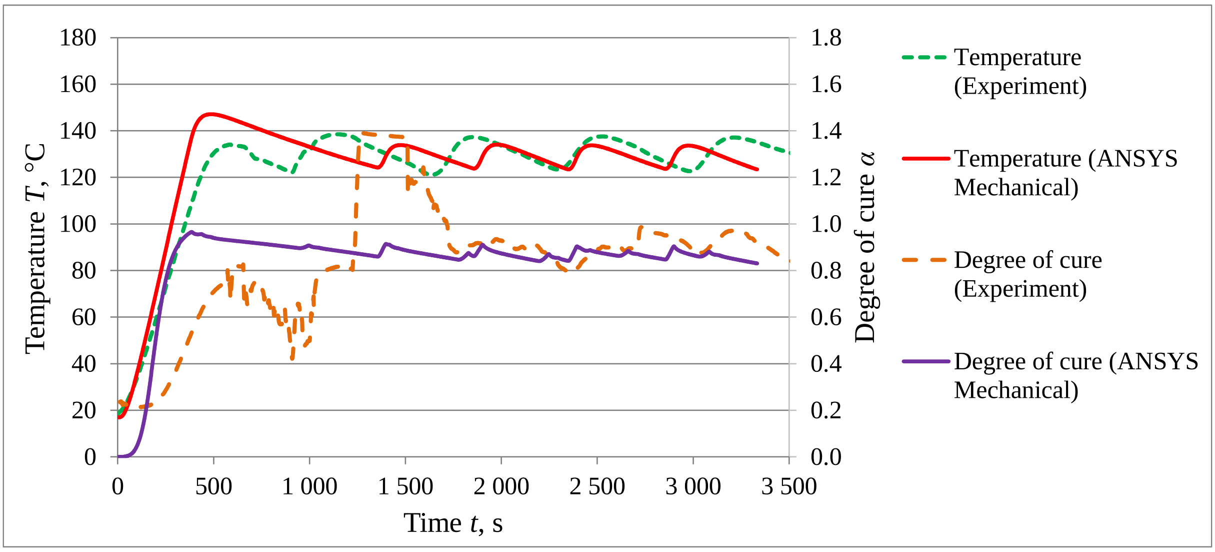

Figure 4.14. Temperature and degree of cure on sensor 3 after correction of the control temperatures.

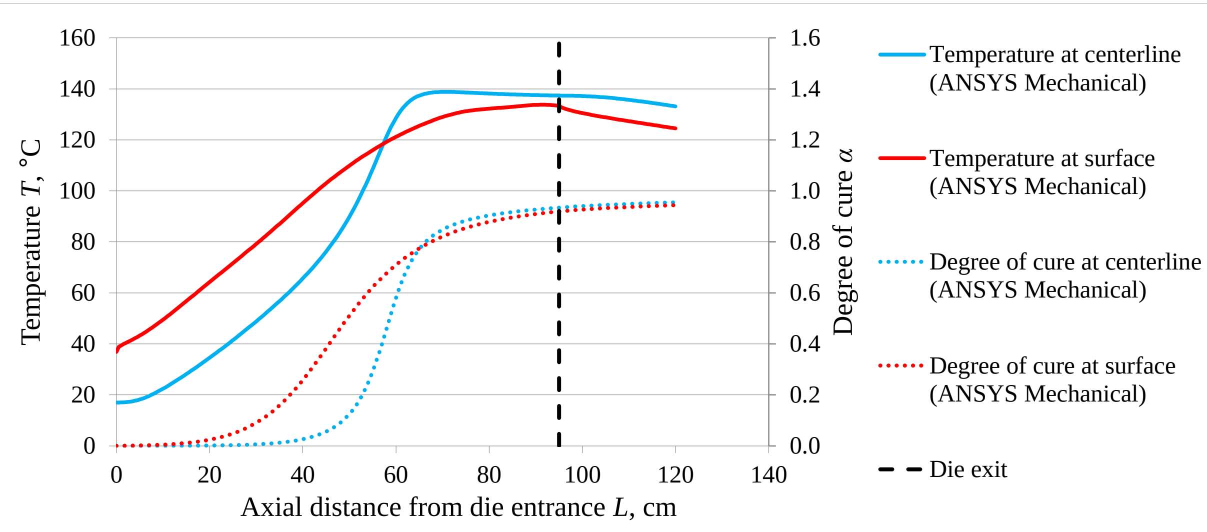

Figure 4.15. Final distribution of temperature and degree of cure along the composite profile after correction of the control temperatures.

4.2.2. Correction of temperature control algorithm

More complex temperature control system (PID controller) has been used in the physical experiment. To bring simulated temperature control algorithm closer to the real, reduction of the control temperature for the first switch-off of the heaters has been applied. Control temperatures have been reduced for 20 °C (Table 4.1, Corrected 2). Experimental measurements together with the results of simulation, temperature and degree of cure obtained on sensors 1-3 with the corrected first and main control temperatures, are presented in Figures 4.16- 4.18. The modified final distribution of the temperature and degree of cure along the composite profile is given in Figure 4.19. Figures 4.16-4.18 demonstrate that simulation temperatures curves have moved down after the first switch-off of the heaters (at time about 400 s from the process beginning) and more close agreement between experimental and simulation results has been obtained with the corrected control temperatures for the first switch-off of the heaters. Disagreement is visible now only for the duration of temperatures cycles.

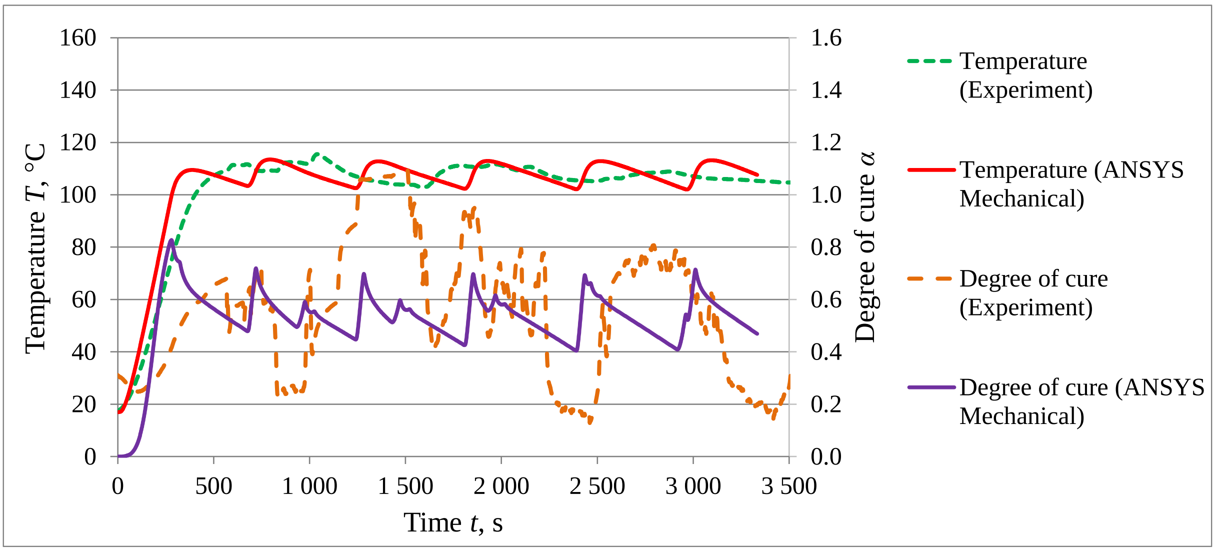

Figure 4.16. Temperature and degree of cure on sensor 1 after correction of temperature control algorithm.

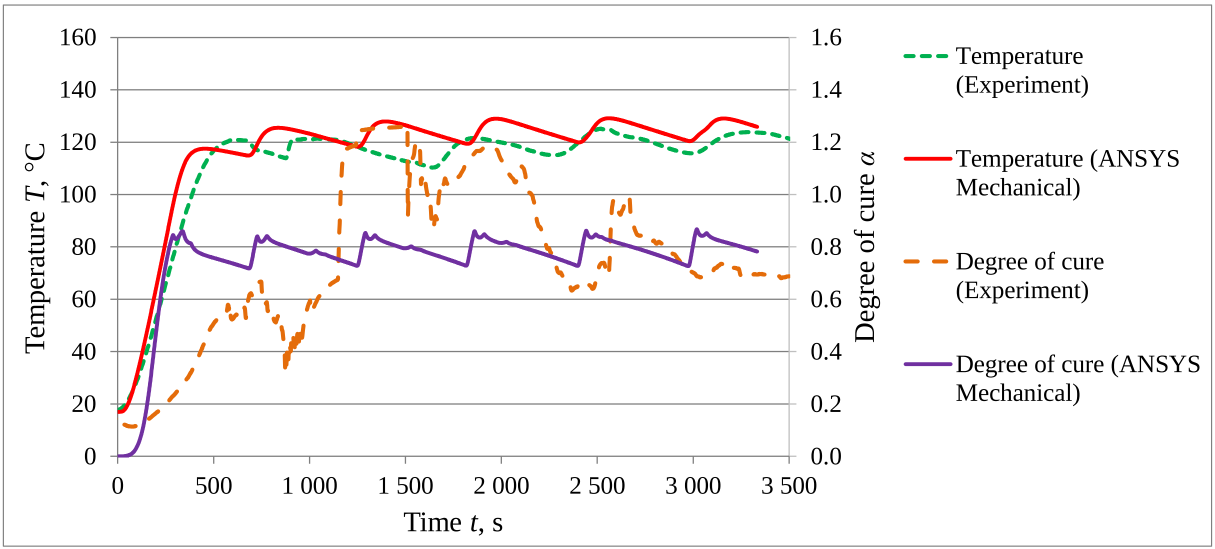

Figure 4.17. Temperature and degree of cure on sensor 2 after correction of temperature control algorithm.

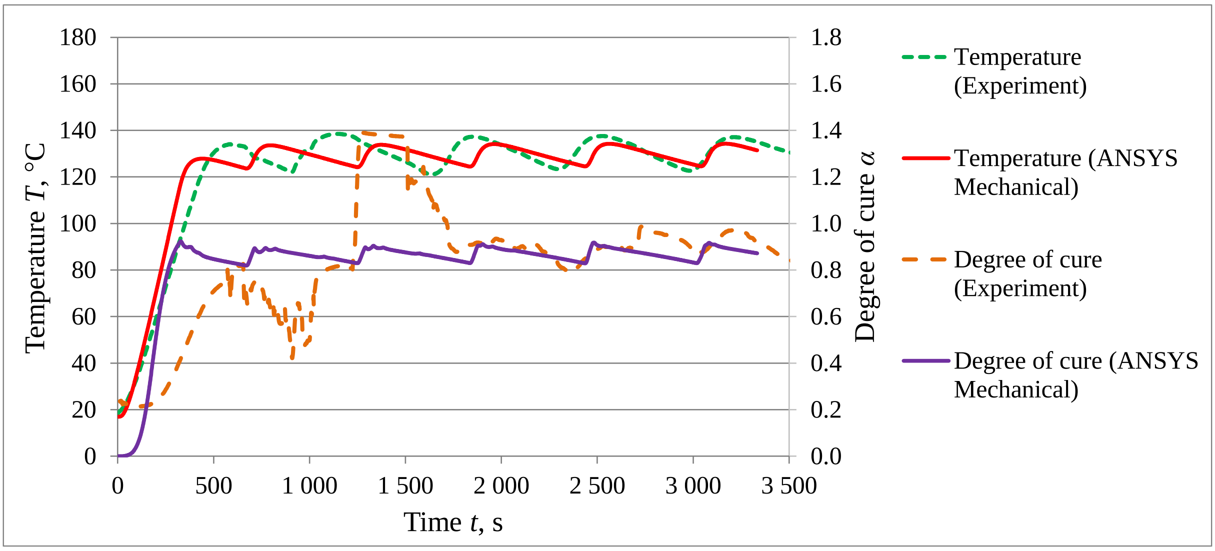

Figure 4.18. Temperature and degree of cure on sensor 3 after correction of temperature control algorithm.

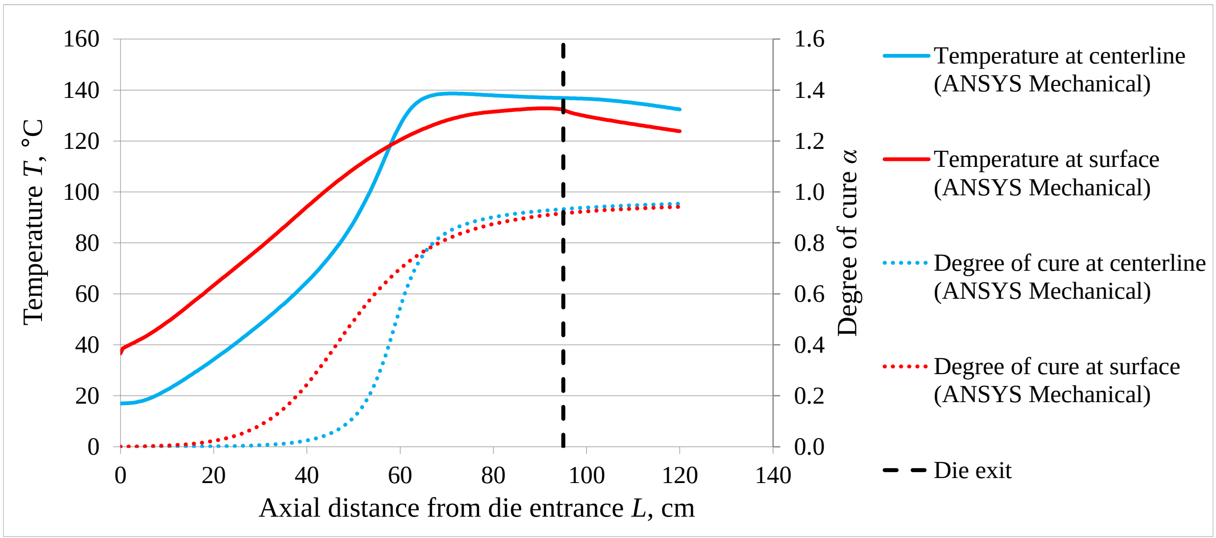

Figure 4.19. Final distribution of temperature and degree of cure along the composite profile after correction of temperature control algorithm.

4.2.3. Correction of die thermal properties

Obviously, that this disagreement is dependent on the value of thermal conductivity of the die material. To avoid this disagreement, the material properties of die have been verified and it has been found that they differ considerably in different material data sheets. Corrected properties are given in Table 4.2.

Experimental measurements together with the results of simulation, temperature and degree of cure obtained on sensors 1-3 with the corrected control temperatures (Table 4.1, Corrected 2) and material properties (Table 4.2), are presented in Figures 4.20-4.22. The modified final distribution of the temperature and degree of cure along the composite profile is given in Figure 4.23. Figures 4.20-4.22 demonstrate that duration of the temperatures cycles has increased considerably after updating of material data with a negligible increase in the amplitude of temperatures cycles. Finally more close agreement between experimental and simulation results has been obtained with the corrected control temperatures and steel thermal properties.

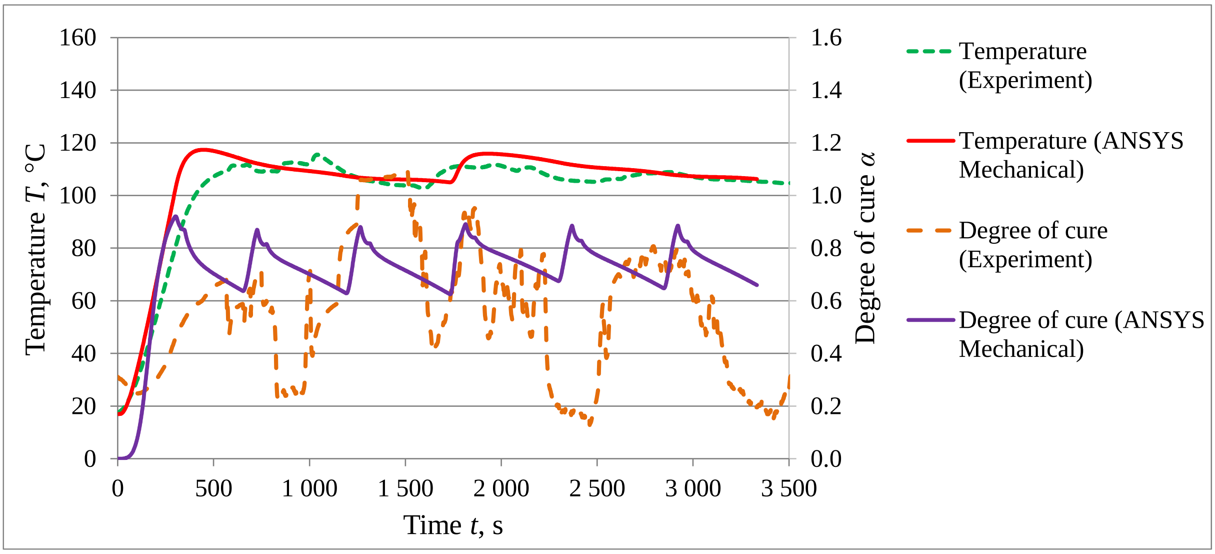

Figure 4.20. Temperature and degree of cure on sensor 1 after correction of the control temperatures and material properties update.

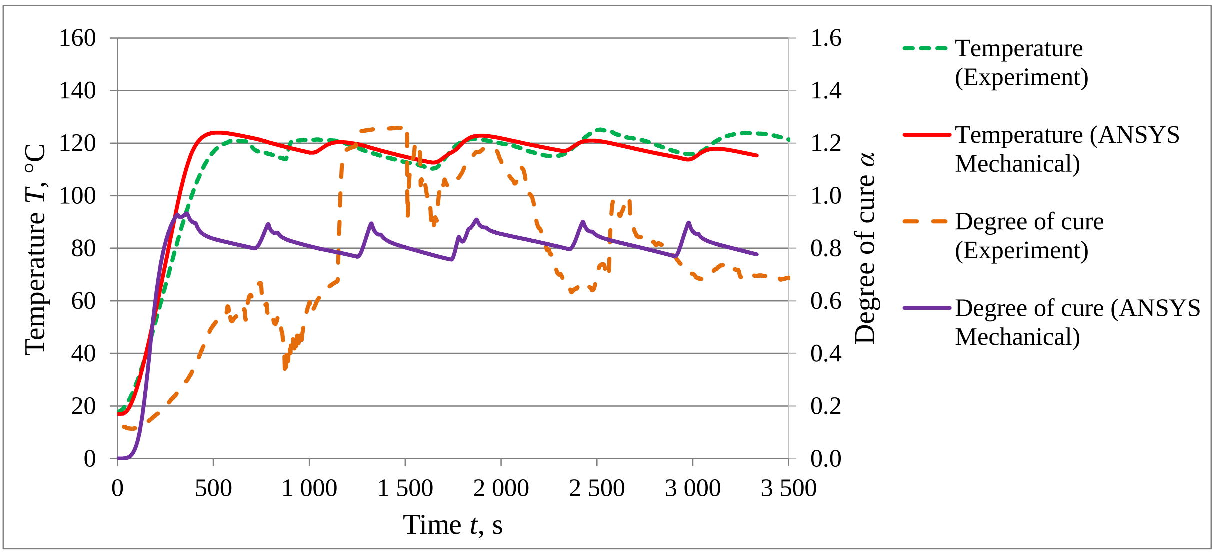

Figure 4.21. Temperature and degree of cure on sensor 2 after correction of the control temperatures and material properties update.

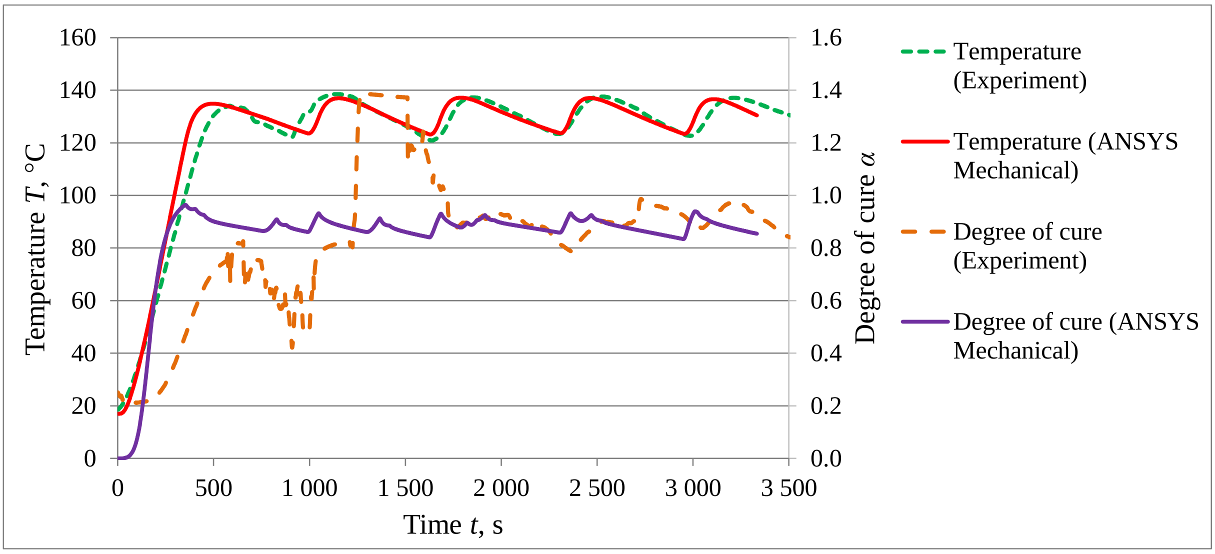

Figure 4.22. Temperature and degree of cure on sensor 3 after correction of the control temperatures and material properties update.

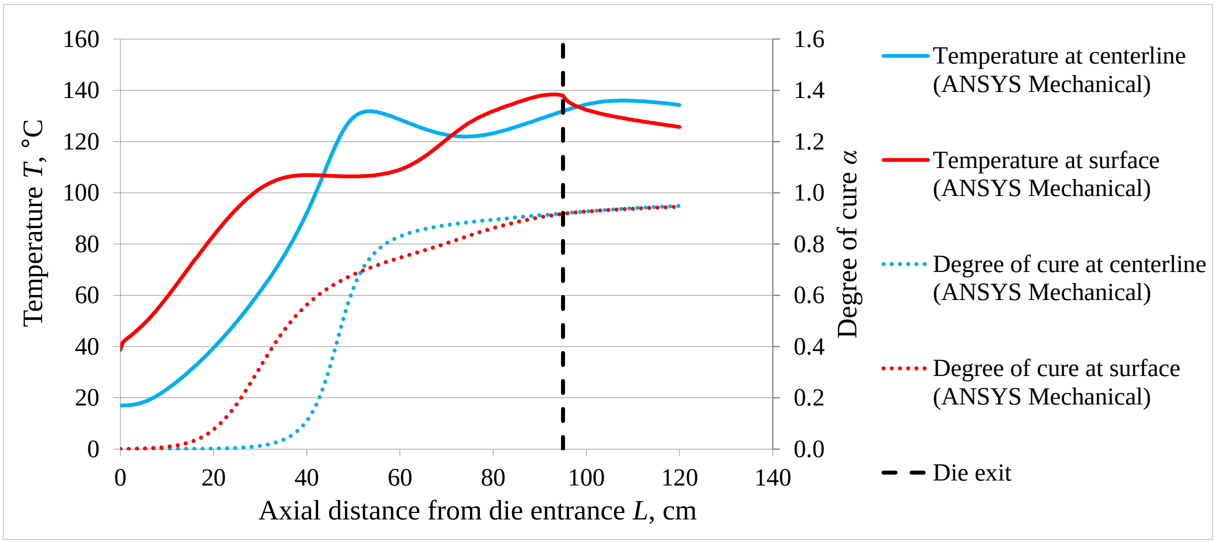

Figure 4.23. Final distribution of temperature and degree of cure along the composite profile after correction of the control temperatures and material properties update.

4.3. Finite element simulation in *ANSYS CFX*

To validate the *ANSYS CFX* based calculation algorithm, the problem in the final formulation has been solved in *ANSYS CFX*.

The finite element model for a simulation of pultrusion has been created in *ANSYS CFX* by using structured hexahedral mesh for composite and unstructured tetrahedral mesh for die. The tetra-element has four nodes and single degree of freedom – temperature. The hexa-element has eight nodes and two degrees of freedom – temperature and extra scalar parameter equal to α. Taking into account symmetry of the examined problem, only a quarter of the die and the composite is modelled. The composite mesh is regular in pull direction and has 43 898 elements and 56 100 nodes with characteristic size of elements 1.5 mm. Die mesh is irregular and has 322 260 elements and 65 440 nodes with characteristic size of elements 1.5 mm for heaters, thermocouples and zones near composite profile and 5 mm for the main part of the die. Fragment of the FE model is presented in Figure 4.24. Due to *ANSYS CFX* software limitations, an isotropic thermal conductivity as lumped composite material property had to be considered with the average value of k_x and k_y (Table 4.2): k_{av} = 0.625 W/(m · °C). The transient analysis with a total simulation time of 3500 s and time step of 0.35 s is applied for a modelling of the pultrusion process.

Results of this simulation together with experiment results and results obtained by *ANSYS Mechanical* are given in Figures 4.25-4.28. Slight difference is observed for temperature and degree of cure curves obtained by *ANSYS Mechanical* and *ANSYS CFX*.

To ensure that this difference is caused by different pultruded material thermal conductivity used in the simulation and is not connected with the simulation algorithm additional simulation has been performed in *ANSYS Mechanical* using averaged lumped thermal conductivity of profile material used in *ANSYS CFX*. Results of this simulation are given in Figures 4.29-4.32. Now it is clear that difference obtained previously is connected only with different material properties used in the simulations.

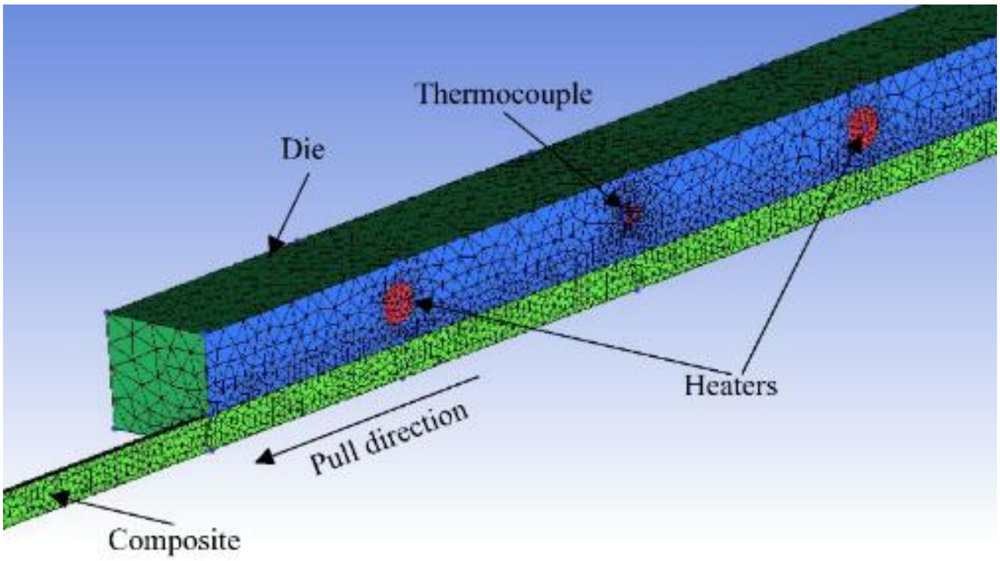

Figure 4.24. Fragment of the finite element model.

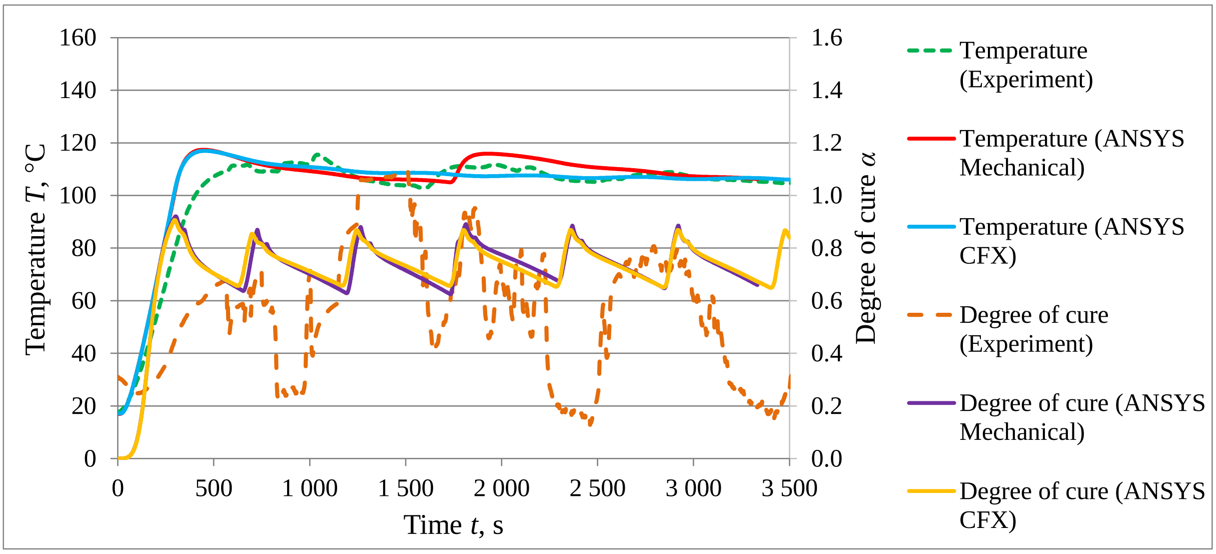

Figure 4.25. Temperature and degree of cure on sensor 1 obtained by *ANSYS Mechanical* and *ANSYS CFX*.

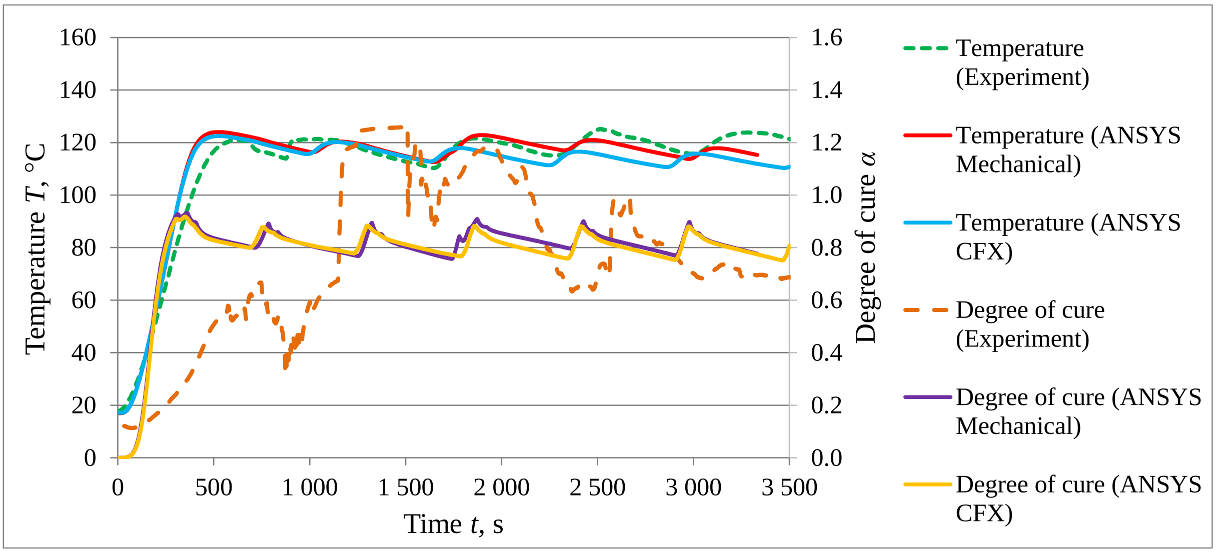

Figure 4.26. Temperature and degree of cure on sensor 2 obtained by *ANSYS Mechanical* and *ANSYS CFX*.

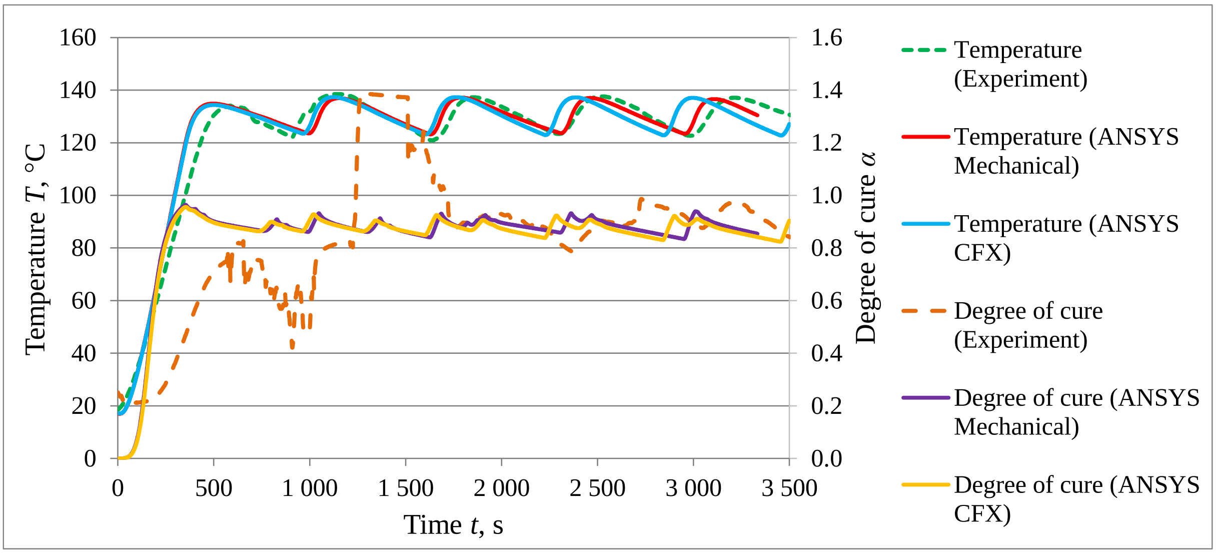

Figure 4.27. Temperature and degree of cure on sensor 3 obtained by *ANSYS Mechanical* and *ANSYS CFX*.

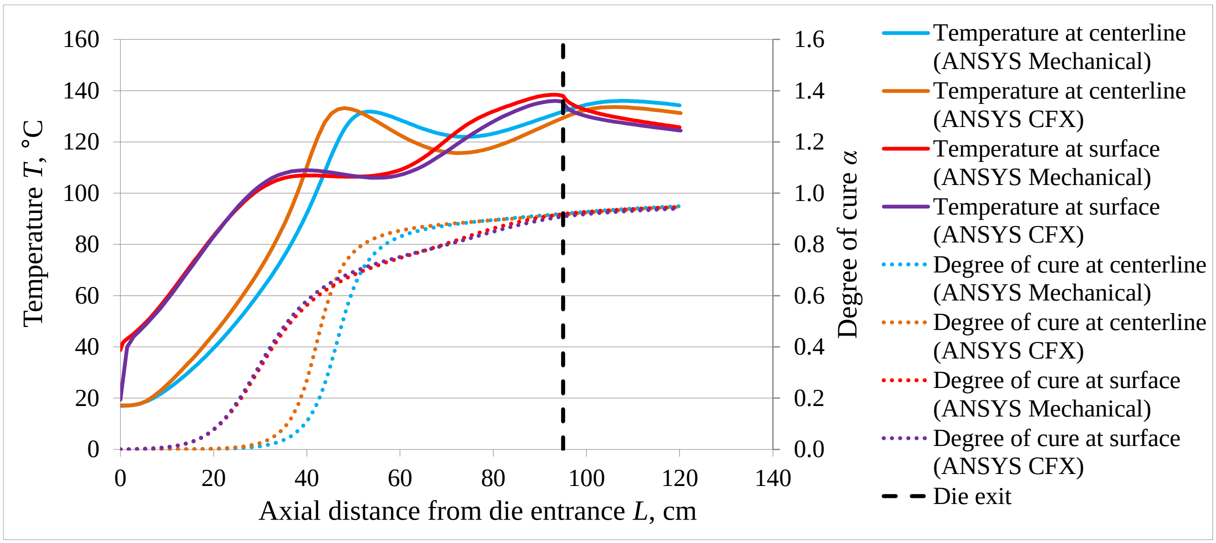

Figure 4.28. Final distribution of temperature and degree of cure along the composite profile obtained by *ANSYS Mechanical* and *ANSYS CFX*.

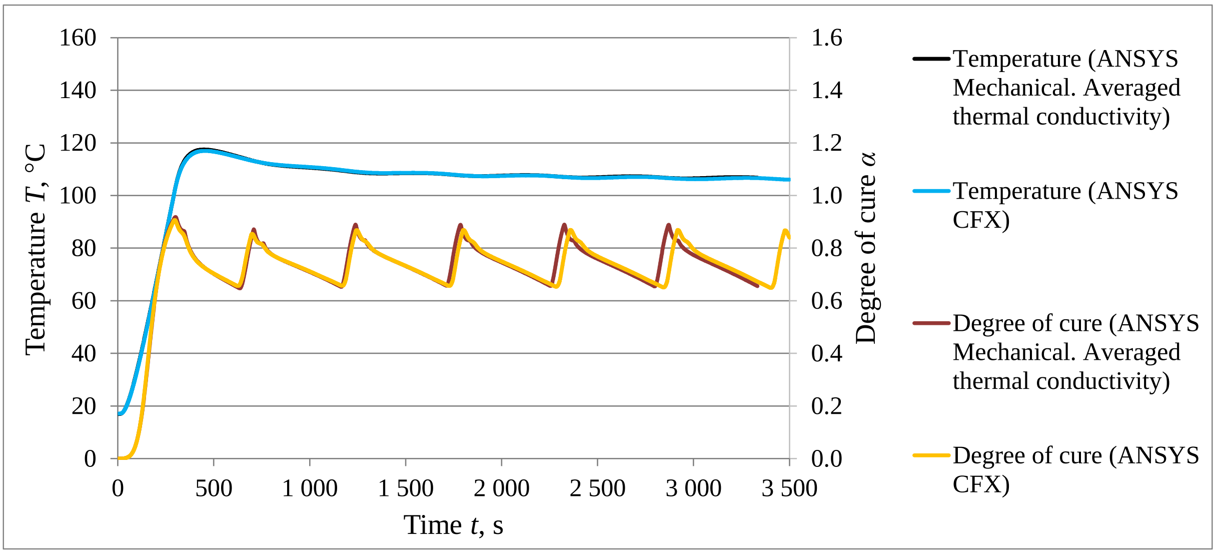

Figure 4.29. Temperature and degree of cure on sensor 1 obtained by *ANSYS Mechanical* and *ANSYS CFX*.

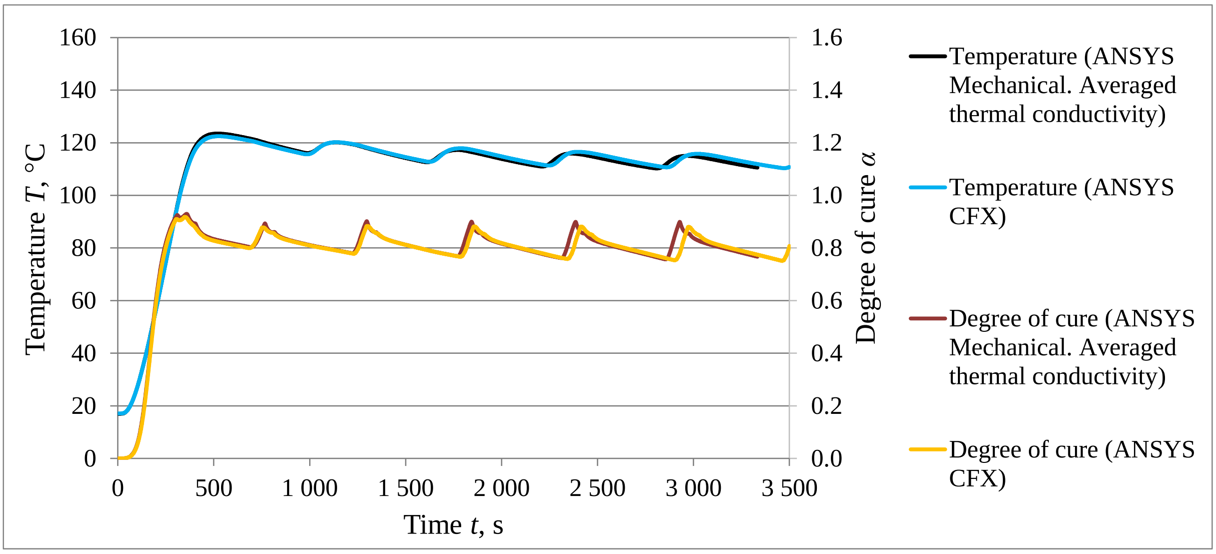

Figure 4.30. Temperature and degree of cure on sensor 2 obtained by *ANSYS Mechanical* and *ANSYS CFX*.

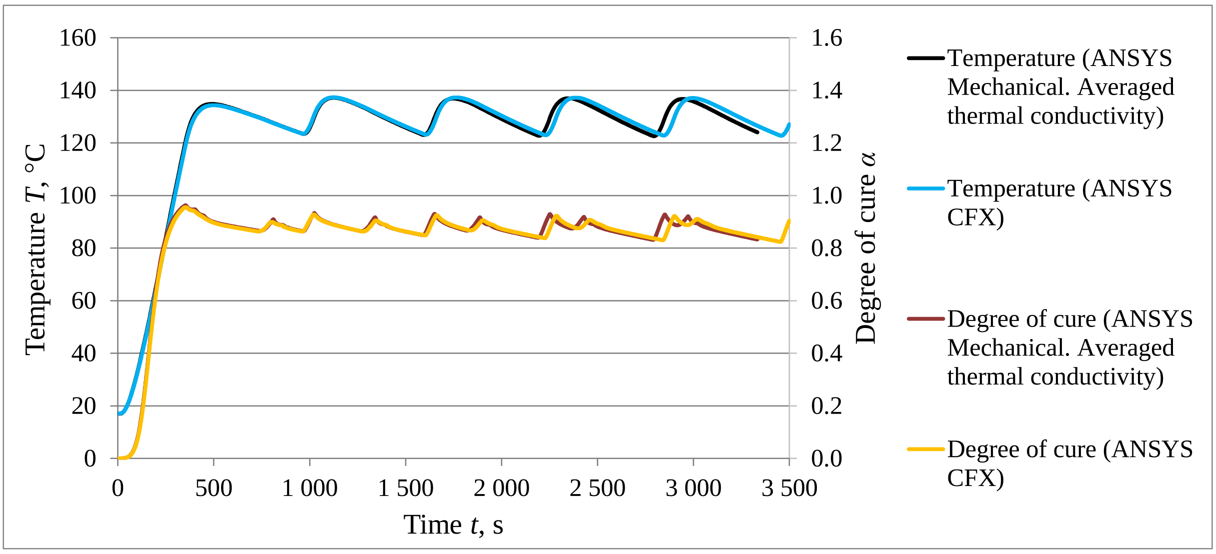

Figure 4.31. Temperature and degree of cure on sensor 3 obtained by *ANSYS Mechanical* and *ANSYS CFX*.

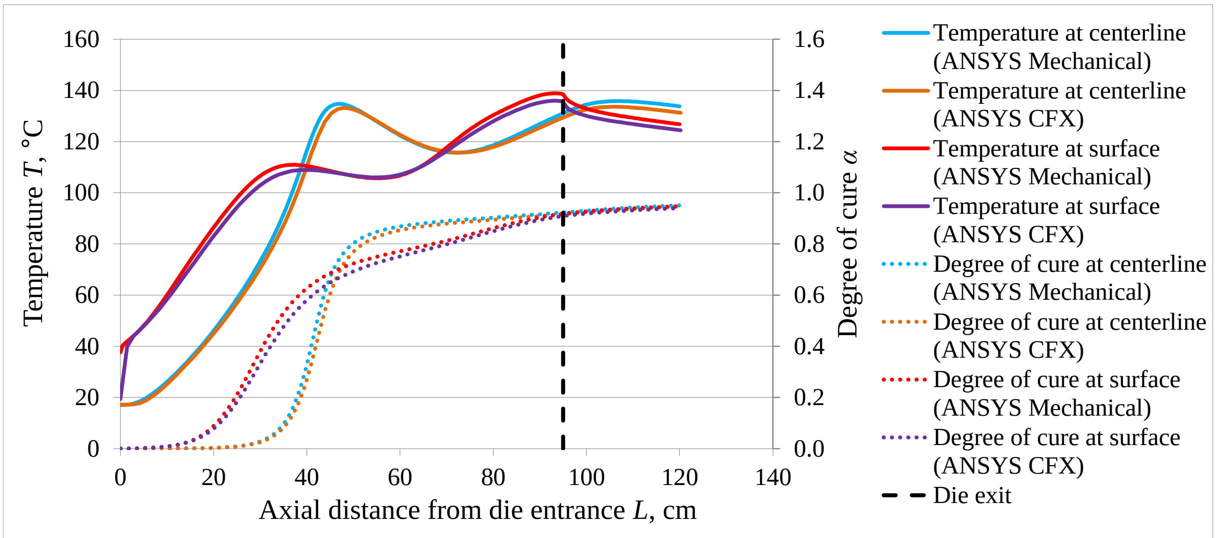

Figure 4.32. Final distribution of temperature and degree of cure along the composite profile.

5. MODELLING OF MICROWAVE ASSISTED PULTRUSION PROCESSES

To provide better understanding of the microwave assisted pultrusion process, to support the pultrusion tooling design and process control, new simulation methodology consisting of two sub-models is developed. Each of the sub-models is constructed by using the general-purpose FE software that results in considerable savings in development time and costs, and also makes available various modelling features of the FE package. In the first step the electromagnetic sub-model is used to evaluate the electric field distribution by using the *COMSOL Multiphysics* software. In the second step an absorption energy field obtained in the composite material is applied as a heating source in the thermochemical sub-model developed in *ANSYS Mechanical* environment to determine temperature and degree of cure fields in the pultruded composite. To demonstrate an application of the developed methodology for the design of technological process, the microwave assisted pultrusion of the cylindrical rod is investigated. Conditions of the advanced pultrusion process, and the temperature and degree of cure fields in the composite material, are determined for the design of modular pultrusion die consisting of microwave block with the ceramic inlet located at the entrance of the steel die. To obtain desired characteristics of the investigated pultrusion process, an influence of the capacity of the absorption energy field, thermal insulation, preheating of steel die, heating of resin bath and reduction of the steel die length on the parameters of pultrusion process are studied.

5.1. Statement of the electromagnetic and thermochemical problems

For a numerical simulation of the microwave assisted pultrusion process it is necessary to solve two coupled multiphysical problems - electromagnetic and thermochemical [15]. The electromagnetic problem is solved with the purpose to determine the electric field distribution and as the result to obtain the absorbed energy field in the composite material which will be used later as a heating source in the subsequent thermochemical problem. Solving the last problem, the temperature and degree of cure fields in the pultruded composite could be estimated.

Using the common approach of a harmonic oscillating electric field $\vec{E}$

$$\vec{E}(\vec{r},t)=\vec{E}(\vec{r})\cdot e^{2\pi i f} \tag{5.1}$$

where $\vec{r}$ is the location vector;
t is a time, s;
f is the microwave frequency, Hz.

Maxwell's equations could be written as following:

$$\nabla\times\nabla\times\vec{E}(\vec{r})-\varepsilon_0\mu_0(2\pi f)^2\varepsilon_r\vec{E}(\vec{r})=\vec{0} \tag{5.2}$$

where ε_0 is the vacuum permittivity, Fa/m;
μ_0 is the magnetic constant, H/m.

This complex valued equation is solved numerically for the amplitudes of the electric field $\vec{E}(\vec{r})$ with respect to the relative permittivity ε_r which for loss dielectric materials like mixtures of glass fibers and polyester resin is a complex function of frequency f, temperature T and degree of cure α:

$$\varepsilon_r(f,T,\alpha)=\varepsilon'(f,T,\alpha)-i\cdot\varepsilon''(f,T,\alpha) \tag{5.3}$$

It can be obtained by the cavity perturbation method [71] at fixed frequencies or Corbino probe measurements [35, 36] with variable frequency. After numerical solution of Equation (5.2), the absorbed microwave energy generated by dielectric losses could be obtained like in paper [63]:

$$Q(\vec{r})=2\pi f\varepsilon_0\varepsilon''\left|\vec{E}(\vec{r})\right|^2 \tag{5.4}$$

The absorption energy Q in the composite material is introduced into corresponding energy equation of the thermochemical problem (Equation (2.1)):

$$\begin{cases} \rho c_p\dfrac{\partial T}{\partial t}-\dfrac{\partial}{\partial x}\left(k_x\dfrac{\partial T}{\partial x}\right)-\dfrac{\partial}{\partial y}\left(k_y\dfrac{\partial T}{\partial y}\right)-\dfrac{\partial}{\partial z}\left(k_z\dfrac{\partial T}{\partial z}\right)-q_b=0 \\ \bar{\rho}\,\bar{c}_p\left(\dfrac{\partial T}{\partial t}+u\dfrac{\partial T}{\partial x}\right)-\dfrac{\partial}{\partial x}\left(\bar{k}_x\dfrac{\partial T}{\partial x}\right)-\dfrac{\partial}{\partial y}\left(\bar{k}_y\dfrac{\partial T}{\partial y}\right)-\dfrac{\partial}{\partial z}\left(\bar{k}_z\dfrac{\partial T}{\partial z}\right)-q-Q=0 \\ \left(\dfrac{\partial\alpha}{\partial t}+u\dfrac{\partial\alpha}{\partial x}\right)=R_r \end{cases} \tag{5.5}$$

Then this problem could be solved numerically by approaches developed in Chapter 2.

5.2. Numerical simulation procedures

The developed algorithms simulate the phenomenon of microwave assisted pultrusion by solving the set of coupled electromagnetic, energy and species equations.

5.2.1. Electromagnetic sub-model

The targeted application of an industrial microwave pultrusion process comes along with two major requirements: the usage of a cost-effective microwave source with a power output in the range of some kW and the capability to generate a homogeneous microwave field distribution for the complete products cross section. As magnetrons provide sufficient power output at fixed frequencies very economically it is obvious to use a magnetron as microwave source working at one of the ISM-frequency-bands (Industrial Scientific and Medical use).

The cross-section of the products is predetermined and the first step of the problem is to design the base model of a microwave set-up with an analytically known field distribution most suitable for the requested cross-section. In a second step, the model is improved numerically towards a homogeneous field distribution and high efficiency of the provided energy. This is performed adjusting the models dimensions and variation of some material properties until the target specifications are reached (Figure 5.1). For the electromagnetic sub-model the FEM software package *COMSOL Multiphysics* is used with the optional radiofrequency (RF) module.

Against standard design drawings, for the simulation of microwave phenomena it is necessary to generate a design defining a closed (e.g. metallic) structure from electric point of view and allocate material properties in every region inside – especially the "air" typically left out as logical region in design drawings – is almost important for wave propagation. On the other hand, the thickness of solid metallic machinery parts is rarely important, because their surfaces usually are treated as perfect electric conductor. The microwave field is reflected at the surface and does not penetrate into the metallic regions – so they can be left out in the drawing.

According to the Nyquist-Shannon sampling theorem [67] for the discrete sampling of a wave function, the maximum element size $x_{\max}$ of the mesh applied to the geometry has to fulfil $x_{\max} < \lambda/2$ with λ - local wavelength. Local wavelength means that λ might be shorten by dielectric materials or influenced by conductive parts so that a good value for the maximum mesh element size is given by $x_{\max} < \lambda_0/20\sqrt{\varepsilon_{\mathrm{r}}}$ with λ_0 - the wavelength in free space and ε_r - the relative permittivity.

For this mesh Equation (5.2) can be solved for the amplitude of the electric field $\vec{E}(\vec{r})$ with respect to the local material properties from Equation (5.3) by iterative or direct solvers in the frequency domain with the fixed frequency f of the magnetron. The wave excitation and thereby the power input is applied by a so called "port" boundary condition provided by the RF – module. Then the absorbed energy Q can be calculated using Equation (5.4) and evaluated regarding homogeneity and efficiency.

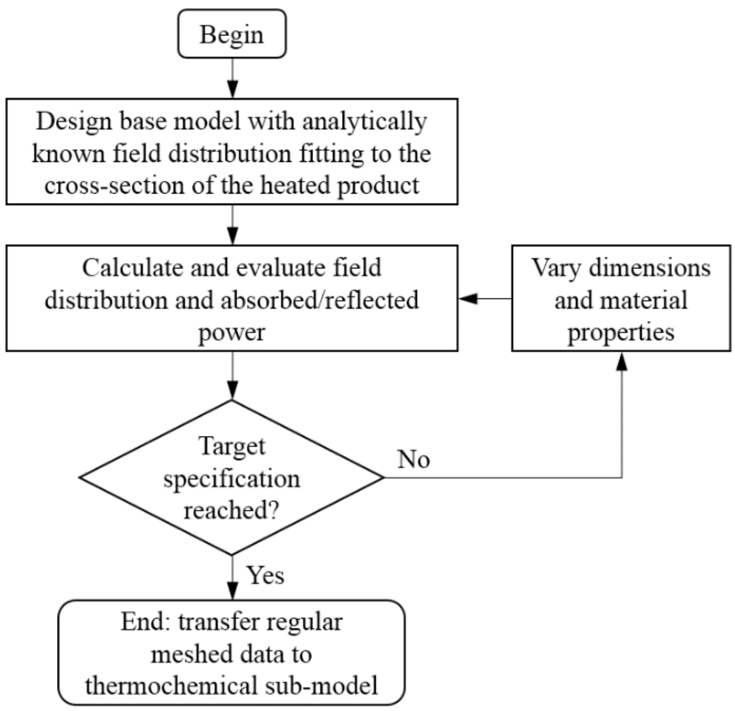

Figure 5.1. Flowchart of the numerical procedure based on *COMSOL Multiphysics*.

5.2.2. Thermochemical sub-model

Thermochemical model (Chapter 2.1) and its numerical implementation for *ANSYS Mechanical* (Chapter 2.2.1) is used for simulation of microwave assisted pultrusion process. Absorption energy field transferred from *COMSOL Multiphysics* is used in *ANSYS Mechanical* as heat energy source.

5.3. Microwave assisted pultrusion of cylindrical rod

To demonstrate an application of the developed methodology for the design of technological process, the microwave assisted pultrusion of the cylindrical rod with the diameter of 16 mm and made of glass fibers *Unifilo 4800 tex* and polyester resin *POLRES 305BV* has been investigated.

5.3.1. Analysis with electromagnetic sub-model

In the present case, the base model has to provide a symmetric cylindrical field distribution with an extended maximum of electrical field covering the products diameter. As starting point, an electric maximum of a standing wave pattern in a shorted rectangular waveguide section is used. To minimize reflection losses the waveguide has been tapered to the dimensions of the pultrusion die. The centerpiece of the microwave system consists out of a ceramic part (ZrO_2) with a 16 mm hole, which has been inserted as a section into the metal pultrusion die. The objective was that the microwave field inside the hole and therefore inside the rod running through that hole is as homogenous as possible. The Zirconium oxide has a very high real part of the permittivity ε', which shortens the wave length of the microwaves. Therefore a magnetron of frequency 915 MHz and a waveguide *WR 975* have been chosen.

Figure 5.2 shows the scheme of the electromagnetic sub-model for microwave pultrusion with the ceramic inlet and coupling of the microwave to the ceramic part with a waveguide. The different color has indicated the different parts and the materials. Dark blue indicates steel (pultrusion die), light blue - air (waveguide), red - ceramic (inlet) and green - product (rod). The dielectric properties ε_r of the glass fiber/polyester resin composition have been measured before with a cavity perturbation method versus temperature and mean values taken at a temperature of T = 60 °C have been used for the calculation of the electric field distribution.

Running through the optimization loop is shown in Figure 5.1 several times, the shape of the ceramic inlay has been adjusted to achieve a homogeneous field distribution inside the rod and a minimized power reflection. Dielectric material properties (dielectric constant ε' and dielectric loss ε'') are specified in Table 5.1.

Figure 5.3 shows the distribution of the resulting absorption energy field Q in different 3D and cross-sectional views for the optimized geometry of the ceramic inlay. In Figures 5.3*a* and 5.3*b* it is obviously, that only the rod inside the ceramic inlet is heated. The microwave coupling and the pultrusion die are not heated by the microwave. Outside of the ceramic inlet the microwave field is close to zero. Figure 5.3*c* shows the cross-section of the absorption energy field in the die and the waveguide. The absorption energy field is homogeneously concentrated in the rod. Additionally a small heating effect inside the ceramic material itself gets visible.

In detail the power density in the cross-section of the rod is about 7000 W/m^3 inside the ceramic inlet but outside the rod it is between 200 and 800 W/m^3 (Figure 5.4). The deviation of the power density is low, therefore the heating is homogenous. The power density is concentrated to the cross-section of the rod. Figure 5.4 shows the power density in the cross-section of the ceramic pultrusion die. The power is concentrated to about 16 mm along the rod with a variation of about 7 %.

5.3.2. Analysis with thermochemical sub-model

The thermochemical analysis means determination of the temperature and degree of cure fields in the composite material travelling in the pultrusion die. In our case the absorption energy field in the composite material determined with *COMSOL Multiphysics* is used as a heating source in the pultrusion process modelled with *ANSYS Mechanical*.

The advanced pultrusion die consists of microwave block with the ceramic inlet located at the entrance of the steel die (Figure 5.5). The thermal properties of steel material used for an advanced die production and the ceramic inlet are given in Table 5.2.

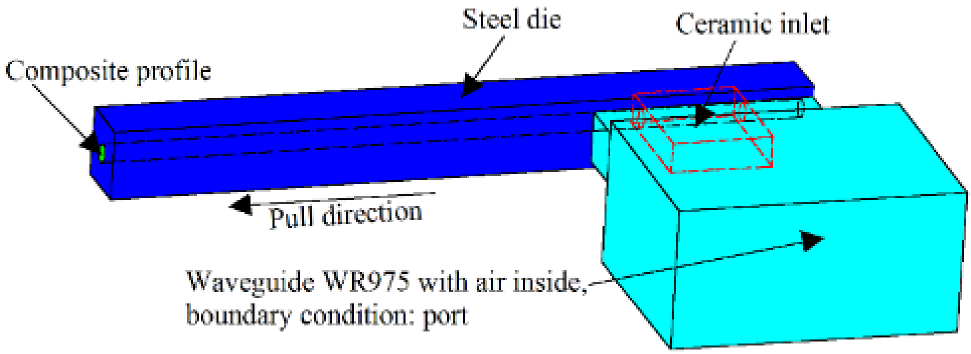

Figure 5.2. Scheme of the electromagnetic model.

Table 5.1.

Parameters of the electromagnetic sub-model

	ε'	ε''
Steel *40Cr*	perfect conductor	
Zirconia ceramic	29	0.2
Lumped composite	5.7	0.32
Air (in waveguide)	1	0

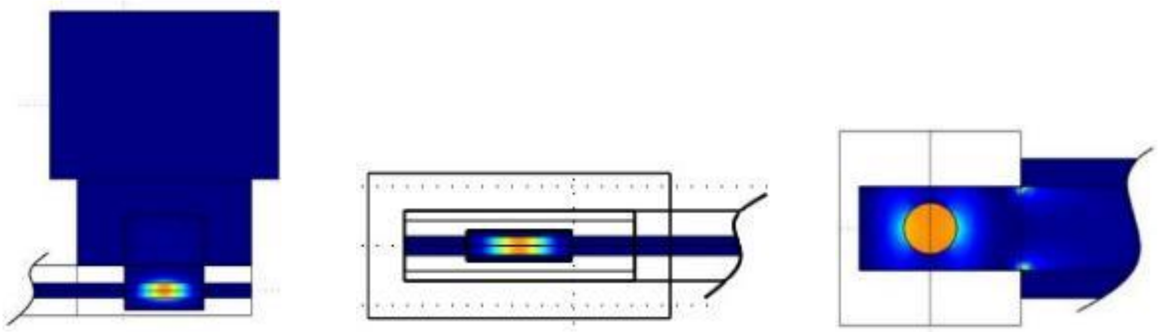

a *b* *c*

Figure 5.3. Distribution of the absorption energy field Q : top-view (*a*), side-view (*b*) and cross-section (*c*).

Heating of the composite profile is realized by using an absorption energy field obtained by *COMSOL Multiphysics*. It is simulated only in the composite material within boundaries of the ceramic inlet. Distribution of the absorption energy in the cross-section of the profile is constant (Figure 5.4) but in the longitudinal direction varies accordingly to the law demonstrated in Figure 5.6. Integrating the curve presented in Figure 5.6 and taking into account area of the profile cross-section, it is possible to obtain the total absorption energy which is equal to 100.2 W. The simulated absorption energy field with the total value of 95.8 W is shown in Figure 5.7. It is necessary to note that temperature control is not applied in this case, and energy source is working continuously. Parameters of the pultrusion process are presented in Table 5.3.

The materials used for a production of the cylindrical rod are glass fibers *Unifilo 4800 tex* (mass content of 70 %) and polyester resin *POLRES 305BV*. Thermal properties of the fiber and resin are given in Table 4.2. The rate of resin reaction is described by using the Kamal-Sourour curing kinetic model (Equation (3.5)) with the parameters presented in Table 3.4. To increase the microwave energy absorption properties of the resin a filler *Martinal* of mass content of 20 % is added to the resin. Thermal properties of the filler and lumped properties of profile material are presented in Table 5.2.

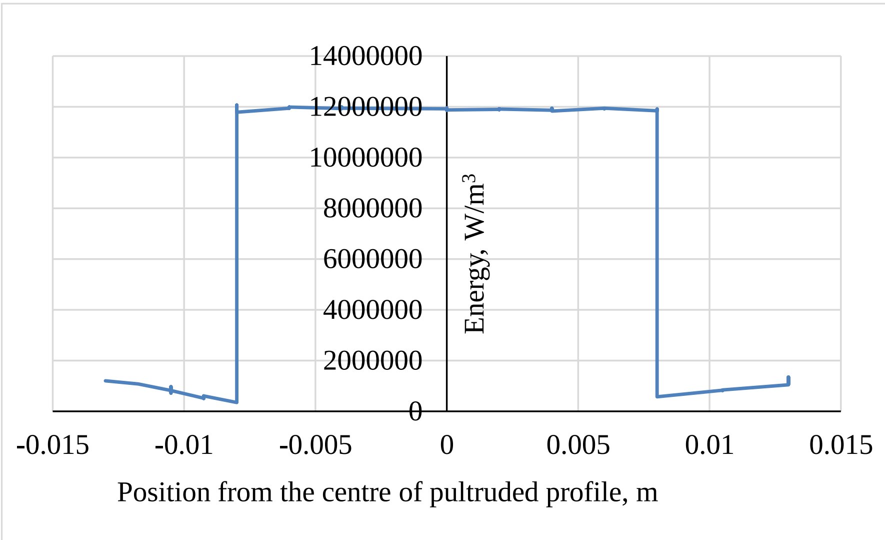

Figure 5.4. Distribution of the absorption energy in the cross-section of the ceramic pultrusion die.

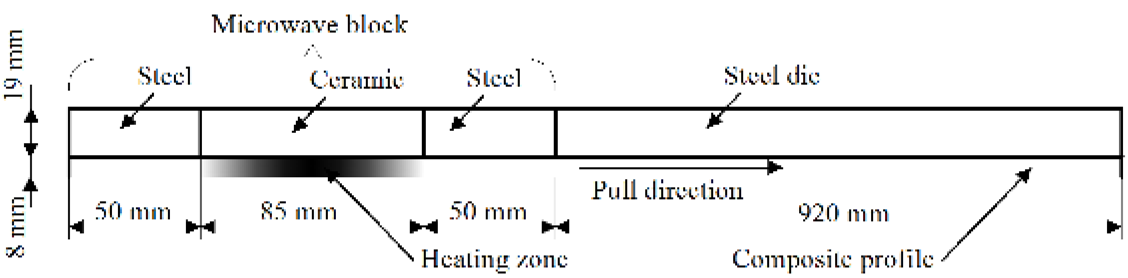

Figure 5.5. Scheme of the advanced pultrusion die.

Table 5.2.

Thermal properties of materials

	ρ, kg/m^3	c_p, J/(kg · °C)	k_x, W/(m · °C)	$k_y = k_z$ W/(m · °C)	Max allowable *T*, °C
Steel *40Cr*	7720	470	42.6	42.6	-
Zirconia ceramic	6000	418	2	2	-
Filler *MARTINAL*	2420	1450	0.21	0.21	280
Lumped composite	1912	1278	0.667	0.468	-

Table 5.3.

Parameters of pultrusion process

Name, unit	Value
Room and resin temperature in the bath, °C	17 or 27 or 37
Pull speed, m/min	0.18 or 0.12 or 0.06

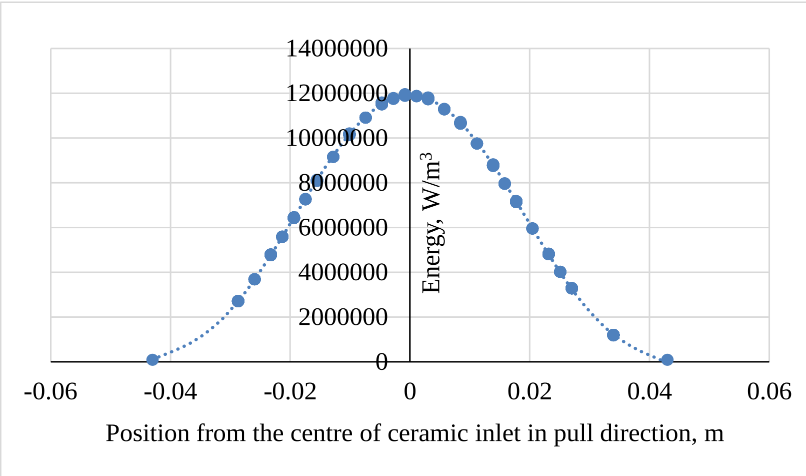

Figure 5.6. Distribution of the absorption energy in the longitudinal direction of the pultruded profile.

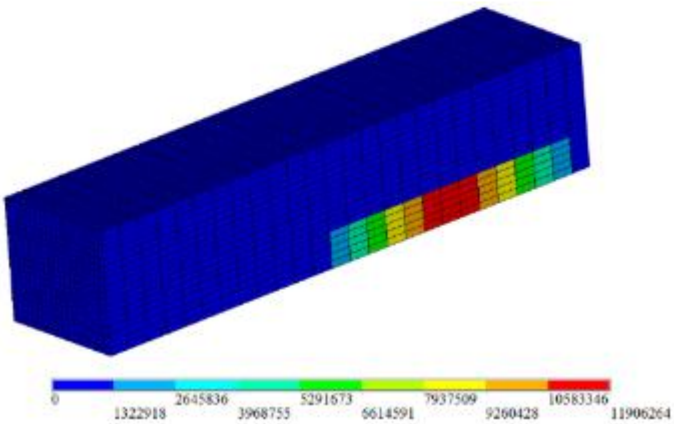

Figure 5.7. Simulation of the absorption energy in the pultruded profile.

The finite element model for a simulation of the cylindrical rod pultrusion has been created in *ANSYS Mechanical* by using 3-D thermal solid finite elements *Solid 70*. Using symmetry of the simulated domain, only a quarter of advanced pultrusion die is modelled. A fragment of the finite element model is presented in Figure 5.8. The finite element mesh is regular in pull direction and has 221 elements along the profile. The total number of finite elements is 74 258 (3978 for the composite, 58 512 for the die, 9728 for the steel part of microwave block and 2040 for the ceramic part). The time step of the solution depends on the pull speed. It is equal to 1.67 s for the speed of 18 cm/min, 2.5 s for the speed of 12 cm/min and 5 s for the speed of 6 cm/min. During this time the composite travels in the pull direction on the distance equals to the dimension of one finite element (5 mm). It is necessary to note that iterations (sub-steps) are not performed in the finite element analysis. Initial conditions are applied at time $t = 0$ when all nodal points of the composite have the room temperature and degree of cure equals to $\alpha = 10^{-10}$.

Results of simulation, temperature and degree of cure obtained in the composite at the die exit in dependence on time, are presented in Figure 5.9 for room temperature 27 °C and pull speed of 12 cm/min. It is necessary to note that process is not steady-state after 55 min from the beginning of the numerical experiment in all tests for the degree of cure at the profile surface.

Results of simulation, temperature and degree of cure at the profile centerline and surface, are given for the time 50 min from starting of the pultrusion process in Figure 5.10 for room temperature 27 °C and pull speed 12 cm/min. It is seen that, as opposed to conventional pultrusion process, now the curing comes considerably faster in the profile centerline than on the surface. So high degree of cure in the profile centerline is reached at the beginning of steel die already for the pultrusion process with pull speed equals to 18 cm/min and room temperature equals to 37 °C. Moreover, full curing in the profile centerline happens already in the ceramic inlet for the pultrusion processes with pull speed equals to 6 cm/min and all examined room temperatures while the degree of cure at the profile surface has not reached high values.

To obtain the high value of the degree of cure at the profile surface in the advanced pultrusion die and to increase the pull speed of the process, improving by this way effectiveness of the pultrusion process, an influence of the following parameters of pultrusion process has been investigated:

- reduction in twice of steel die length,
- application of thermal insulation at all external surfaces of advanced pultrusion die (both steel die and microwave block),
- preheating of steel die, excluding microwave block, with the uniform temperature of 60 °C before the beginning of pultrusion process,
- heating of resin bath (composite) with the temperature of 50 °C for the full duration of pultrusion process.

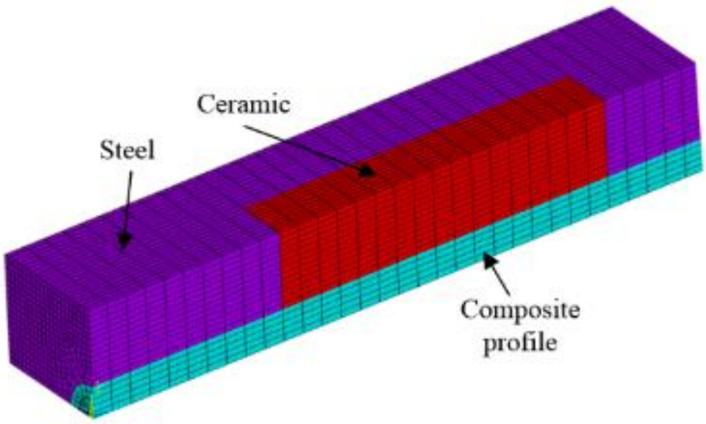

Figure 5.8. Fragment of the finite element model.

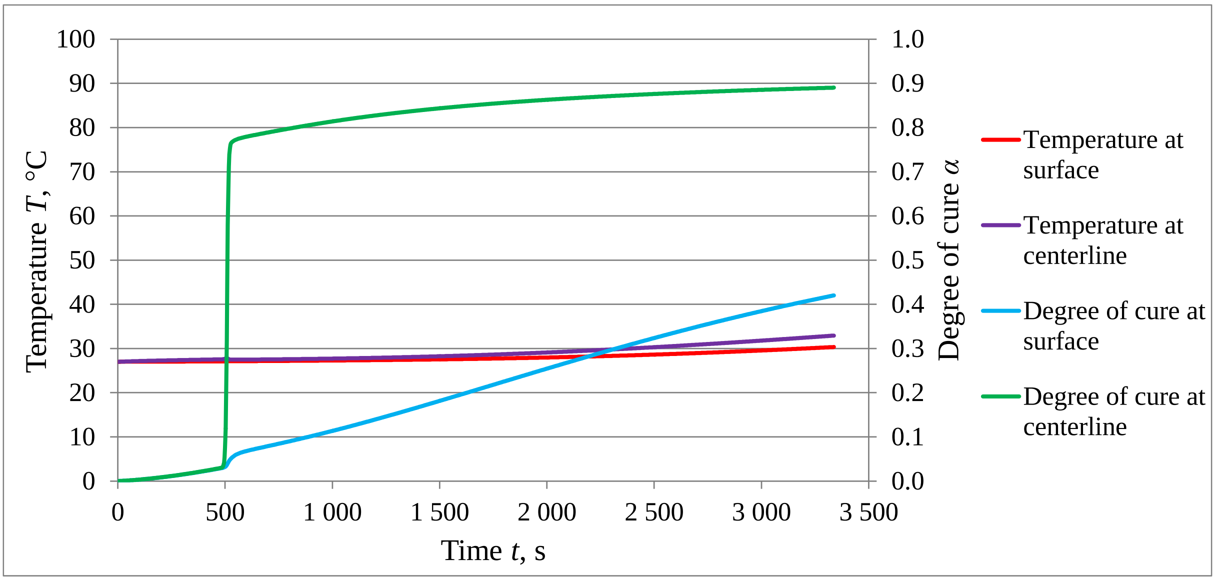

Figure 5.9. Dependence of temperature and degree of cure in the composite at the die exit on time for room temperature 27 °C and pull speed 12 cm/min.

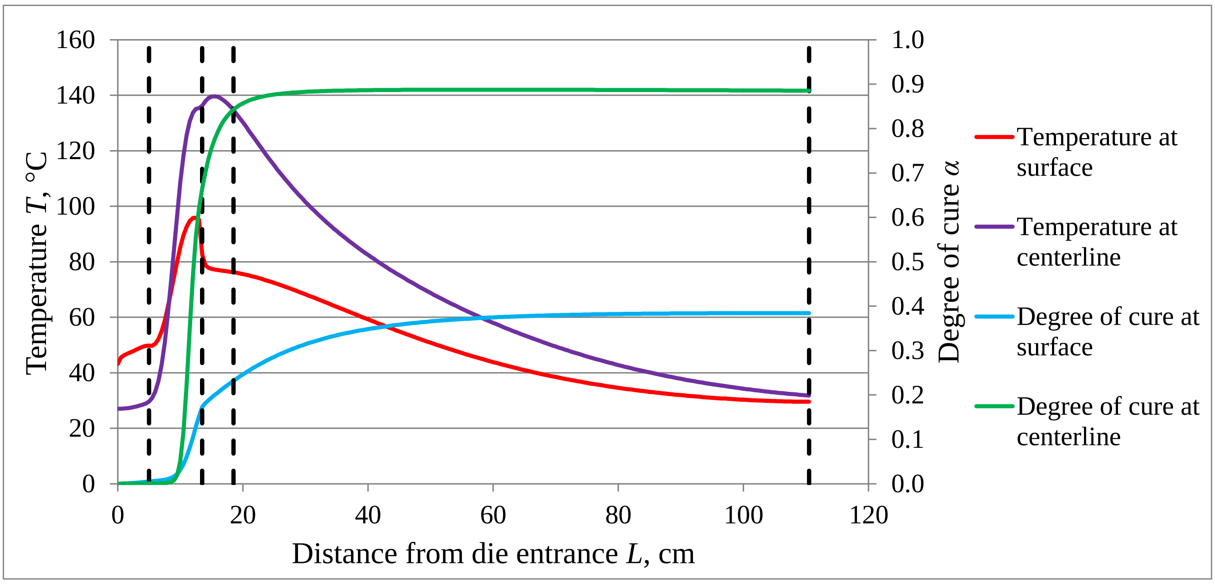

Figure 5.10. Temperature and degree of cure at the profile centerline and surface for room temperature 27 °C and pull speed 12 cm/min.

An influence of the examined factors has been studied for the pultrusion process with the room temperature of 27 °C and pull speed of 12 cm/min. Simulation results are presented in Figures 5.11-5.16.

Figure 5.11 shows that reduction of steel die length has no effect on the degree of cure at the profile surface. However, any reduction of all important parameters has not been observed too. This fact could be used in the design of advanced pultrusion die for a saving of expensive die material. Figure 5.12 demonstrates that an application of thermal insulation at all external surfaces of advanced pultrusion die has increased considerably by 36 % the value of the degree of cure at the profile surface. Figure 5.13 shows that only by preheating of steel die with the temperature of 60 °C before the beginning of pultrusion process, it is possible to increase considerably by 29 % the value of the degree of cure at the profile surface. These effects could be effectively used in the design of advanced pultrusion die. Figure 5.14 demonstrates that heating of resin bath has increased considerably by 44 % the value of the degree of cure at the profile surface that could be used also in the design of advanced pultrusion die. However, it is necessary to note that an effectiveness of the pultrusion process could be not so high since the heating of resin bath is realized for the full duration of pultrusion process.

Joint influence of two factors having large effect on the degree of cure at the profile surface and on the process effectiveness, namely an application of thermal insulation and preheating of steel die, has been investigated additionally. Figure 5.15 shows that by preheating of steel die with the temperature of 60 °C before the beginning of pultrusion process and applying the thermal insulation, it is possible to increase considerably by 79 % the value of the degree of cure at the profile surface. It is necessary to note that joint influence of two examined factors (79 %) is higher than their separate influence summarized together (65 %).

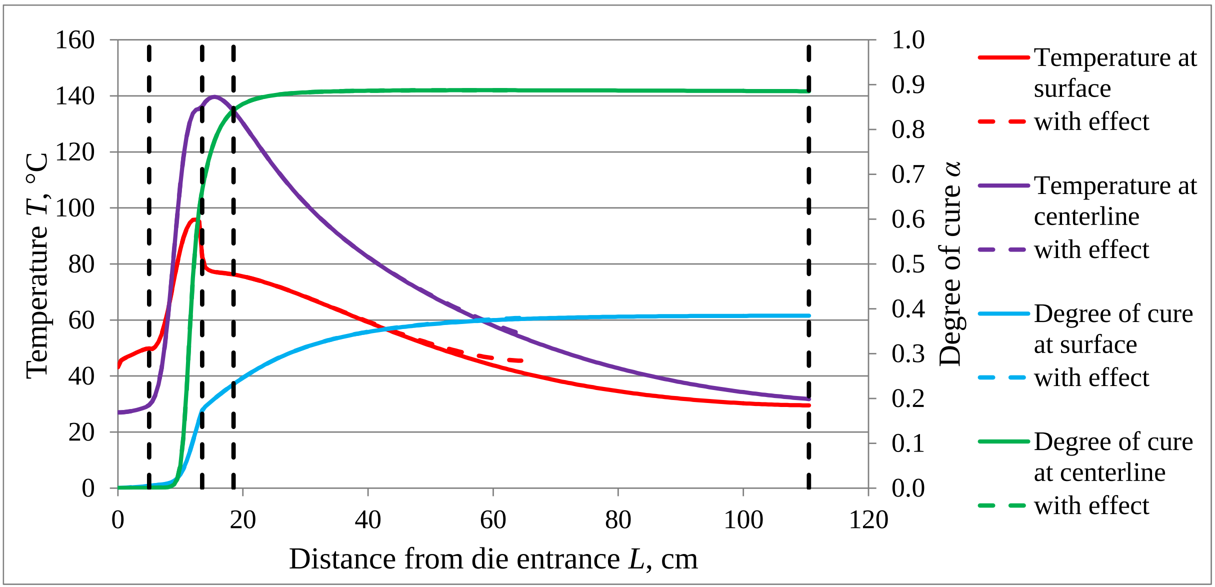

Figure 5.11. Temperature and degree of cure at the profile centerline and surface taking into account the effect of reduction of steel die length.

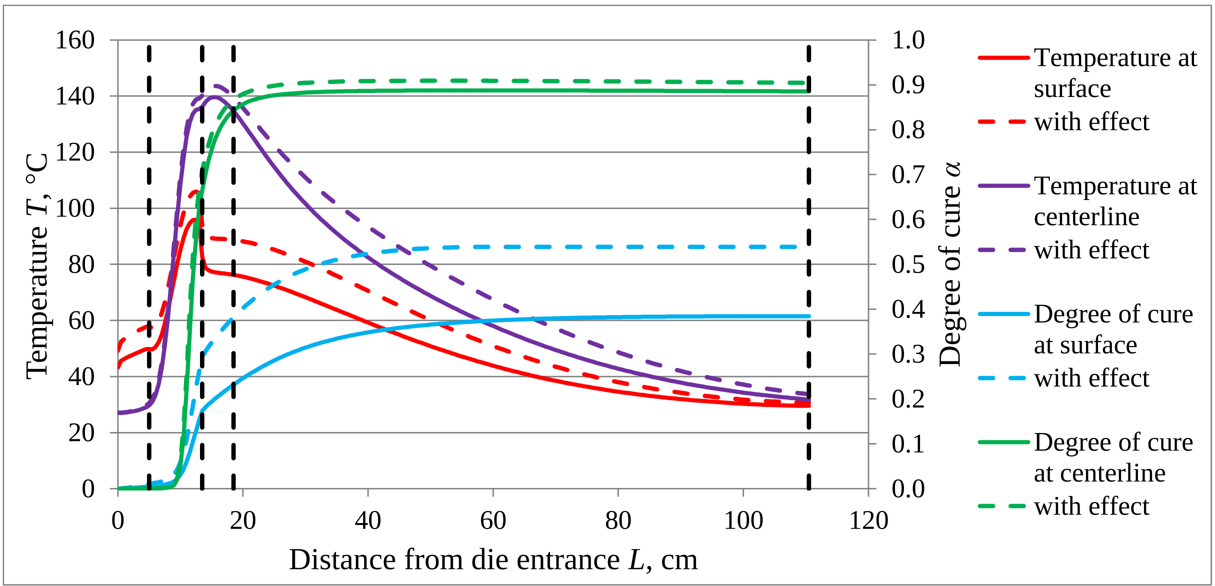

Figure 5.12. Temperature and degree of cure at the profile centerline and surface taking into account the effect of thermal insulation.

To obtain highest values of the degree of cure at the profile surface in the advanced pultrusion die, an influence of the capacity of the absorption energy field on the parameters of pultrusion process has been investigated. It is necessary to note that a distribution of the absorbed energy in the composite profile is not changed while its intensity has been increased proportionally with the coefficients: 1.5, 2.0 and 2.5. Figure 5.16 shows that the high value of the degree of cure at the profile surface could be reached already in the ceramic inlet of the microwave block. However, it is necessary to note that the material temperature in this case could be higher than allowable resin temperature. To avoid overheating of the resin, the pull speed should be increased in the same time that will contribute to the considerable increase of an effectiveness of the microwave assisted pultrusion process.

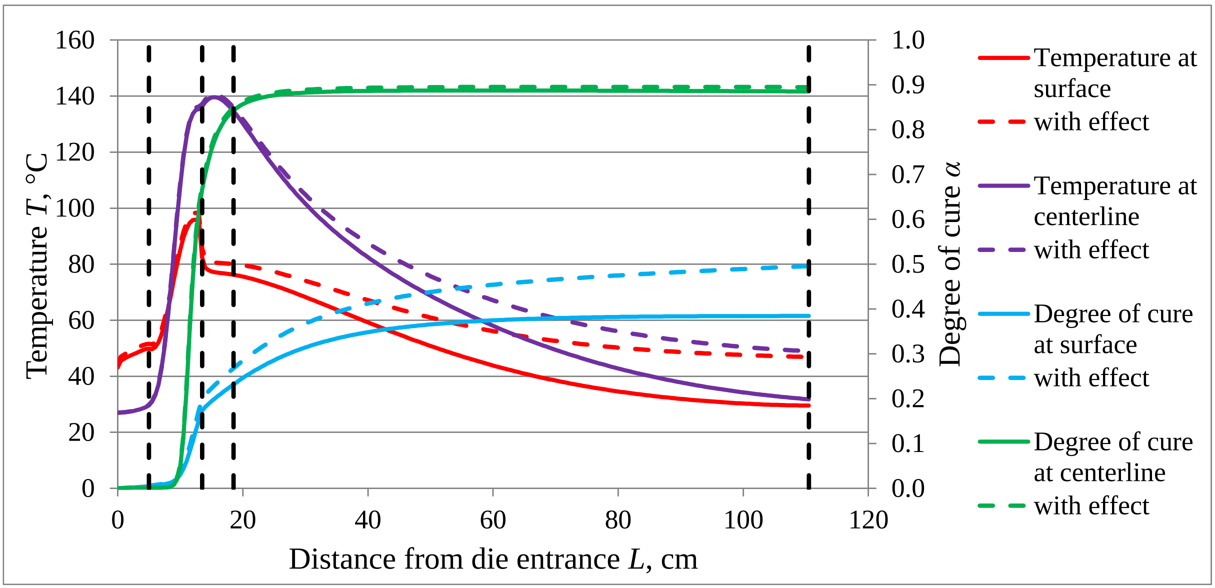

Figure 5.13. Temperature and degree of cure at the profile centerline and surface taking into account the effect of preheating of steel die.

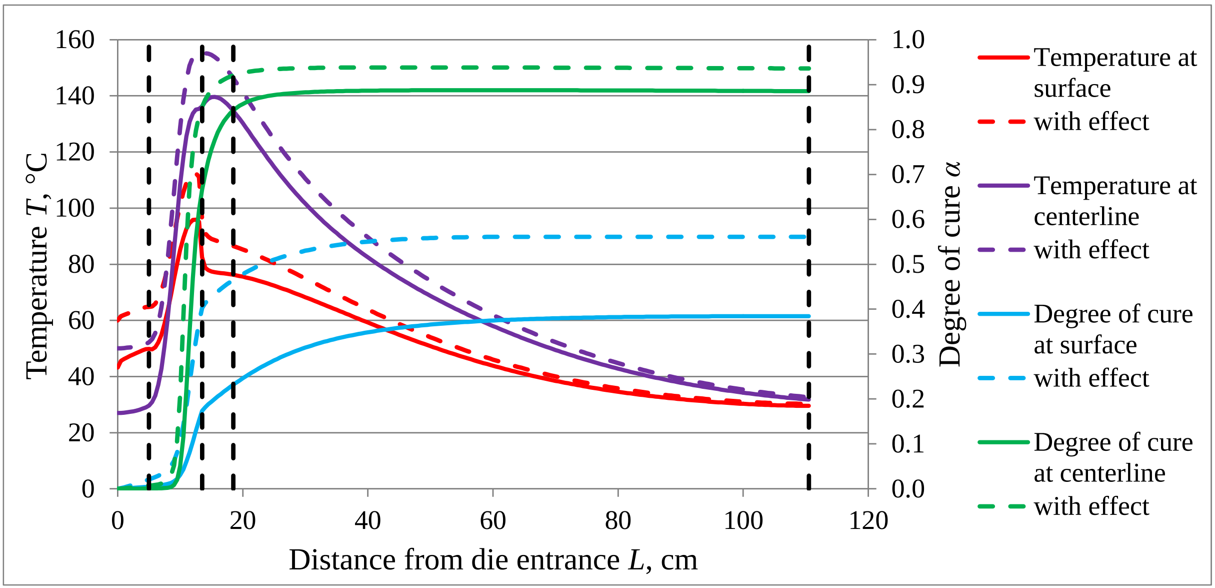

Figure 5.14. Temperature and degree of cure at the profile centerline and surface taking into account the effect of heating of resin bath.

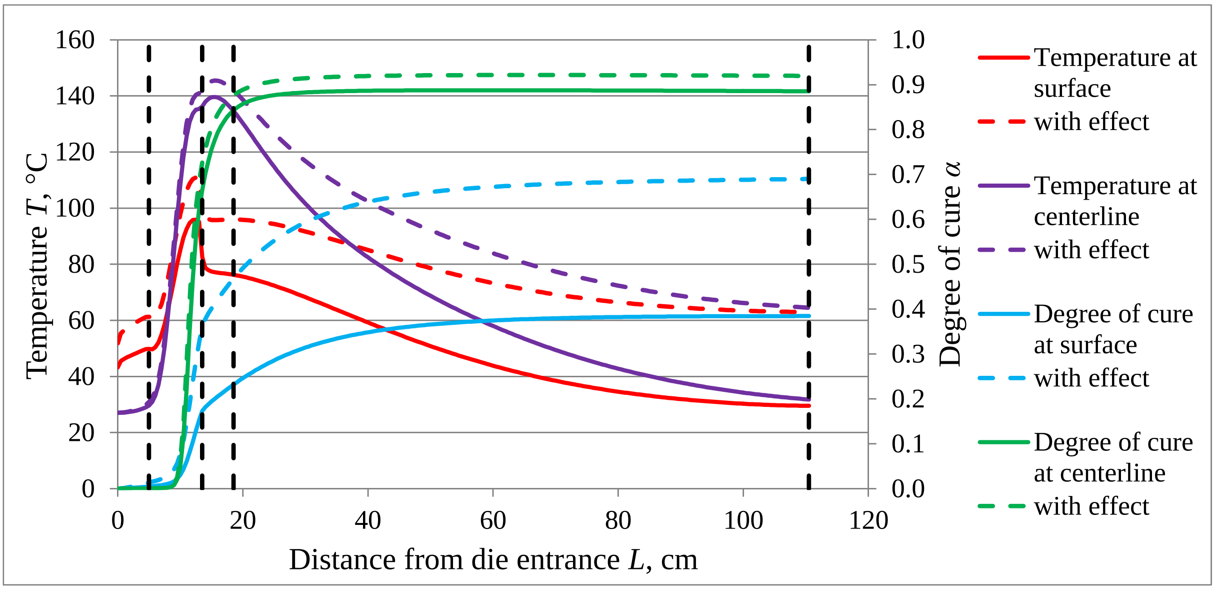

Figure 5.15. Temperature and degree of cure at the profile centerline and surface taking into account the effects of thermal insulation and preheating of steel die.

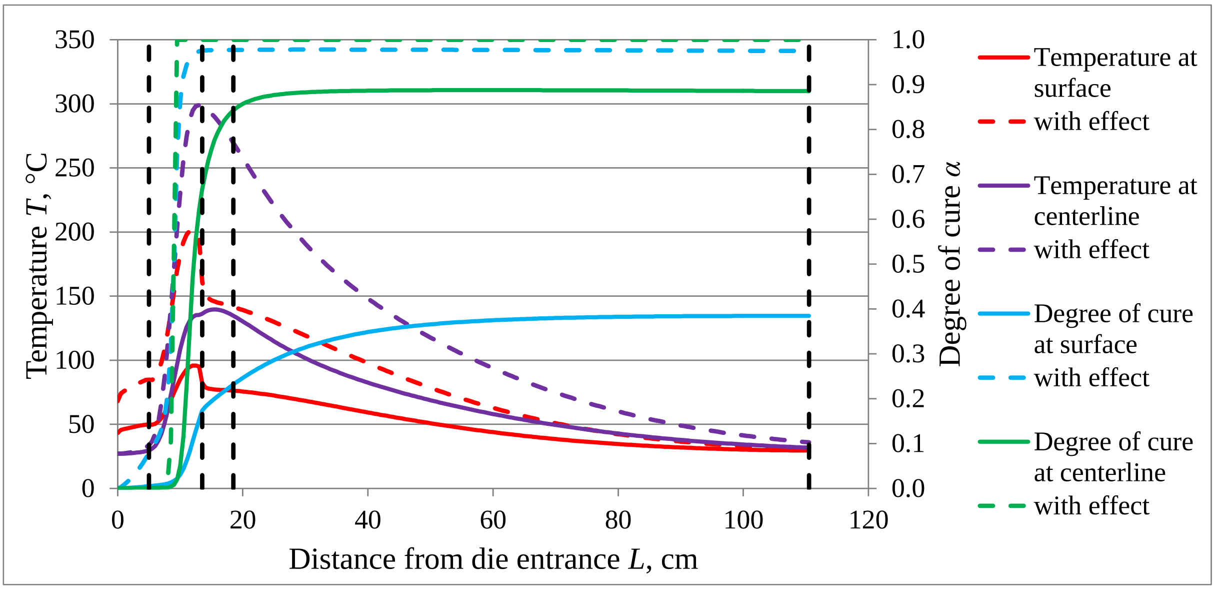

Figure 5.16. Temperature and degree of cure at the profile centerline and surface with the intensity coefficient of the absorption energy field equals to 2.5 (pull speed: 12 cm/min).

6. DESIGN OF MULTIFUNCTIONAL PULTRUSION DIE

The main idea of multifunctional die is to combine profile curing and coating application in one pultrusion die. This advanced process allows to reduce number of manufacturing steps (Figures 1.19 and 1.20). This process is free of VOCs and small particles emission. Also the proposed process has reduced labour and process cost. One more benefit is extraordinary interaction between coating and profile achieved by cure of the coating over a non-fully cured profile. Profile resin degree of cure in range 0.75… 0.85 is required for the best interaction with coating. Scheme of multifunctional pultrusion die is given in Figure 1.21. After the coating application, the profile resin must be fully cured together with coating.

Since the profile resin is cured by microwaves, the profile is heated from centre to surface and curing reaction also starts from centre. Curing reaction is exothermic, therefore theoretically it is possible to cure profile surface and coating by exothermic heat accumulated in profile. Coating injection chamber should be placed as possible closer to the microwave block, because the profile material temperature rises precipitously after the heating zone.

6.1. Multifunctional die with microwave heating

The possibility to cure the coating by the heat generated by microwaves and exothermic profile resin reaction is estimated for the pull speed of 18 cm/min, room temperature of 27 °C and applied microwave energy is 2.35 kW, using modified model used for simulation of microwave assisted pultrusion and shown in Figure 5.5. Coating is applied at distance 100 mm after the microwave block (Figure 6.1). Coating material is epoxy *RESOLTECH RESOLCOAT 2010 FGCS* coat with thermal properties presented in Table 6.1 and curing kinetic parameters presented in Table 3.5. Coating layer thickness is 0.5 mm. Before the injection the coating is preheated to temperature of 50 °C.

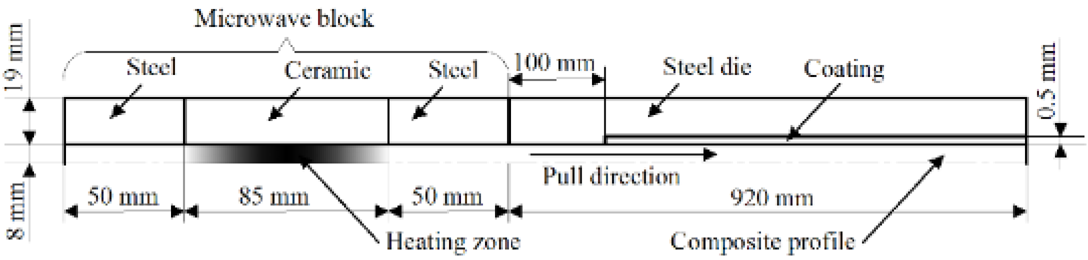

Figure 6.1. Simulation domain.

Table 6.1.

Thermal properties of coating

	ρ, kg/m^3	c_p, J/(kg · °C)	k_x, W/(m · °C)	$k_y = k_z$ W/(m · °C)	Max allowable *T*, °C
Coating *RESOLTECH RESOLCOAT 2010 FGCS*	1500	1630	0.336	0.336	250

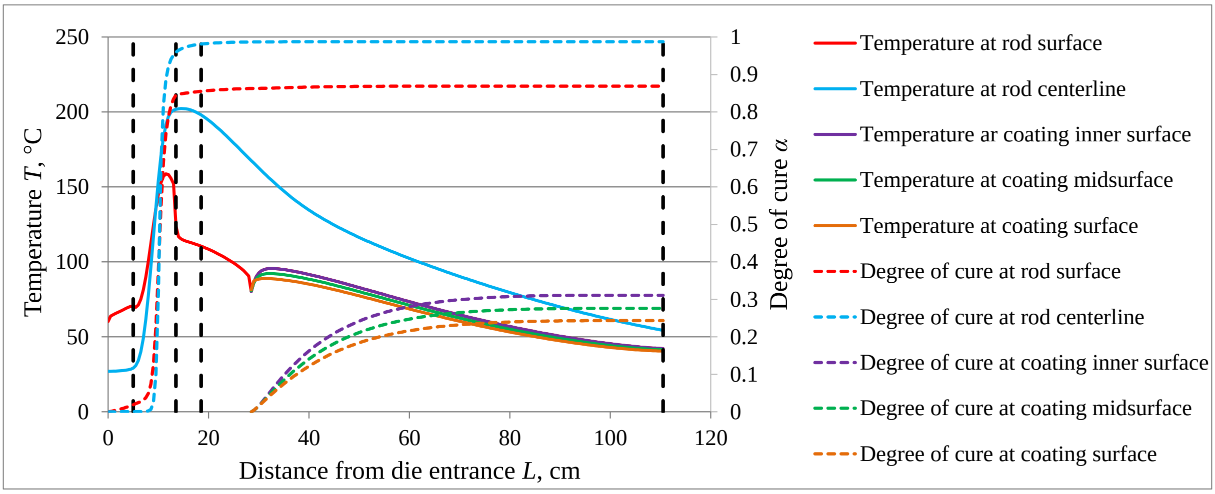

Figure 6.2. Temperature and degree of cure in the profile and coating.

Results of this simulation, temperature and degree of cure at the profile centreline and surface and at the coating inner, middle and outer surfaces are given for the time 50 min from starting of the pultrusion process in Figure 6.2.

In the pultrusion process with microwave heating, the curing is considerably faster on the profile centreline than on the profile surface. So high degree of cure ($\alpha \geq 0.95$) in the profile centreline is reached already at the beginning of steel die right after the microwave block. Degree of cure at the profile surface after the microwave block is equal to the desired value 0.8 (for a good adhesion with coating). It is seen from Figure 6.2 that the applied coating in not completely cured. The degree of cure of the coating on the profile surface is equal to 0.31 but the degree of cure of the coating on its outer surface is 0.24.

To obtain the completely cured coating, an influence of the following parameters of pultrusion process has been investigated:

- application of thermal insulation at all external surfaces of advanced pultrusion tool (both steel die and microwave block),
- preheating of steel die with the uniform temperature of 60 °C before the beginning of pultrusion process,
- joint application of the thermal insulation and preheating of the die.

These simulation results are presented in Figures 6.3-6.5. As it is seen from Figures 6.3-6.5 that thermal insulation and preheating of the pultrusion tool increases the degree of cure in the coating, but does not contribute to its complete curing. Also it is important to note that applying the thermal insulation, the degree of cure of the profile surface increases from 0.85 to 0.9 and for this reason an applied energy could be a little bit decreased. The decrease of the applied microwave energy also is required because of the profile resin overheat (the maximal temperature is about 205 °C and the allowable is 190 °C (Table 4.2)).

All these results show that it is impossible to obtain the complete curing of the applied coating only with the microwave heating and some electrical heaters should be applied in the pultrusion process.

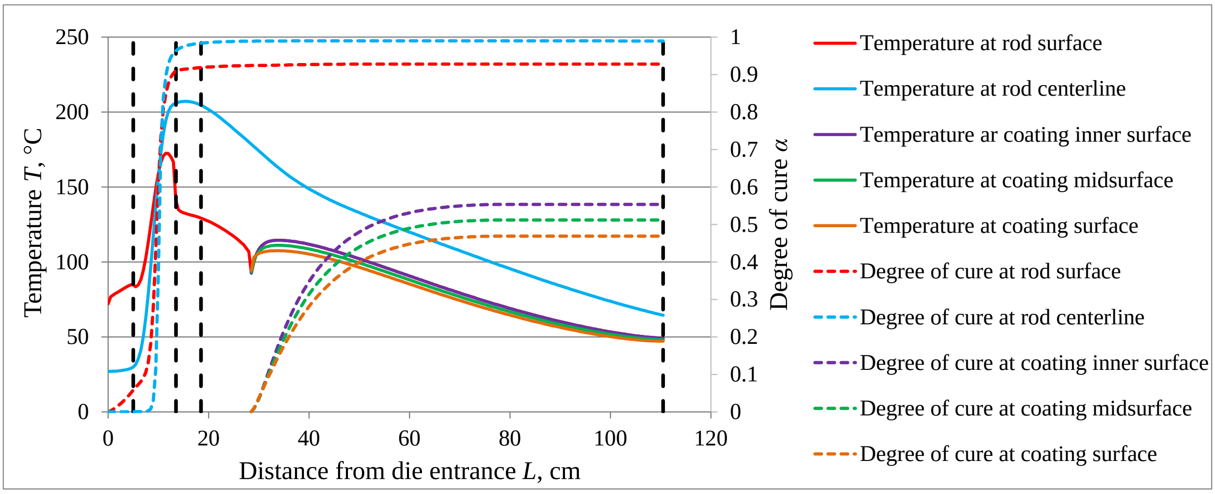

Figure 6.3. Temperature and degree of cure in the profile and coating taking into account the effect of thermal insulation applied to the pultrusion tool.

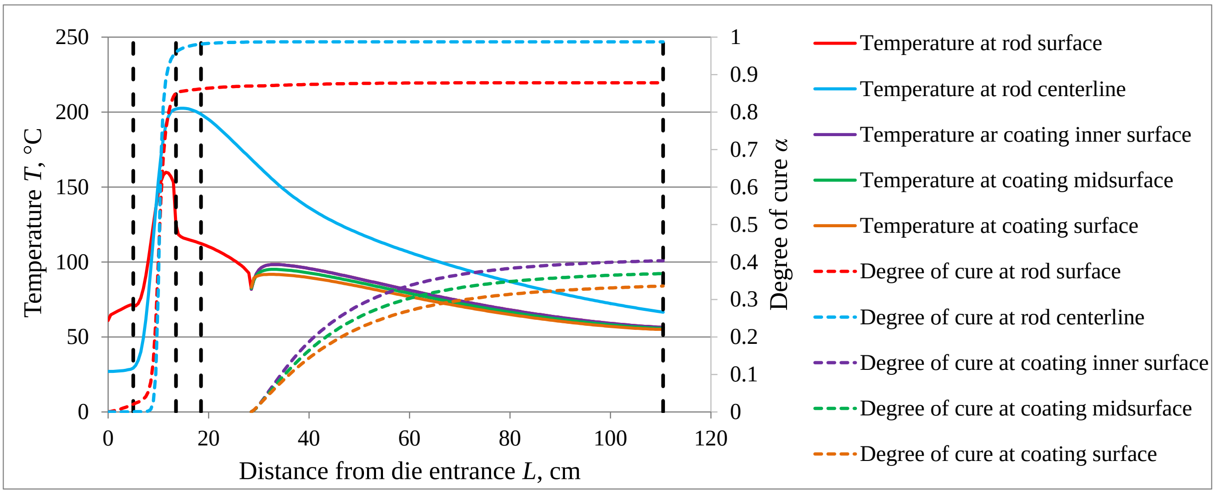

Figure 6.4. Temperature and degree of cure in the profile and coating taking into account the effect of preheating of the pultrusion tool.

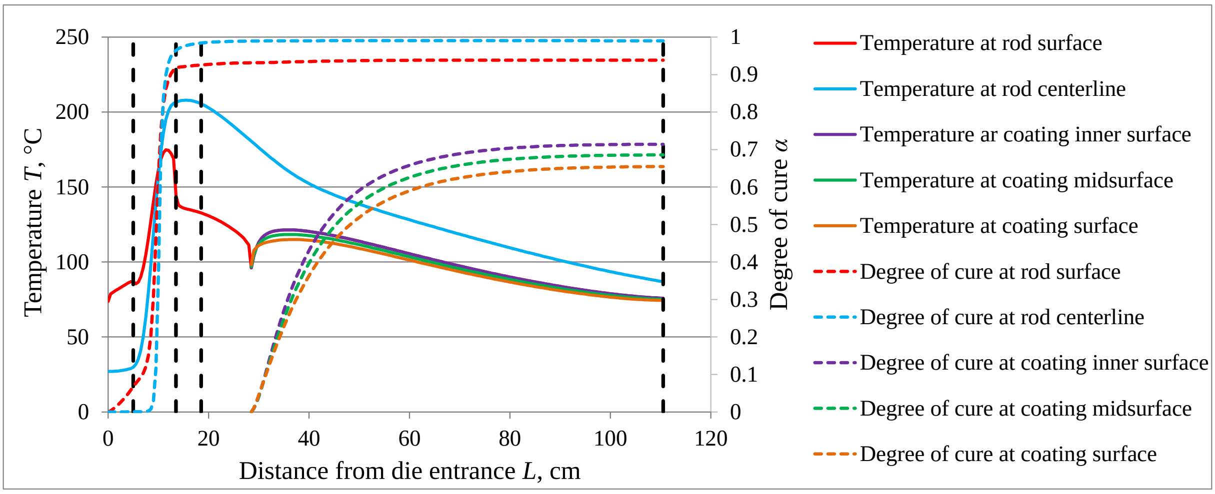

Figure 6.5. Temperature and degree of cure in the profile and coating taking into account both effects of thermal insulation and preheating of the pultrusion tool.

6.2. Multifunctional die with microwave and secondary electrical heating

Two electrical heaters with power of 315 W placed in the distance of 100 mm from the coating injection point and controlled at the temperature 160 °C have been introduced to the multifunctional pultrusion die to evaluate an effectiveness of electric heaters for secondary heating of the pultruded profile. The pull speed and room temperature is the same as in the previous simulations (V = 18 cm/min, T_{room} = 27 °C), but the applied microwave energy is decreased to 1.9 kW to avoid the resin overheat. Scheme of the simulation domain is shown in Figure 6.6. Results of this simulation for the time of 50 min after process starting are shown in Figure 6.7.

The profile and coating resins are not overheated now. The resin at profile centerline is almost completely cured already in the microwave block. The degree of cure at profile surface at the coating injection point is 0.78 that is required for good adhesion between profile and coating. Electric heaters produce energy enough to cure the profile resin at the surface (α = 0.96) and the coating (α = 0.93). Dependency of the temperatures on the thermocouple and the control algorithm of heaters work is shown in Figure 6.8

The results of simulation clearly show that it is possible to obtain completely cured coated profile, but an optimisation problem should be formulated and solved for obtaining of optimal process parameters for different process conditions.

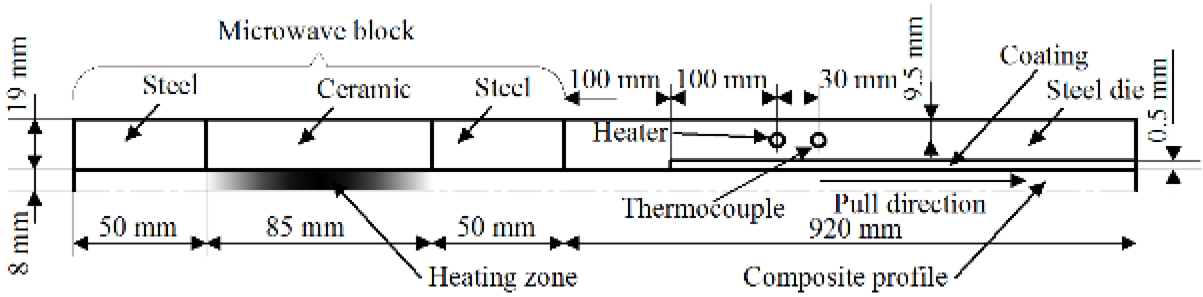

Figure 6.6. Simulation domain.

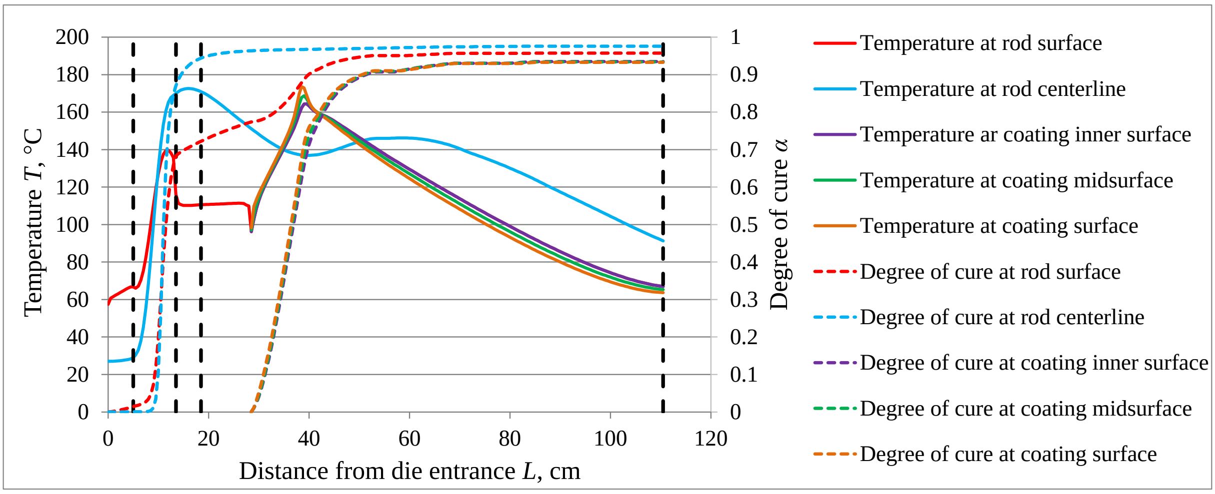

Figure 6.7. Temperature and degree of cure in the profile and coating. Heating: MW and 2 electric heaters. Control temperature: 160 °C.

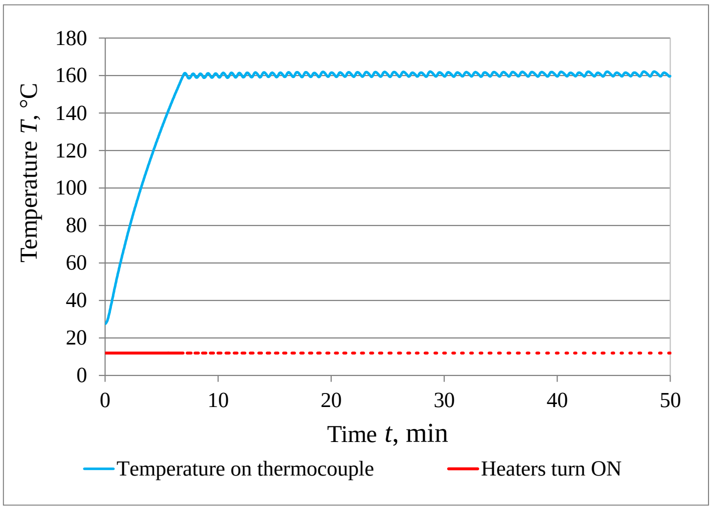

Figure 6.8. Temperature control.

7. OPTIMISATION OF MICROWAVE ASSISTED PULTRUSION PROCESS FOR MULTIFUNCTIONAL DIE

This Chapter describes an optimisation methodology based on the planning of experiments and response surface technique for optimisation of advanced microwave assisted pultrusion process with *in-line* coating technology. The mathematical statement of the optimisation problem is presented and each component of the methodology is described in details.

7.1. Non-direct optimisation methodology

Due to large dimension of the numerical problems to be solved, an optimisation methodology is developed employing the method of experimental design [78] and response surface technique [62]. This methodology is a collection of mathematical and statistical techniques that are useful for the modelling and analysis of problems in which a response of interest is influenced by several variables and the objective is to optimise this response. Optimisation procedure based on experimental design is not only an effective tool for the optimal design of different systems and processes requiring computationally expensive analyses but it also easily combines modelling and optimisation stages and requires less intervention from an analyst in comparison with other approaches. Moreover this approach is general in the sense that it permits to optimise any systems or processes under arbitrary conditions with respect to any objective function (e.g. performance, durability, integrity, reliability, cost) taking into account all practical requirements [4, 19, 20, 21, 22]. An engineering approach of optimisation based on experimental design and response surface technique is presented in Figure 7.1. It is necessary to note that in each of these stages it is possible to solve a problem by different methods.

The basic idea of this approach is that simple mathematical models (response surface) are determined only using the finite element solutions in the reference points of the experimental design. The significant reduction in calculations is achieved in this case in comparison with the conventional optimisation method.

Optimisation methodology is divided into following 5 stages:

- choice of variable parameters and establishment of the domain of search,
- elaboration of plan of experiments for the chosen number of reference points,
- execution of the experiments (numerical simulation),
- determination of simple mathematical models (response surface) from the experimental data,
- minimisation of the selected objective function and obtaining of optimal values of variable parameters.

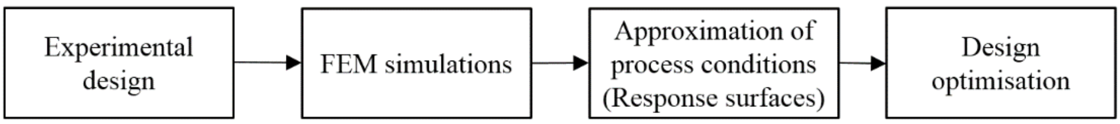

Figure 7.1. Optimisation process.

7.1.1. Experimental design

The plan of experiments can be obtained by different methods: Factorial, D-Optimal, Latin Hypercube, Central Composite, Box-Behnken, Orthogonal Array, Uniform Design, Orthogonal Latin Hypercube, Minimal MSD, MMSD Latin Hypercube, Combined Latin Hypercube D-Optimal, etc. [78]. Then numerical calculations and/or physical experiments are carried out in these points. It is well known that, if for global approximations it is planned to use the second order polynomial functions, the D-Optimal experimental design is the most suitable [8]. The minimal number of design experiments in the optimisation problem is determined in this case as $n = (k+1)(k+2)/2$ where k is the number of design parameters.

In this research the *EDAOpt* software [7] has been used for the generation of the D-Optimal experiment design.

7.1.2. Response surface technique

Different approximation technique can be applied for the numerical and/or physical experiments carried out in the points of the developed plan of experiments. There are Polynomial (Global), Neural Networks, Radial Basis Functions, Kriging, Splines, Rational Functions, etc. [62]. Approximations can be obtained using a conventional un-weighted least square estimation with an elimination of some points and can be performed by the second order polynomials:

$$\overline{F}(x) = \beta_0 + \sum_{i=1}^{K} \beta_i x_i + \sum_{i=1}^{K} \sum_{j=i}^{K} \beta_{ij} x_i x_j \tag{7.1}$$

As stated in [62], there is a considerable practical experience indicating that second–order models work well in solving real response surface problems. In general it is thought that third and higher order polynomials can over–fit data, consequently avoiding construction of global behaviour of the parameters. On the contrary, first order–polynomials are too simple and give prediction errors too high for use in science and engineering.

The error of approximation is calculated by the following expressions

$$\sigma_{err} = \frac{\sum_{i=1}^{N} \left(F(x^i) - \overline{F}(x^i) \right)^2}{N}, \quad \sigma_{err}^0 = \sqrt{\frac{\sum_{i=1}^{N} \left(F(x^i) - \overline{F}(x^i) \right)^2}{N - L}} \tag{7.2}$$

where σ_{err} is the mean squared error;

σ_{err}^0 is the standard deviation;

$F(x^i)$ and $\overline{F}(x^i)$ are the values of original and approximating functions in the sample point x^i of experimental design;

N is the number of points used for an approximation.

The maximal relative error is determined as the maximal relative difference between values obtained by numerical experiment and approximations:

$$\Delta = \max_i \frac{F(x^i) - \overline{F}(x^i)}{F(x^i)} \cdot 100\% \qquad (7.3)$$

7.1.3. Optimisation

The constrained non-linear optimisation problem can be written in the following form:

$$\begin{aligned} &\min F(x); H_i(x) \geq 0; G_j(x) = 0 \\ &i = 1,2,\ldots,I;\ j = 1,2,\ldots,J \end{aligned} \qquad (7.4)$$

where I and J are the numbers of inequality and equality constraints. New version of random search (RS) method [40] and the generalized reduced gradient algorithm (GRG) [49] are used for a solution of the formulated optimisation problem.

The applied RS method is an improved multi-start algorithm with a generation of new start points by exchange of randomly selected point coordinates from the previously found best solution. The search region is moved after each improvement of the objective function and its size is decreased after unsuccessful calculation of the given number of testing points. Continuous variable is assumed as the discrete variable with a large number of levels. In practice 1001 levels are used as the number of levels for continuous variables. However the optimisation process is organised in such a way that even for the continuous variables the initial number of levels is set as 3 or 5, the optimum is found and then the number of levels is increased. The paper [40] presents a short review of the global optimisation methods and comparison of the appropriate software by solving a set of recognized optimisation test problems.

The basic concept of the GRG method entails linearizing the nonlinear objective and constraint functions at a local solution with Taylor expansion equation. Then, the concept of reduced gradient method is employed which divides the variable set into two subsets of basic and non-basic variable and the concept of implicit variable elimination to express the basic variable by the non-basic variable. Finally, the constraints are eliminated and the variable space is deduced to only non-basic variables. The proven efficient method for non-constraints nonlinear programming problems are involved to solve the approximated problem and, then, the next optimal solution for the approximated problem should be found. The processes repeat again until it fulfils the optimal conditions [50].

7.2. Description of technological process

The optimisation of pultrusion process parameters is executed for the rod profile with diameter of 16 mm made of fiberglass *Unfilo 4800 tex* (mass content of 70 %) and polyester resin *POLRES 305BV*. The thermal properties of the fiber and resin are given in Table 4.2, and resin curing kinetic parameters – in Table 3.4. To increase microwave energy absorption properties for the resin, filler *Martinal* with mass content of 20 % is added to the resin. Thermal properties of the filler and lumped properties of profile material are presented in Table 5.2.

The profile is coated by epoxy coating *RESOLTECH RESOLCOAT 2010 FGCS* in the same pultrusion die. The thickness of coating layer is 0.5 mm. The thermal properties of coating are presented in Table 6.1, and curing kinetic parameters – in Table 3.5.

The scheme of pultrusion tool is given in Figure 7.2. Figure 7.3 presents CAD drawing of the tool. The die is made of steel *40Cr* with thermal properties presented in Table 5.2. The thermal properties of ceramic inlet are given in the same table.

Dry glass fibers come into the die and are saturated with the resin in the resin chamber (Figure 7.3) making the composite profile. Heating of the composite profile is realized using microwave energy. Heating system is described in Chapter 5.3.2. The resin is partly cured by the microwave energy to obtain the degree of cure α = 0.75… 0.85 on the profile surface. Then it is coming through the coating chamber where the coating material is applied. This value of the degree of cure is required for a good adhesion between the profile and coating. Then the coating and profile are heated by 8 electrical heaters split to 2 groups and controlled by PID controller and thermocouples located near heaters. The electrical power of each heater is 315 W. Three holes are provided in the die for an installation of *Optimold* monitoring system [39] sensors, which monitor the temperature and the degree of cure on the surface of running profile in real time. *Optimold* system is described in Chapter 4.1.

Scheme of the simulation domain is given in Figure 7.4. Corresponding finite element model presented in Figure 7.5 has been created in *ANSYS Mechanical* by using 3-D thermal solid finite elements *Solid 70*. Using symmetry of the simulated domain, only a quarter of advanced pultrusion die is modelled. The finite element mesh is regular in pull direction and has 124 elements along the profile. The total number of finite elements is 40 974 (3348 for the profile, 588 for the coating, 35 995 for the steel die and 588 for the ceramic part). The time step of the solution depends on the pull speed. It is equal to 2 s for the speed of 30 cm/min, 0.6 s for the speed of 100 cm/min and varies linearly for other speeds in these boundaries. During this time the composite travels in the pull direction on the distance equals to the dimension of one finite element (10 mm). Initial conditions are applied at time $t = 0$ when all nodal points of the composite have the room temperature and degree of cure equals to $\alpha = 10^{-10}$.

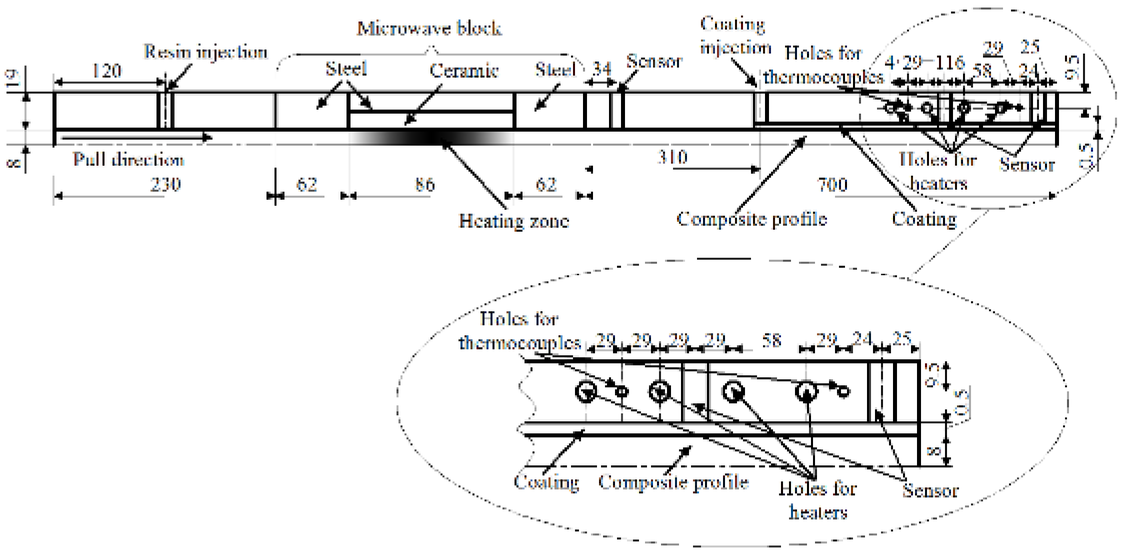

Figure 7.2. Scheme of the pultrusion tool.

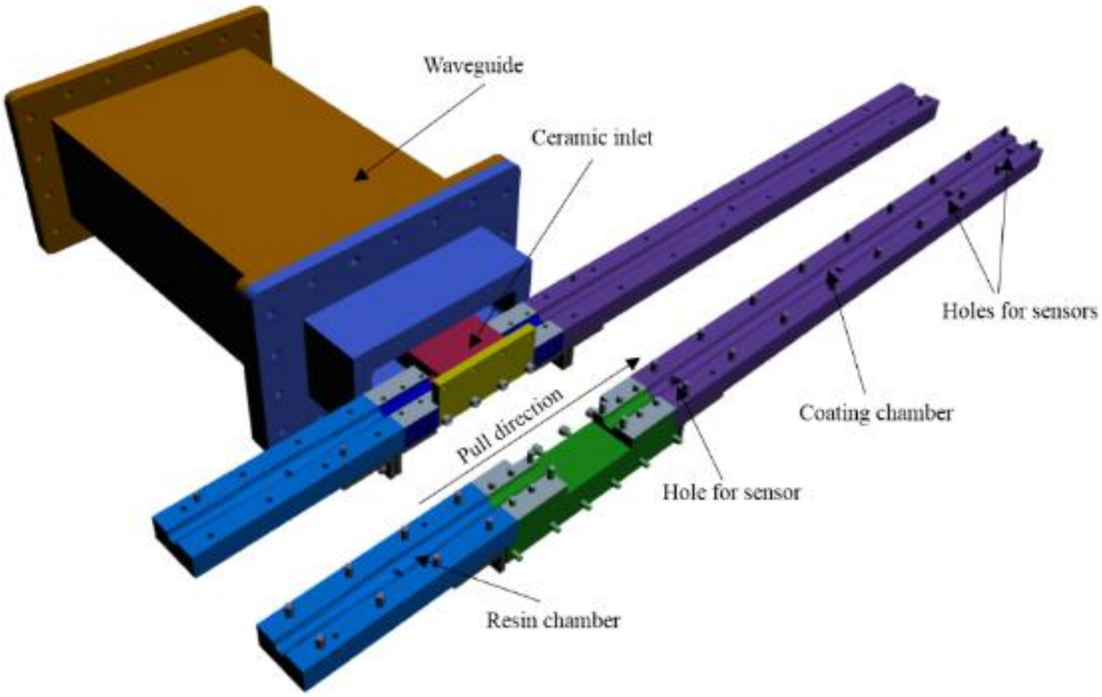

Figure 7.3. CAD drawing of the pultrusion tool.

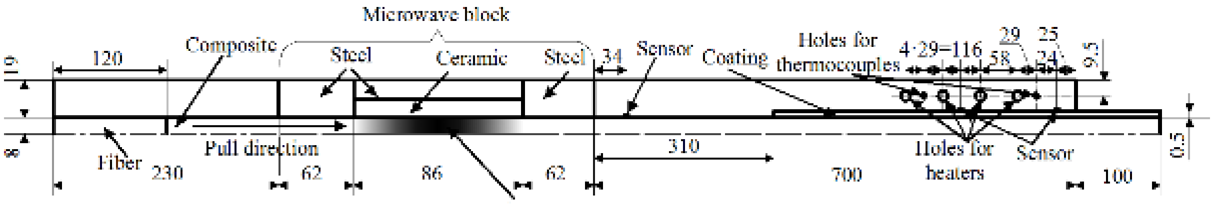

Figure 7.4. Scheme of the simulation domain.

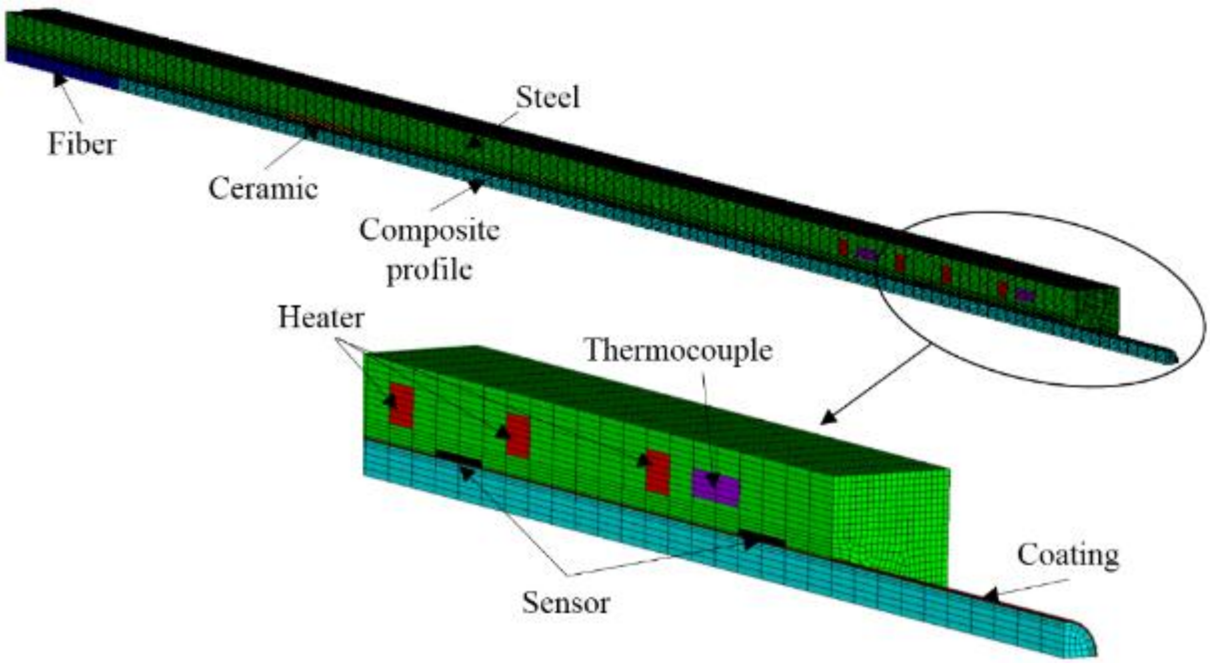

Figure 7.5. FE model of the simulation domain.

7.3. Formulation of optimisation problem

The purpose of optimisation is the minimum of energy (kWh) per meter of coated pultruded profile:

$$\frac{W_{mw} + n \cdot W_{heater} \cdot k_t}{V_{pull}} \rightarrow \min \tag{7.5}$$

where W_{mw} is applied microwave power, kW;

W_{heater} is power of electrical heater, kW;

n is number of electrical heaters;

V_{pull} is pull speed, m/h;

k_t is relative time of heaters work during the simulation time:

$$k_t = \frac{T_{work}}{T_{sim}} \tag{7.6}$$

where T_{work} is time of heaters work, h;

T_{sim} is total simulation time, h.

Some parameters of the process, namely, number and power of electrical heaters and coating preheating temperature are fixed. Their values are given in Table 7.1. Upper and lower bounds (domain of interest) for the variable parameters of the technological process are also listed in Table 7.1.

Constrains are introduced into optimisation procedure with the aim to provide qualitative profile production when profile and coating resins should be completely cured at die exit and materials should not be overheated during the pultrusion process. Constrains of the process are summarized in Table 7.2.

Table 7.1.

Constant and variable parameters of pultrusion process

	constant	min value	max value
Coating preheating temperature, °C	50	-	-
Power of electrical heater, W	315	-	-
Number of electrical heaters	8	-	-
Pull speed, cm/min	-	30	100
Room and resin temperature, °C	-	12	40
Applied microwave energy, kW	-	2	6
Control temperature of electrical heater, °C	-	70	150

Table 7.2.

Constrains of pultrusion process

	min value	max value
Temperature in profile, °C	-	190
Temperature in coating, °C	-	250
Degree of cure at die exit	0.93	-
Degree of cure at coating injection point	0.75	0.85

7.4. Solution of optimisation problem

At the beginning of the optimisation procedure the pultrusion process is simulated with 30 sets of variable parameters generated by D-optimal sampling method [78]. The minimal number of sampling points for the second order polynomial with k variables (design parameters) is $(k+1)(k+2)/2$. It is common practice to use two times greater number of points, therefore 30 sampling points have been used. 2-D views of the plan of experiments are presented in Figure 7.6 and sampling points are given in Appendix (Table A1).

After finite element calculations (results are presented in Table A1 in Appendix), the second order polynomial functions are obtained for simulation results using the conventional unweighted least square method [62] with elimination of some points. The following behaviour functions have been obtained: the maximal temperature of coating (T_{coat}), profile surface (T_{surf}) and centerline (T_{cent}), the degree of cure at die exit for coating (α_{coat}), profile surface (α_{surf}) and centerline (α_{cent}), and on the profile surface for coating injection point ($\alpha_{coat\ inject}$), and the relative time of heaters work (k_t). Approximations using all sampling points are presented in Appendix (Table A2). It is necessary to note that only approximation of k_t directly enters into the objective function (Equation (7.5)). Approximation of temperatures and degrees of cure are used as constrains during the optimisation procedure. It is assumed that constrains for the maximal temperature in profile are satisfied if the profile temperature on centerline and surface is lower than allowed maximal temperature. It is not necessary to check all profile points in this case. Similar assumption is taken for the degree of cure at the die exit.

The standard deviations σ_{err}^{0} and maximal relative errors Δ of approximation functions obtained using all sampling points are presented in Table 7.3. It is seen from Table 7.3 and Table A3 in Appendix that relative errors of approximations are quite large (column Δ) especially for the points with low temperature and degree of cure for a composite material. Since these points are out of interest, it is possible to exclude them from approximations increasing by this way their accuracy narrowing boundaries of the design space. It is necessary to note that no more than 8 points have been excluded from the examined design space. There are points with values lower than 0.25 for the degree of cure and points with values lower than 60 °C for the maximal temperature in composite material. New coefficients of approximation functions are presented in Appendix (Table A4), and relative errors – in column Δ_1 of Table 7.3 and Table A5 in Appendix. It is seen that elimination of some points located out of interest gave the possibility to improve the accuracy of approximations significantly. The maximal relative error of approximations does not exceed 10 % now.

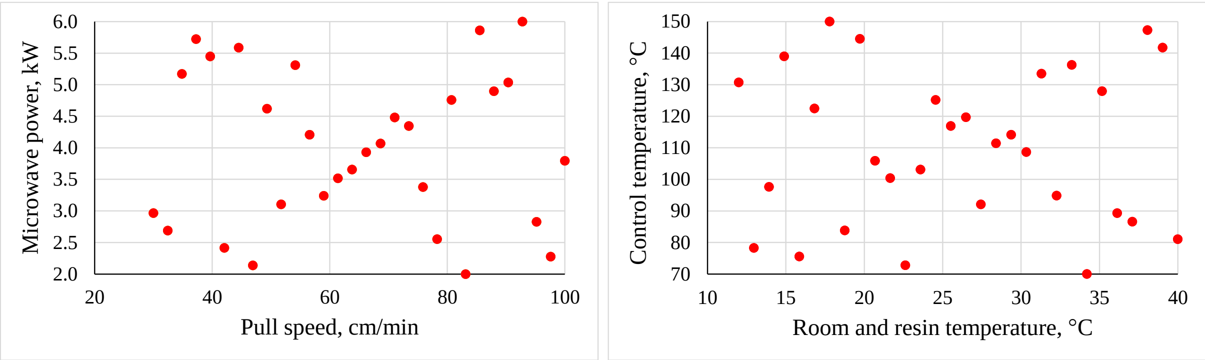

Figure 7.6. 2-D views of the plan of experiments.

Table 7.3.

Standard deviations and relative errors of approximations

Symbol, unit	Approximation with all sampling points		Number of eliminated points	Approximation after elimination of some points	
	σ^0_{err}	Δ, %		σ^0_{err}	Δ_1, %
T_{cent}.°C	8.898	15.8	2	5.516	6.2
α_{cent}	0.0929	479.7	6	0.0349	8.2
T_{surf}, °C	5.446	8.7	0	-	-
α_{surf}	0.0372	16.2	6	0.0317	10.1
$\alpha_{coat\ inject}$	0.0826	1955.9	8	0.0164	10.1
T_{coat}, °C	1.822	2.4	0	-	-
α_{coat}	0.0230	34.2	7	0.0128	4.9
k_t	0.00301	10.0	0	-	-

Then the minimum of the objective function (Equation (7.5)) taking into account constrains presented by approximation functions has been found by two methods: the random search (RS) method [64] using *EDAOpt* optimisation software [7] and the generalized reduced gradient (GRG) algorithm [49] utilized in *Microsoft Excel*.

7.5. Optimisation results

Results of minimisation for the energy consumption by the GRG method are presented in Figure 7.7. Appropriate results obtained by RS method are presented in Figure 7.8. No visible difference is observed in the results obtained by different methods. Since the response surfaces are used instead of the original functions, the optimal result is checked using *ANSYS Mechanical* finite element solution. Good coincidence of results is observed (Table 7.4).

As it is seen from Figures 7.7 and 7.8, the profile material is fully cured (degree of cure more than 0.98), but the coating material is not fully cured (degree of cure 0.93). At the same time the heaters control temperature comes to the upper border of the domain of interest (150 °C), but the pull speed – to the lower one (30 cm/min). Since the degree of cure of coating depends on the pull speed and temperature on the heaters, practically it is not possible to obtain its higher value without changing the corresponding domains of interest in optimisation problem. Taking into account that the maximal coating temperature (158.4 °C) is much less than allowed temperature (250 °C) and the maximal temperature on profile surface (163.2 °C) is also less than allowed temperature (190 °C), it is necessary to increase the heaters control temperature that is possible to make technologically.

By this way the maximal control temperature of heaters work has been increased from 150 °C to 170 °C. To exclude the building of new plan of experiments and time-consuming finite element calculations in each point of the plan, an extrapolation of approximations has been done like presented in Figures 7.9 and 7.10. It is necessary to note that the values of the degree of cure are limited by 1.0. Results of optimisation with modified design space are shown in Figures 7.11 and 7.12.

	Pull speed, cm/min	Room and resin temperature, °C	MW Power, kW	Heaters control temperature, °C	Maximal temperature at centerline, °C	Degree of cure at centerline	Maximal temperature at profile surface, °C	Degree of cure at profile surface	Degree of cure on profile surface at coating injection point	Maximal temperature in coating, °C	Degree of cure in coating	Relative time of heaters work k	Energy consumption, kWh/m
Optimal	31.0	21.3	3.42	150.0	185.68	0.99	163.15	0.98	0.75	158.43	0.93	0.139	0.203
min	30	12	2	70		0.93		0.93	0.75		0.93		
max	100	40	6	150	190		190		0.85	250			

Figure 7.7. Optimal results obtained by the GRG method.

Optimization: COALINE_elimination.prj

Criterion: 1.6667*(X3+0.315*8*Y8)/X1 = 0.202749993509009

Indices No	Min	Type	Max	Criterion=	0.20274999
1) X1:	30	0	100	1) X1=	30.656118
2) X2:	12	0	40	2) X2=	22.015749
3) X3:	2	0	6	3) X3=	3.3816248
4) X4:	70	0	150	4) X4=	150
5) Y1:	0	2	190	5) Y1=	186.16949
6) Y2:	0.93	1	2	6) Y2=	0.99593112
7) Y3:	0	1	190	7) Y3=	163.64049
8) Y4:	0.93	1	2	8) Y4=	0.97614721
9) Y5:	0.75	1	0.85	9) Y5=	0.75000132
10) Y6:	0	1	250	10) Y6=	158.5069
11) Y7:	0.93	1	2	11) Y7=	0.93000024
12) Y8:	0	0	1	12) Y8=	0.13794337

Figure 7.8. Optimal results obtained by the RS method.

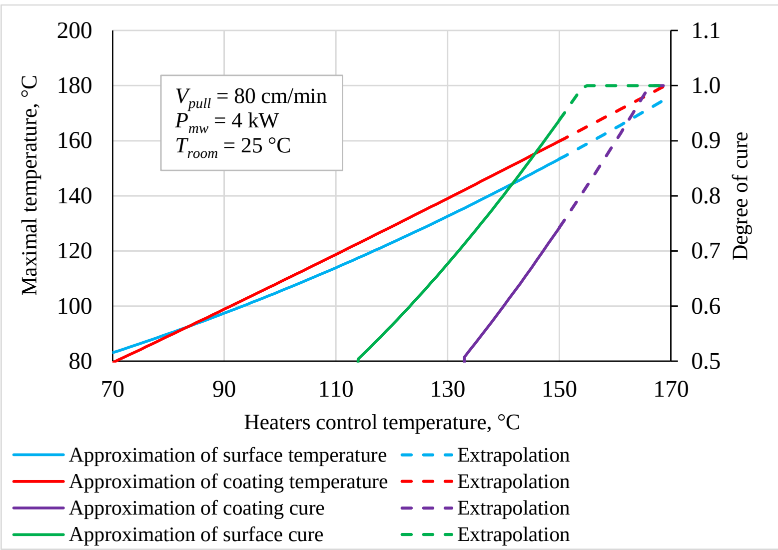

Figure 7.9. Approximated and extrapolated dependences of temperature and degree of cure on heaters control temperature.

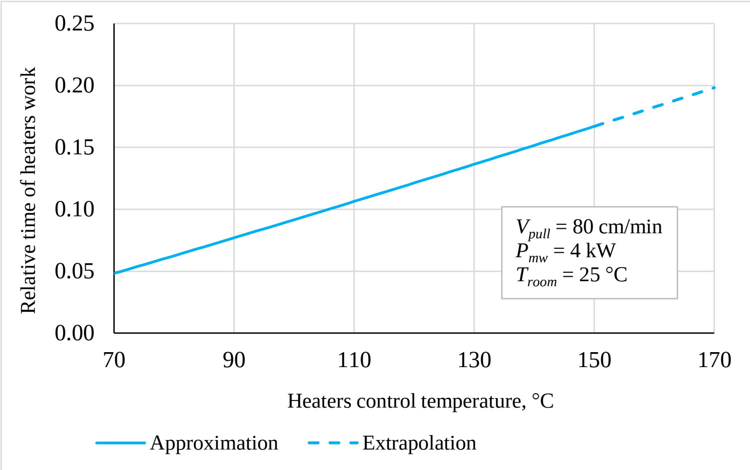

Figure 7.10. Approximated and extrapolated dependence of relative time of heaters work on heaters control temperature.

	Pull speed, cm/min	Room and resin temperature, °C	MW Power, kW	Heaters control temperature, °C	Maximal temperature at centerline, °C	Degree of cure at centerline	Maximal temperature at profile surface, °C	Degree of cure at profile surface	Degree of cure on profile surface at coating injection point	Maximal temperature in coating, °C	Degree of cure in coating	Relative time of heaters work k_t	Energy consumption, kWh/m
Optimal	63.9	40.0	4.98	169.2	165.33	0.93	166.38	1.00	0.75	176.24	1.00	0.153	0.140
min	30	12	2	70		0.93		0.93	0.75		0.93		
max	100	40	6	170	190		190		0.85	250			

Figure 7.11. Optimal results obtained by GRG method for the modified design space.

Optimization: COALINE_elimination.prj

Criterion: 1.667*(X3+0.315*8*Y8)/X1 = 0.139718278809844

Indices No	Min	Type	Max	Criterion=	0.13971828
1) X1:	30	0	100	1) X1=	64.009033
2) X2:	12	0	40	2) X2=	40
3) X3:	2	0	6	3) X3=	4.9785926
4) X4:	70	0	170	4) X4=	169.12372
5) Y1:	0	2	190	5) Y1=	165.19945
6) Y2:	0.93	1	2	6) Y2=	0.93000303
7) Y3:	0	1	180	7) Y3=	166.28756
8) Y4:	0.93	1	2	8) Y4=	1.1452898
9) Y5:	0.75	1	0.85	9) Y5=	0.75000323
10) Y6:	0	1	250	10) Y6=	176.18896
11) Y7:	0.93	1	2	11) Y7=	1.0845412
12) Y8:	0	0	1	12) Y8=	0.15328317

Figure 7.12. Optimal results obtained by RS method for the modified design space.

The optimal values of design parameters together with corresponding values of constrains and objective function obtained by approximations and validated by *ANSYS Mechanical* simulation in the optimal points are listed in Table 7.4, where the relative errors of all constrains and objective function demonstrate high accuracy of the performed optimisation.

Based on the results of optimisation, *Microsoft Excel* tool has been developed for an effective design of microwave assisted pultrusion processes with *in-line* coating technology. As an example of its application, optimal values of design parameters and corresponding constrains for the room temperatures of 20 and 30 °C are presented in Figures 7.13 and 7.14 respectively.

Table 7.4.

Optimal results

	Symbol, unit	Initial domain			Modified domain		
		Approx.	*ANSYS*	*Δ*, %	Approx.	*ANSYS*	*Δ*, %
Design parameters	V_{pull}, cm/min	31.0			64.0		
	T_{room},°C	21.3			40.0		
	P_{mw}, kW	3.42			4.98		
	T_{cont}, °C	150.0			169.3		
Constrains	T_{cent}, °C	185.7	175.8	5.63	165.3	180.9	-8.62
	α_{cent}	0.99	0.97	2.06	0.93	0.98	-5.10
	T_{surf}, °C	163.2	155.1	5.22	166.4	177.0	-5.99
	α_{surf}	0.98	0.94	4.26	1.00	0.95	5.26
	$\alpha_{coat\ inject}$	0.75	0.69	8.70	0.75	0.77	-2.60
	T_{coat}, °C	158.4	157.2	0.76	176.2	181.3	-2.81
	α_{coat}	0.93	0.89	4.49	1.00	0.90	11.11
	k_t	0.139	0.141	-1.42	0.153	0.143	6.99
Objective function, Wh/m		203	203	0.00	140	140	0.00

	Pull speed, cm/min	Room and resin temperature, °C	MW Power, kW	Heaters control temperature, °C	Maximal temperature at centerline, °C	Degree of cure at centerline	Maximal temperature at profile surface, °C	Degree of cure at profile surface	Degree of cure on profile surface at coating injection point	Maximal temperature in coating, °C	Degree of cure in coating	Relative time of heaters work k_t	Energy consumption, kWh/m
Optimal	36.9	20.0	3.87	150.6	181.56	0.93	161.77	1.00	0.75	158.10	0.93	0.141	0.191
min	30	20	2	70		0.93		0.93	0.75		0.93		
max	100	20	6	170	190		190		0.85	250			

Figure 7.13. Optimal results obtained by GRG method for the room temperature of 20 °C.

	Pull speed, cm/min	Room and resin temperature, °C	MW Power, kW	Heaters control temperature, °C	Maximal temperature at centerline, °C	Degree of cure at centerline	Maximal temperature at profile surface, °C	Degree of cure at profile surface	Degree of cure on profile surface at coating injection point	Maximal temperature in coating, °C	Degree of cure in coating	Relative time of heaters work k_t	Energy consumption, kWh/m
Optimal	48.7	30.0	4.38	153.2	174.77	0.93	164.09	1.00	0.75	160.47	0.93	0.137	0.162
min	30	30	2	70		0.93		0.93	0.75		0.93		
max	100	30	6	170	190		190		0.85	250			

Figure 7.14. Optimal results obtained by GRG method for the room temperature of 30 °C.

8. CONCLUSIONS

The present investigations have been carried out to develop new simulation and optimisation methodology for the design of advanced microwave assisted pultrusion processes with *in-line* coating technology. The developed methodology uses different finite element codes for a simulation of the manufacturing process, and planning of experiments and response surface technique - for the process optimisation. The proposed simulation methodology has been validated by using the results published in scientific literature and obtained from physical experiments. New optimal solutions have been obtained for the advanced technological process. The following general conclusions can be drawn based on the results presented in the Thesis:

1. Conventional pultrusion processes, their simulation and optimisation are widely considered in the scientific literature. Advanced microwave assisted pultrusion processes are studied considerably less, no optimisation problems have been solved for this new technological process. The design of pultrusion dies with *in-line* coating technology is not mentioned in scientific literature.
2. The developed and successfully validated numerical approaches for a simulation of pultrusion processes are reliable and can be used for investigation of pultrusion processes. The first procedure has been developed in *ANSYS Mechanical* environment and based on the mixed time integration scheme and nodal control volumes method to decouple the coupled energy and species equations. Movement of the resin-saturated composite has been simulated by shifting the temperature and degree of cure fields after each calculation step. Within each time step the species equation has been solved outside the software by using the control volume method to obtain the degree of cure at each nodal point. An effect of the convection and exothermic terms on temperature has been computed from the known temperatures of the previous time step. The algorithm allows an obtaining a temperature field for the current time step by solving of the remaining transient heat conduction problem. The second procedure has been performed by using *ANSYS CFX* software. The cure reaction in this case has been introduced as an additional variable. The developed procedures have been successfully validated by the results from literature and physical experiment that gave the possibility to compare the developed algorithms in their applicability for an accurate thermochemical simulation of pultrusion processes without and with a temperature control and by this way to define their advantages and limitations. Good agreement between present finite element results and published results as well as results of trial has been observed for the temperature and degree of cure fields in all test problems studying the pultrusion of flat plate, I-beam and two different cylindrical rod profiles. Some difference between experimentally measured and simulated degrees of cure has been observed for the resin at the gelation stage. However, this disagreement is practically disappeared for the resin which is almost fully cured.
3. The proposed methodology for a building of the curing kinetic models has been successfully validated for an epoxy resin described in open literature. The best precision has been obtained with the Kamal-Sourour model. An engineering tool based on *Microsoft Excel* code has been developed by using the proposed methodology. This tool has been successfully applied for a building of the curing kinetic models of polyester resin and epoxy coating with high microwave absorption properties used in the advanced pultrusion processes

4. During an experimental validation of the developed algorithms for a simulation of pultrusion processes, it has been shown that conditions of transient process are very sensitive to the variation of initial data (process parameters). An appropriate methodology for the correction and obtaining the correct set of initial data using experimental results has been demonstrated.
5. New simulation methodology based on *COMSOL Multiphysics* and *ANSYS Mechanical* has been developed for simulation and investigation of advanced microwave assisted pultrusion process. Parameters of the microwave assisted pultrusion process, and the temperature and degree of cure fields in the composite material have been determined for the design of advanced pultrusion die. Simulation results show that the developed technology gives the possibility to ensure a homogeneous curing of the composite profile and to obtain high values of the degree of cure in the cured composite. To improve effectiveness of the microwave assisted pultrusion process, an influence of different process parameters has been additionally investigated. Based on the obtained results, the following recommendations could be done for technologists designing advanced pultrusion dies:
    - More effective is to apply the thermal insulation at all external surfaces of advanced pultrusion die or to preheat a steel die before the beginning of pultrusion process if the highest value of the degree of cure at the profile surface is required.
    - To obtain largest effect on the degree of cure at the profile surface and to increase the process effectiveness, joint application of both factors, namely an application of thermal insulation and preheating of steel die, should be realized.
    - The heating of resin bath could be used also to obtain the highest values of the degree of cure at the profile surface. However, an effectiveness of the pultrusion process in this case is not so high since the heating of resin bath should be organized for the full duration of pultrusion process.
    - The reduction of steel die length has no effect on the degree of cure at the profile surface. However, this effect could be used in the design of advanced pultrusion die for saving of expensive die material.
6. It has been shown that it is impossible to obtain the complete curing of the profile and applied coating only with the microwave heating taking into account all process conditions and constrains in the case of *in-line* coating technology. Some electrical heaters should be applied in the pultrusion process to cure coating.
7. It has been shown that process conditions (temperature and degree of cure) are very sensitive to the variation of process parameters (pull speed, applied energy, controlled and room temperatures). Determination of appropriate process conditions is possible only by formulation and solution of optimisation problem. This task has been successfully solved with the purpose to define the minimum of energy consumption. As a result of optimisation, *Microsoft Excel* tool for determination of optimal process conditions in dependence on taken design parameters has been created.

The results of the present Thesis are the part of the collaborative European project “Development of an Innovative Manufacturing Process for the In-Line Coating of Pultruded Composites” (*COALINE*) under *FRAMEWORK 7* program. The main aim of the project is to develop an innovative manufacturing process for the *in-line* coating of pultruded composites. The data obtained from investigations are intended for the most experienced European companies, research institutes and academic institutions working in the field of pultrusion. The development of new modelling and optimisation methodologies for the design of advanced pultrusion processes will allow further expansion of investigations in this field.

For the future research and design studies, the pultrusion of thin-walled profiles should be studied. Additionally, the thermomechanical problem of the pultrusion taking into account pull forces and friction between pultruded product and pultrusion die should be considered.

APPENDIX

Detailed data obtained in Chapter 7 are presented in this Appendix

Table A1.

Sampling points and obtained results of numerical simulations

Exp. No	Plan				Results							
	V_{pull}, cm/min	T_{room}, °C	W_{mw}, kW	$T_{control}$, °C	T_{cent}, °C	α_{cent}	T_{surf}, °C	α_{surf}	$\alpha_{coat.inj}$	T_{coat}, °C	α_{coat}	k_t
1	54.14	12.00	5.31	130.69	178.97	0.970	137.30	0.850	0.630	137.82	0.650	0.120
2	68.62	25.52	4.07	116.90	125.61	0.790	125.35	0.660	0.140	125.13	0.400	0.108
3	78.28	34.21	2.55	70.00	77.06	0.170	71.62	0.086	0.030	71.95	0.041	0.043
4	100.00	13.93	3.79	97.59	60.78	0.038	94.99	0.150	0.006	102.74	0.110	0.126
5	44.48	36.14	5.59	89.31	196.11	0.990	165.96	0.900	0.890	108.86	0.380	0.038
6	95.17	39.03	2.83	141.72	85.97	0.170	140.82	0.760	0.034	154.19	0.540	0.156
7	87.93	17.79	4.90	150.00	105.30	0.400	152.79	0.860	0.043	159.59	0.680	0.177
8	58.97	33.24	3.24	136.21	132.52	0.850	142.65	0.850	0.220	144.03	0.680	0.120
9	90.34	40.00	5.03	81.03	149.73	0.900	103.81	0.430	0.300	100.83	0.130	0.031
10	66.21	29.38	3.93	114.14	135.70	0.860	123.48	0.650	0.210	123.27	0.390	0.096
11	61.38	24.55	3.52	125.17	118.16	0.740	131.74	0.740	0.120	132.43	0.510	0.121
12	92.76	31.31	6.00	133.45	153.46	0.910	145.71	0.810	0.310	145.63	0.560	0.122
13	34.83	22.62	5.17	72.76	209.60	0.990	169.90	0.900	0.900	94.70	0.290	0.034
14	83.10	14.90	2.00	138.97	52.76	0.012	134.30	0.710	0.003	145.81	0.570	0.189
15	85.52	15.86	5.86	75.52	128.12	0.770	87.40	0.210	0.110	86.97	0.072	0.054
16	97.59	27.45	2.28	92.07	57.51	0.029	88.62	0.120	0.007	98.46	0.082	0.104
17	71.03	28.41	4.48	111.38	143.61	0.890	121.86	0.630	0.250	121.64	0.350	0.092
18	32.41	37.10	2.69	86.55	172.15	0.970	122.69	0.740	0.690	93.87	0.290	0.041
19	75.86	18.76	3.38	83.79	75.42	0.160	84.21	0.130	0.020	89.10	0.073	0.086
20	46.90	35.17	2.14	127.93	120.67	0.730	134.11	0.810	0.140	137.54	0.630	0.110
21	49.31	32.28	4.62	94.83	182.81	0.980	132.85	0.800	0.770	107.92	0.330	0.049
22	37.24	16.83	5.72	122.41	211.36	0.990	170.61	0.920	0.900	129.09	0.680	0.100
23	80.69	30.34	4.76	108.62	136.94	0.850	119.49	0.550	0.190	119.26	0.290	0.090

Continuation of Table A1

24	42.07	12.97	2.41	78.28	90.47	0.430	80.84	0.210	0.044	81.47	0.120	0.075
25	39.66	38.07	5.45	147.24	209.92	0.990	177.29	0.960	0.930	154.63	0.870	0.108
26	56.55	21.66	4.21	100.34	156.73	0.930	109.66	0.600	0.380	109.36	0.300	0.077
27	51.72	20.69	3.10	105.86	114.62	0.720	112.16	0.560	0.110	111.88	0.330	0.098
28	30.00	19.72	2.97	144.48	172.86	0.970	150.50	0.930	0.610	152.58	0.860	0.136
29	73.45	26.48	4.34	119.66	127.44	0.800	128.53	0.670	0.140	128.34	0.410	0.112
30	63.79	23.59	3.66	103.10	114.34	0.700	110.02	0.480	0.100	111.01	0.260	0.094

Table A2.

Coefficients of approximation functions using all sampling points

	T_{cent}	α_{cent}	T_{surf}	α_{surf}	$\alpha_{coat.inj}$	T_{coat}	α_{coat}	k_t
const	$-1.7\cdot10^{1}$	$-1.5\cdot10^{0}$	$2.8\cdot10^{1}$	$-7.6\cdot10^{-1}$	$-3.4\cdot10^{-1}$	$-5.8\cdot10^{0}$	$-2.2\cdot10^{-1}$	$3.0\cdot10^{-2}$
V_{pull}	$-3.6\cdot10^{0}$	$-1.9\cdot10^{-2}$	$-2.5\cdot10^{0}$	$-2.5\cdot10^{-2}$	$-2.6\cdot10^{-2}$	$-5.8\cdot10^{-1}$	$-4.1\cdot10^{-3}$	$-9.7\cdot10^{-5}$
T_r	$3.4\cdot10^{0}$	$3.3\cdot10^{-2}$	$4.1\cdot10^{0}$	$4.1\cdot10^{-2}$	$1.8\cdot10^{-2}$	$2.5\cdot10^{-1}$	$1.1\cdot10^{-2}$	$-1.4\cdot10^{-3}$
W_{mw}	$4.4\cdot10^{1}$	$1.7\cdot10^{-1}$	$3.1\cdot10^{1}$	$2.8\cdot10^{-1}$	$2.7\cdot10^{-1}$	$1.1\cdot10^{1}$	$-9.4\cdot10^{-3}$	$-7.1\cdot10^{-3}$
T_{cont}	$2.0\cdot10^{0}$	$3.5\cdot10^{-2}$	$2.0\cdot10^{-1}$	$1.2\cdot10^{-2}$	$1.1\cdot10^{-2}$	$1.1\cdot10^{0}$	$3.0\cdot10^{-3}$	$7.6\cdot10^{-4}$
$(V_{pull})^2$	$1.4\cdot10^{-2}$	$-3.7\cdot10^{-5}$	$1.3\cdot10^{-2}$	$4.2\cdot10^{-5}$	$2.0\cdot10^{-3}$	$2.0\cdot10^{-3}$	$1.2\cdot10^{-5}$	$4.6\cdot10^{-6}$
$V_{pull} \cdot T_r$	$1.5\cdot10^{-2}$	$1.8\cdot10^{-4}$	$-6.6\cdot10^{-3}$	$1.6\cdot10^{-7}$	$2.8\cdot10^{-3}$	$2.8\cdot10^{-3}$	$1.3\cdot10^{-5}$	$-8.3\cdot10^{-6}$
$V_{pull} \cdot W_{mw}$	$-8.6\cdot10^{-3}$	$3.2\cdot10^{-3}$	$-2.2\cdot10^{-1}$	$-4.2\cdot10^{-4}$	$-2.4\cdot10^{-3}$	$-2.4\cdot10^{-3}$	$-2.1\cdot10^{-4}$	$-8.3\cdot10^{-5}$
$V_{pull} \cdot T_{cont}$	$-8.9\cdot10^{-4}$	$-3.2\cdot10^{-5}$	$1.1\cdot10^{-2}$	$1.3\cdot10^{-4}$	$2.2\cdot10^{-3}$	$2.2\cdot10^{-3}$	$-9.9\cdot10^{-6}$	$5.7\cdot10^{-6}$
$(T_r)^2$	$-1.1\cdot10^{-2}$	$-3.5\cdot10^{-4}$	$-4.6\cdot10^{-2}$	$-1.9\cdot10^{-4}$	$-3.7\cdot10^{-3}$	$-3.7\cdot10^{-3}$	$-3.7\cdot10^{-5}$	$-1.1\cdot10^{-5}$
$T_r \cdot W_{mw}$	$-1.9\cdot10^{-1}$	$-1.2\cdot10^{-3}$	$8.5\cdot10^{-2}$	$-6.8\cdot10^{-4}$	$5.1\cdot10^{-4}$	$5.0\cdot10^{-2}$	$-4.4\cdot10^{-5}$	$1.2\cdot10^{-4}$
$T_r \cdot T_{cont}$	$-1.6\cdot10^{-2}$	$-9.9\cdot10^{-5}$	$-9.2\cdot10^{-3}$	$-1.9\cdot10^{-4}$	$-1.9\cdot10^{-4}$	$-2.2\cdot10^{-3}$	$-5.6\cdot10^{-5}$	$4.4\cdot10^{-6}$
$(W_{mw})^2$	$-6.0\cdot10^{-1}$	$-6.6\cdot10^{-3}$	$8.7\cdot10^{-1}$	$3.0\cdot10^{-3}$	$4.3\cdot10^{-3}$	$-1.6\cdot10^{-1}$	$1.2\cdot10^{-2}$	$1.6\cdot10^{-4}$
$W_{mw} \cdot T_{cont}$	$-7.7\cdot10^{-2}$	$-1.2\cdot10^{-3}$	$-1.5\cdot10^{-1}$	$-1.7\cdot10^{-3}$	$-1.6\cdot10^{-4}$	$-7.7\cdot10^{-2}$	$-3.5\cdot10^{-4}$	$-1.3\cdot10^{-6}$
$(T_{cont})^2$	$-4.7\cdot10^{-3}$	$-1.1\cdot10^{-4}$	$2.7\cdot10^{-3}$	$-6.7\cdot10^{-6}$	$-2.5\cdot10^{-5}$	$5.7\cdot10^{-4}$	$4.2\cdot10^{-5}$	$7.6\cdot10^{-7}$

Table A3.

Relative errors of approximations using all sampling points

Exp.	T_{cent}, °C			α_{cent}			T_{surf}, °C		
No	Exp.	Appr.	Δ, %	Exp.	Appr.	Δ, %	Exp.	Appr.	Δ, %
1	178.97	169.88	5.1	0.97	0.88	9.3	137.30	137.63	-0.2
2	125.61	127.96	-1.9	0.79	0.78	1.4	125.35	123.83	1.2
3	77.06	79.92	-3.7	0.17	0.21	-25.5	71.62	71.39	0.3
4	60.78	64.47	-6.1	0.04	0.08	-104.5	94.99	89.84	5.4
5	196.11	211.53	-7.9	0.99	1.11	-12.0	165.96	165.50	0.3
6	85.97	89.08	-3.6	0.17	0.22	-30.7	140.82	145.68	-3.5
7	105.30	113.84	-8.1	0.40	0.46	-15.5	152.79	151.99	0.5
8	132.52	129.05	2.6	0.85	0.77	9.9	142.65	137.53	3.6
9	149.73	148.66	0.7	0.90	0.87	3.3	103.81	99.71	3.9
10	135.70	132.35	2.5	0.86	0.82	5.1	123.48	123.27	0.2
11	118.16	124.58	-5.4	0.74	0.76	-2.1	131.74	128.47	2.5
12	153.46	149.45	2.6	0.91	0.92	-0.6	145.71	144.60	0.8
13	209.60	203.61	2.9	0.99	0.92	6.9	169.90	162.91	4.1
14	52.76	44.41	15.8	0.01	-0.05	479.7	134.30	136.31	-1.5
15	128.12	127.46	0.5	0.77	0.73	5.6	87.40	93.24	-6.7
16	57.51	52.91	8.0	0.03	-0.07	342.1	88.62	90.79	-2.4
17	143.61	137.89	4.0	0.89	0.86	3.8	121.86	123.70	-1.5
18	172.15	165.54	3.8	0.97	0.90	7.7	122.69	126.51	-3.1
19	75.42	79.18	-5.0	0.16	0.33	-104.3	84.21	81.34	3.4
20	120.67	126.13	-4.5	0.73	0.82	-12.8	134.11	126.73	5.5
21	182.81	177.14	3.1	0.98	1.01	-3.4	132.85	139.35	-4.9
22	211.36	219.84	-4.0	0.99	1.09	-10.0	170.61	167.81	1.6
23	136.94	136.08	0.6	0.85	0.85	0.2	119.49	120.40	-0.8
24	90.47	93.35	-3.2	0.43	0.42	2.5	80.84	80.78	0.1
25	209.92	205.42	2.1	0.99	0.93	5.7	177.29	179.16	-1.1
26	156.73	142.48	9.1	0.93	0.85	9.1	109.66	119.15	-8.7
27	114.62	122.21	-6.6	0.72	0.75	-3.6	112.16	111.98	0.2
28	172.86	173.14	-0.2	0.97	1.00	-3.1	150.50	154.19	-2.5
29	127.44	129.52	-1.6	0.80	0.78	1.9	128.53	126.81	1.3
30	114.34	119.67	-4.7	0.70	0.72	-2.7	110.02	110.75	-0.7

Continuation of Table A3

Exp. No	α_{surf} Exp.	α_{surf} Appr.	Δ, %	$\alpha_{coat.inj}$ Exp.	$\alpha_{coat.inj}$ Appr.	Δ, %	T_{coat}, °C Exp.	T_{coat}, °C Appr.	Δ, %
1	0.85	0.81	4.9	0.63	0.54	15.1	137.82	135.75	1.5
2	0.66	0.65	1.6	0.14	0.18	-26.2	125.13	125.42	-0.2
3	0.09	0.09	-3.2	0.03	0.03	-6.1	71.95	73.89	-2.7
4	0.15	0.13	16.2	0.01	0.02	-287.8	102.74	102.97	-0.2
5	0.90	0.94	-4.9	0.89	0.98	-9.9	108.86	108.62	0.2
6	0.76	0.79	-4.3	0.03	0.03	18.6	154.19	155.45	-0.8
7	0.86	0.89	-3.0	0.04	0.14	-225.5	159.59	158.06	1.0
8	0.85	0.82	4.1	0.22	0.18	16.7	144.03	144.54	-0.4
9	0.43	0.41	5.3	0.30	0.34	-13.6	100.83	99.42	1.4
10	0.65	0.66	-0.9	0.21	0.21	0.3	123.27	123.16	0.1
11	0.74	0.72	3.3	0.12	0.17	-40.6	132.43	132.75	-0.2
12	0.81	0.78	4.0	0.31	0.23	26.7	145.63	145.84	-0.1
13	0.90	0.85	5.8	0.90	0.89	1.0	94.70	92.66	2.2
14	0.71	0.71	0.6	0.00	-0.05	1955.9	145.81	147.20	-1.0
15	0.21	0.24	-12.4	0.11	0.11	-3.3	86.97	88.45	-1.7
16	0.12	0.11	12.0	0.01	0.00	138.2	98.46	96.08	2.4
17	0.63	0.64	-1.4	0.25	0.23	8.7	121.64	121.49	0.1
18	0.74	0.76	-2.1	0.69	0.65	5.3	93.87	95.48	-1.7
19	0.13	0.15	-11.9	0.02	-0.04	312.1	89.10	88.49	0.7
20	0.81	0.79	3.0	0.14	0.20	-41.1	137.54	134.26	2.4
21	0.80	0.77	3.9	0.77	0.61	20.4	107.92	108.44	-0.5
22	0.92	0.95	-3.6	0.90	0.97	-8.1	129.09	131.37	-1.8
23	0.55	0.59	-7.4	0.19	0.20	-6.9	119.26	120.34	-0.9
24	0.21	0.22	-4.4	0.04	0.08	-92.0	81.47	81.37	0.1
25	0.96	0.96	0.1	0.93	0.93	-0.4	154.63	154.49	0.1
26	0.60	0.59	1.2	0.38	0.30	20.4	109.36	109.33	0.0
27	0.56	0.56	-0.9	0.11	0.19	-76.30	111.88	112.15	-0.2
28	0.93	0.95	-2.2	0.61	0.57	6.6	152.58	153.23	-0.4
29	0.67	0.67	0.5	0.14	0.17	-24.1	128.34	128.85	-0.4
30	0.48	0.52	-9.2	0.10	0.15	-50.1	111.01	110.61	0.4

Continuation of Table A3

Exp. No	α_{coat} Exp.	α_{coat} Appr.	Δ, %	k_t Exp.	k_t Appr.	Δ, %
1	0.65	0.64	1.0	0.12	0.12	-1.9
2	0.40	0.40	-0.1	0.11	0.11	1.1
3	0.04	0.03	27.6	0.04	0.04	2.4
4	0.11	0.08	27.5	0.13	0.13	0.9
5	0.38	0.38	0.4	0.04	0.03	8.8
6	0.54	0.56	-3.7	0.16	0.16	0.3
7	0.68	0.69	-1.5	0.18	0.18	0.9
8	0.68	0.63	7.0	0.12	0.12	-2.5
9	0.13	0.12	4.6	0.03	0.03	1.0
10	0.39	0.39	0.8	0.10	0.10	-0.4
11	0.51	0.50	1.6	0.12	0.12	0.6
12	0.56	0.54	4.0	0.12	0.12	-1.1
13	0.29	0.27	7.6	0.03	0.03	-1.2
14	0.57	0.57	-0.8	0.19	0.19	-0.6
15	0.07	0.10	-34.2	0.05	0.05	-1.1
16	0.08	0.09	-11.4	0.10	0.11	-2.7
17	0.35	0.36	-2.0	0.09	0.09	-0.9
18	0.29	0.31	-6.2	0.04	0.04	-2.0
19	0.07	0.07	7.1	0.09	0.08	3.9
20	0.63	0.61	2.7	0.11	0.11	2.1
21	0.33	0.33	-0.3	0.05	0.05	-10.0
22	0.68	0.68	0.6	0.10	0.10	3.3
23	0.29	0.31	-6.3	0.09	0.09	1.8
24	0.12	0.12	-0.1	0.07	0.08	-0.2
25	0.87	0.89	-2.0	0.11	0.11	-0.7
26	0.30	0.30	-1.3	0.08	0.08	-6.9
27	0.33	0.34	-4.3	0.10	0.10	1.3
28	0.86	0.87	-0.9	0.14	0.14	-0.1
29	0.41	0.41	-1.1	0.11	0.11	1.5
30	0.26	0.28	-9.6	0.09	0.09	3.1

Table A4.

Coefficients of approximation functions after elimination of sampling points

	T_{cent}	α_{cent}	α_{surf}	$\alpha_{coat.inj}$	α_{coat}
const	$2.3 \cdot 10^{1}$	$-1.0 \cdot 10^{0}$	$5.0 \cdot 10^{-1}$	$4.4 \cdot 10^{-2}$	$1.1 \cdot 10^{-2}$
V_{pull}	$-4.9 \cdot 10^{0}$	$-4.2 \cdot 10^{-2}$	$-1.7 \cdot 10^{-2}$	$-3.1 \cdot 10^{-2}$	$-2.1 \cdot 10^{-3}$
T_r	$1.8 \cdot 10^{0}$	$-3.8 \cdot 10^{-2}$	$3.4 \cdot 10^{-2}$	$3.5 \cdot 10^{-2}$	$1.9 \cdot 10^{-2}$
W_{mw}	$8.3 \cdot 10^{1}$	$8.6 \cdot 10^{-1}$	$7.9 \cdot 10^{-2}$	$4.8 \cdot 10^{-1}$	$-9.2 \cdot 10^{-2}$
T_{cont}	$8.9 \cdot 10^{-1}$	$3.0 \cdot 10^{-2}$	$-5.6 \cdot 10^{-3}$	$-6.9 \cdot 10^{-3}$	$-2.0 \cdot 10^{-3}$
$(V_{pull})^2$	$1.7 \cdot 10^{-2}$	$-5.4 \cdot 10^{-5}$	$-8.2 \cdot 10^{-5}$	$-1.8 \cdot 10^{-4}$	$-5.7 \cdot 10^{-5}$
$V_{pull} \cdot T_r$	$2.7 \cdot 10^{-2}$	$3.3 \cdot 10^{-4}$	$1.4 \cdot 10^{-4}$	$3.5 \cdot 10^{-4}$	$9.4 \cdot 10^{-5}$
$V_{pull} \cdot W_{mw}$	$1.7 \cdot 10^{-1}$	$6.3 \cdot 10^{-3}$	$2.8 \cdot 10^{-5}$	$5.6 \cdot 10^{-3}$	$-4.9 \cdot 10^{-5}$
$V_{pull} \cdot T_{cont}$	$-2.9 \cdot 10^{-3}$	$1.5 \cdot 10^{-5}$	$1.4 \cdot 10^{-4}$	$-9.2 \cdot 10^{-6}$	$1.7 \cdot 10^{-5}$
$(T_r)^2$	$8.5 \cdot 10^{-3}$	$5.2 \cdot 10^{-4}$	$-2.3 \cdot 10^{-4}$	$-1.5 \cdot 10^{-4}$	$-2.1 \cdot 10^{-4}$
$T_r \cdot W_{mw}$	$-6.2 \cdot 10^{-1}$	$-4.8 \cdot 10^{-3}$	$-4.8 \cdot 10^{-4}$	$-4.8 \cdot 10^{-3}$	$-5.7 \cdot 10^{-4}$
$T_r \cdot T_{cont}$	$1.3 \cdot 10^{-3}$	$2.0 \cdot 10^{-4}$	$-1.9 \cdot 10^{-4}$	$-1.1 \cdot 10^{-4}$	$-8.3 \cdot 10^{-5}$
$(W_{mw})^2$	$-6.4 \cdot 10^{0}$	$-9.2 \cdot 10^{-2}$	$1.8 \cdot 10^{-2}$	$-5.2 \cdot 10^{-2}$	$2.3 \cdot 10^{-2}$
$W_{mw} \cdot T_{cont}$	$2.4 \cdot 10^{-2}$	$-1.5 \cdot 10^{-3}$	$-1.3 \cdot 10^{-3}$	$3.7 \cdot 10^{-4}$	$-4.1 \cdot 10^{-4}$
$(T_{cont})^2$	$-3.6 \cdot 10^{-3}$	$-1.3 \cdot 10^{-4}$	$6.2 \cdot 10^{-5}$	$4.0 \cdot 10^{-5}$	$6.4 \cdot 10^{-5}$

Table A5.

Relative errors of approximations after elimination of sampling points

Exp. No	T_{cent}, °C Exp.	Appr.	Δ, %	α_{cent} Exp.	Appr.	Δ (%)	α_{surf} Exp.	Appr.	Δ, %
1	178.97	172.31	3.7	0.97	0.96	1.5	0.85	0.84	1.5
2	125.61	128.42	-2.2	0.79	0.79	0.6	0.66	0.64	3.4
3	77.06	74.07	3.9	0.17	-	-	0.09	-	-
4	60.78	57.22	5.8	0.04	-	-	0.15	-	-
5	196.11	196.05	0.0	0.99	0.98	1.4	0.90	0.94	-4.4
6	85.97	86.66	-0.8	0.17	-	-	0.76	0.77	-1.1
7	105.30	109.17	-3.7	0.40	0.42	-4.4	0.86	0.88	-2.9
8	132.52	131.29	0.9	0.85	0.85	0.2	0.85	0.85	-0.1
9	149.73	152.46	-1.8	0.90	0.89	0.6	0.43	0.43	0.9
10	135.70	134.83	0.6	0.86	0.85	1.5	0.65	0.65	-0.2
11	118.16	120.55	-2.0	0.74	0.72	2.6	0.74	0.72	2.0
12	153.46	148.14	3.5	0.91	0.90	1.5	0.81	0.80	1.3
13	209.60	206.49	1.5	0.99	0.97	1.7	0.90	0.89	1.5
14	52.76	-	-	0.01	-	-	0.71	0.69	2.5
15	128.12	131.46	-2.6	0.77	0.77	-0.1	0.21	-	-
16	57.51	-	-	0.03	-	-	0.12	-	-
17	143.61	140.64	2.1	0.89	0.89	0.4	0.63	0.63	0.4
18	172.15	175.21	-1.8	0.97	0.95	1.9	0.74	0.73	1.4
19	75.42	76.63	-1.6	0.16	-	-	0.13	-	-
20	120.67	118.13	2.1	0.73	0.74	-2.0	0.81	0.82	-0.7
21	182.81	179.99	1.5	0.98	1.06	-8.2	0.80	0.76	4.7
22	211.36	218.56	-3.4	0.99	1.01	-1.7	0.92	0.93	-0.7
23	136.94	139.21	-1.7	0.85	0.88	-3.0	0.55	0.56	-1.8
24	90.47	92.32	-2.0	0.43	0.45	-4.7	0.21	-	-
25	209.92	211.04	-0.5	0.99	0.98	0.8	0.96	0.96	0.5
26	156.73	147.05	6.2	0.93	0.91	2.0	0.60	0.60	0.4
27	114.62	118.04	-3.0	0.72	0.70	2.6	0.56	0.58	-4.4
28	172.86	170.48	1.4	0.97	0.97	-0.2	0.93	0.93	-0.5
29	127.44	130.87	-2.7	0.80	0.80	-0.4	0.67	0.65	3.1
30	114.34	119.22	-4.3	0.70	0.69	1.4	0.48	0.53	-10.1

Continuation of Table A5

Exp. No	$\alpha_{coat.inj}$ Exp.	Appr.	Δ, %	α_{coat} Exp.	Appr.	Δ, %
1	0.63	0.63	0.5	0.65	0.65	0.5
2	0.14	0.14	1.0	0.40	0.40	1.1
3	0.03	-	-	0.04	-	-
4	0.01	-	-	0.11	-	-
5	0.89	0.90	-0.9	0.38	0.39	-2.5
6	0.03	-	-	0.54	0.55	-1.1
7	0.04	-	-	0.68	0.69	-1.6
8	0.22	0.23	-4.2	0.68	0.66	2.8
9	0.30	0.30	-0.4	0.13	-	-
10	0.21	0.22	-5.5	0.39	0.39	0.9
11	0.12	0.11	10.1	0.51	0.51	-0.8
12	0.31	0.31	-0.2	0.56	0.56	0.8
13	0.90	0.90	0.2	0.29	0.29	1.3
14	0.00	-	-	0.57	0.56	1.4
15	0.11	0.11	-1.6	0.07	-	-
16	0.01	-	-	0.08	-	-
17	0.25	0.27	-8.9	0.35	0.35	-0.3
18	0.69	0.69	-0.6	0.29	0.28	3.0
19	0.02	-	-	0.07	-	-
20	0.14	0.13	5.0	0.63	0.64	-1.7
21	0.77	0.75	2.7	0.33	0.33	-0.5
22	0.90	0.90	-0.3	0.68	0.68	0.1
23	0.19	0.18	7.5	0.29	0.28	1.9
24	0.04	-	-	0.12	-	-
25	0.93	0.93	0.2	0.87	0.87	-0.1
26	0.38	0.39	-1.3	0.30	0.29	1.8
27	0.11	0.11	-0.7	0.33	0.34	-3.4
28	0.61	0.61	-0.1	0.86	0.86	-0.1
29	0.14	0.14	2.2	0.41	0.41	0.5
30	0.10	-	-	0.26	0.27	-4.9

REFERENCES

[1] Akishin P., Barkanov E. and Bondarchuk A. Finite Element Modelling and Analysis of Conventional Pultrusion Processes. IOP Conference. Series: Materials Science and Engineering, 96, 012012, 10 p, 2015.

[2] Akishin P., Barkanov E., Miazza N. and Galvez S. Curing Kinetic Models of Resins for Microwave Assisted Pultrusion. Key Engineering Materials, 721, pp. 92-96, 2017.

[3] Akishin, P., Aniskevich, A., Aniskevich, K., Kulakov, V. Numerical Modeling of Heat Transfer in an Orthotropic I-Beam. Mechanics of Composite Materials, 49, 3, pp. 267-276, 2013.

[4] Akishin, P., Barkanov, E. Weight Optimisation of Composite Bandage used for Repair of Pipe with Volumetric Surface Defect. In: *Innovative Solutions in Repair of Gas and Oil Pipelines*. Sofia: Bulgarian Society for Non-destructive Testing Publishers, 2016, pp. 172-182.

[5] Arkhangel'skii I.V., Dunaev A.V., Makarenko I.V., Tikhonov N.A., Belyaev S.S., Tarasov A.V. Non-isothermal kinetic methods. Workbook and laboratory manual. Berlin: Edition Open Access, 2013, 73 p.

[6] ASTM E 698. Standard test method for Arrhenius kinetic constants for thermally unstable materials.

[7] Auzins J., Janushevskis A., Janushevskis J., Skukis E. Software EDAOpt for Experimental Design, AnalysisandMulti-Objective Robust Optimization. In: *Proceedings of the International Conference on Engineering and Applied Sciences Optimisation*, Kos Island, Greece, 2014, 23 p.

[8] Auzins, J. Direct Optimization of Experimental Designs. In: *Proceedings of the 10th AIAA/ISSMO Multidisciplinary Analysis and Optimization*, Albany, USA, 2004, V. 274578, 12 p.

[9] Bai J. Advanced Fibre-reinforced Polymer Composites for Structural Applications. Cambridge: Woodhead Publishing, 2013, 928 p.

[10] Baran I. Pultrusion: State-of-the-art Process Models. Shawbury: Smithers Rapra Technology, 2015, 211 p.

[11] Baran I., Hattel J. H., Tutum C. C. Thermo-Chemical Modeling Strategies for the Pultrusion Process, Applied Composite Materials, vol. 20, pp. 1247-1263, 2013.

[12] Baran I., Tutum C. C., and Hattel J. H. The effect of Thermal Contact Resistance on the Thermosetting Pultrusion Process, Composites Part B: Engineering, 45, pp. 995-1000, 2013.

[13] Baran I., Tutum C.C., Hattel J.H. Probabilistic analysis of a thermosetting pultrusion process, Science and Engineering of Composite Materials, 23(1), pp. 67-76, 2014.

[14] Baran I., Tutum C.C., Hattel J.H. Reliability Estimation of the Pultrusion Process Using the First-Order Reliability Method (FORM), Applied Composite Materials, 20, pp. 639-653, 2013.

[15] Barkanov E., Akishin P., Emmerich R. and Graf M. Numerical Simulation of Advanced Pultrusion Processes with Microwave Heating. In: *Proceedings of the VII European Congress on Computational Methods in Applied Sciences and Engineering*, Crete, Greece, 2016, pp. 7720-7738.

[16] Barkanov E., Akishin P., Miazza N. L. and Galvez S. ANSYS-Based Algorithms for a Simulation of Pultrusion Processes. Mechanics of Advanced Materials and Structures, 24, 5, pp. 377-384, 2017.
[17] Barkanov E., Akishin P., Miazza N. L. and Galvez S. Numerical Simulation of Pultrusion Processes: Algirithms' Comparative Study. In: *Proceedings of the 10th International Conference on Composite Science and Technology*, Lisbon, Portugal, 2015, 12 p.
[18] Barkanov E., Akishin P., Miazza N. L., Galvez S. and Pantelelis N. Experimental Validation of Thermo-Chemical Algorithm for a Simulation of Pultrusion Processes. IOP Conference. Series: Journal of Physics (accepted).
[19] Barkanov E., Eglitis E., Almeida F., Bowering M.C., Watson G. Weight Optimal Design of Composite Lateral Wing Upper Covers Made of Composite Materials, Engineering Optimization, 48(9), pp. 1618-1637, 2016.
[20] Barkanov E., Gluhih S., Kovalov A. Optimal Design of the Active Twist for Helicopter Rotor Blades with C-Spar, Mechanics of Advanced Materials and Structures, 15(3-4), pp. 325-334, 2008.
[21] Barkanov E., Lvov I., and Akishin P. Optimal Design of Composite Repair Systems of Transmission Pipelines. In: *Non-destructive Testing and Repair of Pipelines*. Cham: Springer, 2017, pp. 387-401.
[22] Barkanov E.N., Rikards R.B., Chate A.K. Optimization of Sandwich Structures with Damping Properties, Mechanics of Composite Materials, 1, pp. 485-487, 1993.
[23] Carlone P., Baran I., Hattel J. H., Palazzo G. S. Computational Approaches for Modeling the Multiphysics in Pultrusion Process, Advances in Mechanical Engineering, Article ID 301875, 14 p., 2013.
[24] Carlone P., Palazzo G. S. and Pasquino R. Pultrusion Manufacturing Process Development: Cure Optimization by Hybrid Computational Methods. Computers and Mathematics with Applications, 53, pp. 1464-1471, 2007.
[25] Carlone P., Palazzo G.S. Numerical modeling of the microwave assisted pultrusion process. International Journal of Material Forming, 1 (1), pp. 1323-1326, 2008.
[26] Carlone P., Palazzo G.S., and Pasquino R. Pultrusion Manufacturing Process Development by Computational Modeling and Methods, Mathematical and Computer Modeling, 44, pp. 701-709, 2006.
[27] Chachad Y. R., Roux J. A., Vaughan J. G. and Arafat E. S. Thermal Model for Three-Dimensional Irregular Shaped Pultruded Fiberglass Composites, Journal of Composite Materials, 30/6, pp. 692-721, 1996.
[28] Chachad Y. R., Roux J. A., Vaughan J. G. Three-dimensional characterization of pultruded fiberglass-epoxy composite materials. Journal of Reinforced Plastics and Composites, 14, pp. 495-512, 1995.
[29] Chen C.-H. and Wang W.-S. The Development of Glass Fiber Reinforced Polystyrene for Pultrusion. II: Effect of Processing Parameters for Optimizing the Process, Polymer Composites, 19/4, pp. 423-430, 1998.
[30] Coelho R. M. L. and Calado V. M. A. An Optimization Procedure for the Pultrusion Process Based on a Finite Element Formulation, Polymer Composites, 23/3, pp. 329-341, 2002.
[31] Ding Z, Li S, Lee LJ. Influence of heat transfer and curing on the quality of pultruded composites. II: Modelling and simulation. Polymer Composites, 23(5), pp. 957-69, 2002.

[32] Goldsworthy W.B. Apparatus for producing elongated articles from fiber-reinforced plastic material. US patent US2871911 A, 1959.

[33] Hackett R. M., Zhu S.-Z. Two-Dimensional Finite Element Model of the Pultrusion Process, Journal of Reinforced Plastics and Composites, 11, pp. 1322-1351, 1992.

[34] Han C.D., Lee D.S., and Chin H.B. Development of a Mathematical Model for the Pultrusion Process, Polymer Engineering and Science, 26/6, pp. 393-404, 1986.

[35] Hewlett-Packard: Basics of measuring the dielectric properties of materials, Application Note 1217-1, Hewlett-Packard Co., 1992.

[36] Hewlett-Packard: HP-Network Analyzer 8720 D + Dielectric Probe Kit 85070B: User´s Manual, 1993.

[37] Howald A.M. Meyer L.S. Shaft for Fishing Rods. US patent US2571717 A, 1951.

[38] http://www.lucintel.com/pultrusion_market_2021.aspx, 15 August 2017.

[39] http://www.synthesites.com/ipage.php?p=9&l=11, 16 February 2017.

[40] Janushevskis A., Akinfiev T., Auzins J., Boyko A. A Comparative Analysis of Global Search Procedures. Proceedings of the Estonian Academy of Sciences Engineering, 10 (4), pp. 236-250, 2004.

[41] Joshi S. C., Lam Y. C. Three-Dimensional Finite-Element/Nodal-Control-Volume Simulation of the Pultrusion Process with Temperature-Dependent Material Properties Including Resin Shrinkage, Composite Science and Technology, 61, pp. 1539-1547, 2001.

[42] Joshi S.C., and Lam Y.C. Integrated Approach for Modeling Cure and Crystallization Kinetics of Different Polymers in 3D Pultrusion Simulation, Journal of Materials Processing Technology, 174, pp. 178-182, 2006.

[43] Joshi S.C., Lam Y.C., Tun U.W. Improved cure optimization in pultrusion with pre-heating and die-cooler temperature. Composites: Part A, 34, pp. 1151-1159, 2003.

[44] Joshi S.C., Lam Y.C., Zaw K. Optimization for quality thermosetting composites pultrudate through die heater layout and power control. In: *Proceedings of the 16th International Conference on Composite Materials*, Kyoto, Japan, 2007, 7 p.

[45] Kayser T., Link G., Seitz T., Nuss V., Dittrich J., Jelonnek J., Heidbrink F., Ghomeshi R. An applicator for microwave assisted pultrusion of carbon fiber reinforced plastic. In: *Proceedings of the 2014 IEEE MTT-S International Microwave Symposium*, Florida, USA, 2014, 4 p.

[46] Khan WA, Methven J. Determination of the duty cycle in thermoset pultrusion. In: *Hinduja S and Li L, editors. Proceedings of the 36th International MATADOR Conference*, London: Springer, 2010. pp. 75-78.

[47] Kim D.H., Lee W.I., Friedrich K. A model for a thermoplastic pultrusion process using commingled yarns. Composites science and technology, 61(8), pp. 1065-1077, 2001.

[48] Kissinger H. E. Reaction kinetics in differential thermal analysis. National Bureau of Standards, 29(11), pp. 1702–1706, 1957.

[49] Lasdon L. S., Fox R. L., Rather M. W. Nonlinear optimization using the generalized reduced gradient method. Revue française d'automatique, d'informatique et de recherche opérationnelle. Recherche opérationnelle, 8(3), pp. 73-103, 1974.

[50] Lee H-T., Chen S-H., Kang H-Y. A Study of Generalized Reduced Gradient Method with Different Search Directions. Journal of Measurement Management, 1(1), pp. 25-38, 2004.

[51] Lee W.I., Loos A.C., Springer G.S. Heat of reaction, degree of cure, and viscosity of Hercules 3501-6 resin, Journal of Composite Materials, 16, pp. 510-520, 1982.

[52] Li J., Joshi S.C., Lam Y.C. Curing Optimization for pultruded composite sections. Composite Science and Technology, 62, pp. 457-467, 2002.
[53] Liang G., Garg A., Chandrashekhara K. Cure Characterization of Pultruded Soy-Based Composites, Journal of Reinforced Plastics and Composites, 24/14, pp. 1509-1520, 2005.
[54] Lin M., Hawley M.C. Preliminary tests of the application of continuous microwave technique to pultrusion. In: *Proceedings of the 38 International SAMPE Symposium and Exhibition*, Anaheim, USA, 1993, pp. 436-445.
[55] Liu L., Yi S., Ong L.S., Chian K.S., Osiyemi S., Lim S.H., Su F. Chemothermal modeling and finite-element analysis for microwave cure process of underfill in flip-chip packaging, IEEE Transactions on Electronics Packaging Manufacturing, 28 (4), pp. 355-363, 2005.
[56] Liu X. L., Crouch I. G., Lam Y. C. Simulation of heat transfer and cure in pultrusion with a general-purpose finite element package. Composites Science and Technology, 60, pp. 857-864, 2000.
[57] Liu X. L., Hillier W. Heat Transfer and Cure Analysis for the Pultrusion of a Fiberglass-Vinyl Ester I Beam, Composite Structures, 47, pp. 581-588, 1999.
[58] Liu X.-L. Numerical modelling on pultrusion of composite I beam. Composites: Part A, 32, pp. 663-681, 2001.
[59] Maffezzoli A, Trivisano A, Opalicki M, Mijovic J, Kenny JM. Correlation between dielectric and chemorheological properties during cure of epoxy-based composites. Journal of Materials Science, 29(3), pp. 800-808, 1994.
[60] Metaxas A.C., Meredith R.J. Industrial microwave heating, IEEE Power Engineering Series 4. London: Peter Peregrinus Limited, 1983, 357 p.
[61] Methven J.M., Ghaffariyan S.R., Abidin A.Z. Manufacture of fiber-reinforced composites by microwave assisted pultrusion. Polymer Composites, 21 (4), pp. 586-594, 2000.
[62] Myers R. H., Montgomery D. C. Response surface methodology: Process and product optimization using designed experiments. New York: John Wiley & Sons, 1976, 714 p.
[63] Püschner H. Wärme durch Mikrowellen. Eindhoven: Philips Technische Bibliothek, 1964, 325 p.
[64] Rao S.S. Engineering Optimisation: Theory and Practice. New York: John Wiley & Sons, 2009, 840 p.
[65] Roux J.A., Vaughan J. G., Shanku R., Arafat E. S., Bruce J. L., Johnson V. R. Comparison of Measurements and Modeling for Pultrusion of a Fiberglass/Epoxy I-Beam, Journal of Reinforced Plastics and Composites, 17/17, pp. 1557-1579, 1998.
[66] Sacks J., Welch W.J., Mitchell T.J., Wynn H.P. Design and analysis of computer experiments. Statistical science, 4(4), pp. 409–435, 1989.
[67] Shannon C.E. Communication in the presence of noise. Proceedings of the Institute of Radio Engineers, 37 (1), pp. 10-21, 1949.
[68] Shokrieh M.M., Aghdami A.M. A dynamic model to simulate the time dependent pultrusion process of Glass/Polyester Composites, Applied Composite Materials, 18, pp. 585-601, 2011.
[69] Smith A.C., McMillan A.M., Hawley M.C. Microwave pultrusion of graphite/epoxy composites using single frequency and variable frequency processing techniques. In: *Proceedings of the 30 International SAMPE Technical Conference*, San Antonio, USA, 1998, pp. 213-225.
[70] Starr T.F. Pultrusion for Engineers. Cambridge: Woodhead Publishing, 2000, 303 p.

[71] Sucher M., Fox J. Handbook of microwave measurements, Vol. II, 3rd Edition. New York: Polytechnic Press., 1963, 340 p.
[72] Suranto B. R., Ye L., Mai Y. W. Simulation of temperature and curing profiles in pultruded composite rods. Composite Science and Technology, 58, pp. 191-197, 1998.
[73] Tena I, Sarrionandia M, Torre J, Aurrekoetxea J. The effect of process parameters on ultraviolet cured out of die bent pultrusion process. Composites: Part B, 89, pp. 9-17, 2016.
[74] Thostenson E.T., Tchou W. Microwave and conventional curing of thick-section thermoset composite laminates: experiment and simulation. Polymer Composites, 22(2), pp. 197-212, 2001.
[75] Tutum C.C., Deb K., Baran I. Constrained efficient Global Optimization for pultrusion process, Materials and Manufacturing Processes, 30(4), pp. 538-551, 2015.
[76] Valliappan M., Roux J. A., Vaughan J. G., Arafat E. S. Die and post-die temperature and cure in graphite/epoxy composites. Composites: Part B, 27B, pp. 1-9, 1996.
[77] Witten E. Composites Market Report 2012: Market Developments, Trends, Challenges and Opportunities, 2012.
[78] Wu C.F.J., Hamada M. Experiments: Planning, Analysis, and Parameter Design Optimisation. New York: John Wiley & Sons Inc., 2000, 630 p.